



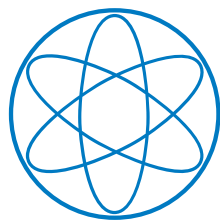
TECHNISCHE UNIVERSITÄT MÜNCHEN

Phenomenology of dark matter scenarios with non-minimal coupling to gravity

DISSERTATION

by

JOEL SEBASTIAN INGENHÜTT



PHYSIK-DEPARTMENT T30D, TUM
& MAX-PLANCK-INSTITUT FÜR PHYSIK



TECHNISCHE UNIVERSITÄT MÜNCHEN

PHYSIK-DEPARTMENT T30D

Phenomenology of dark matter scenarios with non-minimal coupling to gravity

JOEL SEBASTIAN INGENHÜTT

Vollständiger Abdruck der von der Fakultät für Physik der Technischen Universität München zur Erlangung des akademischen Grades eines

Doktors der Naturwissenschaften

genehmigten Dissertation.

Vorsitzender: Prof. Dr. Stefan Schönert
Prüfer der Dissertation: 1. Prof. Dr. Alejandro Ibarra
2. Hon.-Prof. Dr. Wolfgang Hollik

Die Dissertation wurde am 20.03.2019 bei der Technischen Universität München eingereicht und durch die Fakultät für Physik am 16.04.2019 angenommen.

Abstract

Although a large number of astronomical and cosmological observations have corroborated the case for the existence of dark matter, its particle nature and properties remain unknown. In particular, the origin of the extremely long lifetime of the dark matter particle is not fully understood. This thesis studies the phenomenological implications of a non-minimal coupling to gravity in various dark matter scenarios. Through this interaction, dark matter is shown to decay into visible sector particles via Planck-mass suppressed operators, connecting its small decay width with the weakness of gravitational interactions. For a scalar singlet, a scalar doublet and a fermionic singlet dark matter candidate, data from gamma-ray, cosmic-ray and neutrino experiments as well as observations of the cosmic microwave background are used to constrain the size of this gravity portal. Further limits are derived through an analysis of dark matter production via coannihilations in the early Universe. Finally, a possible connection between dark matter decay and cosmic inflation is explored.

Zusammenfassung

Obgleich eine Vielzahl astronomischer und kosmologischer Beobachtungen Hinweise für die Existenz dunkler Materie geliefert haben, sind deren Teilchennatur und -eigenschaften nach wie vor unbekannt. Speziell der Ursprung der äußerst langen Lebensdauer des Dunkelmaterieteilchens ist nicht vollständig verstanden. Diese Dissertation untersucht die phänomenologischen Auswirkungen einer nichtminimalen Kopplung an Gravitation in mehreren theoretischen Szenarien dunkler Materie. Es wird gezeigt, wie dunkle Materie durch diese Wechselwirkung in Teilchen sichtbarer Materie zerfallen kann. Dass die hierfür relevanten Operatoren durch Potenzen der Planck-Masse unterdrückt sind, lässt eine Verbindung der kleinen Zerfallsbreite mit der Schwachheit gravitativer Wechselwirkungen zu. Für ein skalares Singulett, ein skalares Dublett sowie ein fermionisches Singulett erlauben es Messungen der kosmischen Gamma- und Teilchenstrahlung, des Neutrinoflusses sowie des kosmischen Mikrowellenhintergrunds, die maximale Stärke dieser Kopplung zu beschränken. Weitere Einschränkungen ergeben sich aus einer Berechnung der Produktion dunkler Materie durch Koannihilationsprozesse im frühen Universum. Zuletzt wird ein möglicher Zusammenhang zwischen dem Zerfall dunkler Materie und kosmologischer Inflation untersucht.

Contents

1	Introduction	5
2	The dark and the visible sector	9
2.1	The dark matter puzzle	9
2.2	Indirect detection	10
2.3	Dark matter production in the early Universe	12
2.4	Dark matter stability	14
2.5	Dark and visible matter in curved spacetime	15
3	Theories with non-minimal coupling to gravity	21
3.1	Non-minimal coupling to gravity	22
3.2	Weyl transformation	24
3.3	Modification of the electroweak vacuum	27
3.4	A note on the cosmological constant	28
4	Dark matter decays from non-minimal coupling to gravity	31
4.1	Scalar singlet dark matter	32
4.2	Scalar (inert) doublet dark matter	35
4.3	Fermionic dark matter	37
4.4	Dark matter decay in simplified models	38
5	Decay phenomenology	41
5.1	Scalar singlet dark matter above the GeV scale	42
5.2	Low-mass scalar singlet dark matter	46
5.3	Scalar (inert) doublet dark matter	50
5.4	Fermionic dark matter	54
5.5	Higher-order corrections	58
6	Constraints from cosmology	61
6.1	Constraints from the cosmic microwave background	61
6.2	Constraints from dark matter production	63
6.2.1	Relic abundance from coannihilations	64
6.2.2	Relic abundance from (inverse) decays	69
6.2.3	Total relic abundance	71
7	Inflation in non-minimally coupled scenarios	73
7.1	Scalar field dynamics	73
7.2	Inflation with non-minimal coupling to gravity	74

8	Conclusions	77
	Appendices	79
A	Feynman Rules	79
A.1	Scalar singlet above 1 GeV	79
A.2	Low-mass scalar singlet	81
A.3	Scalar doublet	81
A.4	Fermion singlet	85
B	Generating Feynman rules with <i>FeynRules</i>	87
C	Computing decay rates with <i>MadGraph</i>	89
D	High-multiplicity phase-space integrals	91
E	Energy spectra of cascade decays	95
	Bibliography	99

Chapter 1

Introduction

At the present day, we have a very advanced understanding of fundamental physics. On microscopic scales, the standard model of particle physics [1] unifies the description of electromagnetism and the weak and strong nuclear forces. Since its finalization in the 1970s, its predictions have been verified experimentally time and time again, the latest example being the detection of the Higgs boson at the Large Hadron Collider (LHC) [2, 3]. Meanwhile, the Lambda-Cold Dark Matter (Λ CDM) model of concordance cosmology [4] has been tremendously successful at describing the dynamics of our Universe at the largest observable scales, on the basis of general relativity. Among other astronomical and cosmological observables, it can explain the shape of the anisotropy spectrum of the cosmic microwave background (CMB) to astonishing precision [5]. However, despite the individual success of these two theories, a description of nature through a combination of the standard model and Λ CDM cosmology leaves certain questions unanswered, *e.g.* related to the origin of neutrino masses, the strongly hierarchical mass spectrum of the known particles or the nature of dark matter. These gaps in our understanding undeniably prove the existence of new physics beyond these respective standard models, and a tremendous amount of effort, both experimental and theoretical, is being put into closing them.

With respect to the last of the examples given above, over the past decades, a large number of astronomical and cosmological observations have corroborated the case for some form of non-luminous, or “dark” matter [6]. On galactic length scales, a large discrepancy is observed between the motion of stars in spiral galaxies and the predictions of Newtonian gravity based on the attraction of the visible galactic matter [7, 8]. Arguably the most likely explanation for this phenomenon is the presence of a dark matter halo that extends far beyond the visible matter distribution. Depending on the size and luminosity of the galaxy, it is thought to be responsible for a dominant, or at least significant, fraction of the total mass [9]. Alternatively, one would have to conclude that the known laws of gravity do not apply at these scales and have to be modified [10]. At larger scales, the behavior of a number of galaxy clusters exhibits a similar mismatch between their visible and total matter. Concretely, their center of mass, as determined from gravitational lensing observations, is spatially offset from the center of their visible matter distribution, identified through its x-ray emission [11, 12]. Finally, more and more precise measurements of the cosmic microwave background by the COBE [13], WMAP [14] and Planck [5] missions have enabled us to pinpoint the parameters of the Λ CDM model. In this framework, cosmological observations can be explained with a minimal set of parameters, under very general assumptions — one of which, however, is the presence of a cold dark matter component in the cosmic fluid that dominates over the visible matter energy density by roughly a factor of five.

The list of proposed candidates for dark matter is extensive, ranging in mass from ultra-

light scalar fields [15, 16] to more “traditional” examples of particle dark matter inspired by supersymmetry or other “new physics” scenarios [17, 6], all the way up to macroscopic objects such as primordial black holes [18, 19]. This diversity follows from the fact that so far, the presence of dark matter has only been established through its gravitational effects on visible matter, as described above. Determining whether there are other, non-gravitational interactions between dark and visible matter is one of the most pressing tasks of astroparticle physics today, in the hope that these interactions, if present, will allow us to learn more about the nature and origin of dark matter.

For a long time, one of the most popular candidates has been the weakly interacting massive particle (WIMP), *i.e.* an electrically neutral particle with a mass around the electroweak scale and couplings comparable to those of the weak nuclear force. The theoretical motivation for this type of dark matter candidate is strong, since it appears in many extensions of the standard model, *e.g.* as the neutralino in supersymmetric models [17]. Moreover, its weak-scale mass and coupling mean that a population of these particles was in thermal equilibrium with the visible sector in the early Universe, giving rise to the “correct” present-day dark matter abundance, under some simplifying assumptions [6]. Most intriguingly, however, such a dark matter particle could be accessible to the Large Hadron Collider at CERN [20, 21], leave a trace in one of the direct detection experiments operating all over the world [22, 23, 24, 25, 26], or lead to exotic signals in gamma-ray [27], cosmic-ray [28] or neutrino experiments [29] through annihilations or decays. In the absence of a conclusive signal in either of these three detection strategies, however, it seems prudent to remain open to dark matter theories beyond the WIMP paradigm, *e.g.* those with different thermal histories [30, 31] or additional hidden sector dynamics [32, 33], as well as to the full range of possible masses.

Among the properties to be addressed by any such theory should be the exceptional longevity of the dark matter particle [34]. In the visible sector, only very few particles share its stability on cosmological timescales: the electron and the lightest neutrino, for example, are both absolutely stable, protected by electric charge conservation and Lorentz symmetry, respectively. The stability of the proton, on the other hand, seems to be an “accidental” consequence of the matter content of the standard model and its combination of gauge charges [35, 36]. In a similar way, there are multiple possible explanations for dark matter stability. Often, an agnostic standpoint is taken by postulating the existence of a global symmetry by hand that forbids dark matter decay. This is not strictly necessary, however: if the dark matter particle is very light and weakly coupled to the visible sector [37, 38], its total width might be suppressed sufficiently by small couplings and phase-space factors. Alternatively, the dark matter field could be part of a high-dimensional gauge multiplet [39] or Lorentz representation [40], which would severely restrict renormalizable interactions with the standard model. As another option, a dark gauge symmetry might exist, making the lightest charged “dark” particle absolutely stable analogously to the electron [41, 42]. If the first approach is pursued and a global symmetry is assumed to be in place, it is usually taken to be exact. However, similarly to the case of the proton, *a priori* there is no reason why the global symmetry should be conserved at higher energy scales. In particular, on very general grounds, gravity is not expected to conserve global symmetries [43, 44]. Therefore, the possibility that dark matter stability is spoiled by gravitational effects has to be taken seriously in this scenario [45, 46, 47, 48].

This thesis deals with the phenomenological implications of a certain type of non-minimal coupling between the dark matter quantum field and gravity, specifically with its impact on dark matter stability. In chapter 2, a brief review of our current knowledge about the dark and visible sector particles and their interactions will be given. This will set the stage for the introduction of non-minimally coupled dark matter scenarios in chapter 3. First, the general form of the

effective operators induced through non-minimal coupling will be discussed, followed by an outline of how dark matter decay proceeds through them. Two remarks address the modification of the electroweak vacuum as well as the value of the cosmological constant. Chapter 4 details the interaction Lagrangian induced by non-minimal coupling for a scalar singlet, a scalar $SU(2)_L$ doublet and a fermionic singlet. Chapter 5 deals with the decay phenomenology of each of these candidates in turn, deriving constraints on the strength of the non-minimal coupling in each case. Some implications of a non-minimally coupled scalar field for cosmology will be discussed in chapter 6, in particular its impact on the cosmic microwave background and prospects for dark matter production in the early Universe. Chapter 7 explores a possible connection between dark matter decay and inflation in non-minimally coupled scenarios. Conclusions will be presented in chapter 8. A set of appendices provides details on the interaction vertices of the dark matter candidates discussed in this thesis (A), on the software packages utilized in the numerical computations (B, C), as well as on the calculation of high-multiplicity phase-space integrals (D) and cascade decay spectra (E).

This dissertation builds on the previous studies of

- [49] Sebastian Ingehütt. Dark matter decays from non-minimal coupling to gravity. Master's thesis, Technical University of Munich, 11 2015.

Parts of the results, as well as some of the figures, have been published in

- [50] Oscar Catà, Alejandro Ibarra, and Sebastian Ingehütt. Dark matter decays from non-minimal coupling to gravity. *Phys. Rev. Lett.*, 117(2):021302, 2016. [arXiv:1603.03696](#), [doi:10.1103/PhysRevLett.117.021302](#),
- [51] Oscar Catà, Alejandro Ibarra, and Sebastian Ingehütt. Dark matter decay through gravity portals. *Phys. Rev.*, D95(3):035011, 2017. [arXiv:1611.00725](#), [doi:10.1103/PhysRevD.95.035011](#),
- [52] Oscar Catà, Alejandro Ibarra, and Sebastian Ingehütt. Sharp spectral features from light dark matter decay via gravity portals. *JCAP*, 1711(11):044, 2017. [arXiv:1707.08480](#), [doi:10.1088/1475-7516/2017/11/044](#).

Chapter 2

The dark and the visible sector

2.1 The dark matter puzzle

The question about the nature of dark matter has been with us for many decades now, sparked by astronomical observations on multiple distance scales. As early as the 1920s, there was evidence for the existence of some unseen matter in our galaxy [53], based on the comparison of the observed rotational velocities of stars within the Milky Way with the predictions of Newtonian gravity. Follow-up studies in the 1930s corroborated this picture [54]. On larger scales, the dynamics of clusters of galaxies showed a similar behavior. Specifically for the Coma cluster it was found that most of its mass had to be “dark” in order to explain the large dispersion in the velocity distribution of its constituents [55, 56].

By the 1970s, technological advances had made it possible to determine galactic rotation curves with much greater accuracy. A detailed study of 21 spiral galaxies confirmed that these rotation curves did indeed not fall at large radii, but kept rising instead [7]. Complementary observations by radio telescopes supported this picture [57], further strengthening the case for dark matter in galaxies. On the scale of galaxy clusters, by the end of the 1990s it had become possible to perform complementary determinations of their mass by measuring gravitational lensing effects [58]. More recently still, spatial separation between the dark and luminous matter distributions has been shown to exist in some systems [11, 12], which are thought to be a result of the particular histories of these clusters. Finally, a last line of evidence for dark matter emerged with the detailed measurement of the acoustic peaks in the cosmic microwave background [14, 5]. These tightly constrain the parameters of the Λ CDM model, among them the physical density parameter

$$\Omega_{\text{DM}} h^2 \simeq 0.12 [5], \quad (2.1)$$

quantifying the total amount of dark matter in the Universe.

By now, a rough picture of the properties and distribution of dark matter has emerged, from cosmological down to galactic scales:

- The total amount of dark matter in the Universe is roughly five times that of baryonic matter [5].
- Dark matter was non-relativistic already in the early Universe, enabling it to form over- and underdensities in the primordial plasma. These density fluctuations provided the seeds for structure formation, leading to the large-scale structures we observe today [4].

- Galaxies typically host a dark matter halo of appreciable size, which extends to radii exceeding those of the outermost visible objects. This halo usually accounts for the bulk of the total galactic mass [7, 8], although exceptions to this rule might exist [59, 60, 61, 62].
- Dark matter interacts very weakly with ordinary matter; specifically, it does not emit sizable amounts of electromagnetic radiation. It is also stable on cosmological timescales.

Several questions remain open, however:

- What is dark matter made of? What are its fundamental constituents, and what are their properties?
- Does dark matter interact non-gravitationally with baryonic matter? What shape do these interactions take?
- Does dark matter self-interact? Does it decay?
- How was dark matter produced in the early Universe?

Today, a rich experimental program aims to find answers to these questions. In particular, based on the assumption that dark matter is made up of elementary particles like ordinary matter, three main strategies are being pursued at present: direct detection, indirect detection and collider searches. In the direct detection approach, one tries to observe scattering events between dark matter particles and atomic nuclei. Various experiments use different target materials and different read-out techniques: for dark matter masses around 10–1000 GeV, liquid noble gas detectors currently provide the strongest bounds [25, 23, 24]. Today, their sensitivity is mostly limited by target volume [63, 64]. For lower dark matter masses, the main challenge is to remain sensitive to lower recoil energies. Solid state detectors perform best in this regime [26, 22]. In the future, reaching and pushing beyond the so-called “neutrino floor” caused by coherent scattering of neutrinos off target nuclei will be vital, and techniques to obtain directional information are being studied [65, 66, 67, 68]. If the dark matter particle is not too heavy, one could also hope to produce it in the high-energy proton-proton collisions conducted at CERN’s Large Hadron Collider. Generally speaking, events with large amounts of missing transverse energy would be a likely signature at the ATLAS [69] or CMS [70] experiments, as the dark matter particle is expected to pass through these detectors without interacting. Of course, depending on the dark matter model, other signatures, such as invisible Higgs decays or displaced vertices, are possible [71] and are actively being searched for in the data [72, 73].

2.2 Indirect detection

Finally, as dark matter is thought to be abundant throughout the Universe, one can attempt to detect it indirectly, by observing the final-state particles of dark matter scattering or decay events. This requires a precise measurement of the photon [74], neutrino [75] or cosmic ray fluxes [76, 77] at Earth. The main difficulty here is to accurately quantify the astrophysical background fluxes and associated uncertainties [78]. For gamma rays specifically, sensitivity can be improved significantly by choosing appropriate observation targets that are expected to have a high concentration of dark matter [79] and, ideally, low astrophysical background fluxes [27]. Any model of decaying or annihilating dark matter producing additional photons can then be constrained by the non-observation of exotic signals in the data. Focussing on the scenario of

decaying dark matter, there are two contributions to the total isotropic photon flux at Earth,

$$\frac{d\Phi}{dE_\gamma} = \frac{d\Phi_{\text{EG}}}{dE_\gamma} + \frac{d\Phi_{\text{MW}}}{dE_\gamma}, \quad (2.2)$$

corresponding to extragalactic photons and those produced within the Milky Way, respectively.

The first, cosmological, component is given by integrating the differential decay rate over redshift z , taking into account the expansion of the Universe parametrized by the Hubble parameter $H(z)$ [80],

$$\frac{d\Phi_{\text{EG}}}{dE_\gamma} = \frac{1}{4\pi} \frac{\Omega_{\text{DM}} \rho_{\text{c},0}}{m_{\text{DM}}} \int_0^\infty \frac{dz}{H(z)} e^{-\tau(E_\gamma(z),z)} \sum_f \left(\Gamma_{\text{DM} \rightarrow f} \frac{dN^{(f)}}{dE_\gamma} ((1+z)E_\gamma) \right). \quad (2.3)$$

Here, $\rho_{\text{c},0} = 4.9 \times 10^{-6} \text{ GeV cm}^{-3}$ [4] is the present-day value of the critical density of the Universe, m_{DM} is the dark matter mass, and

$$H(z) = H_0 \sqrt{\Omega_{\text{m}} (1+z)^3 + \Omega_{\Lambda}} \quad (2.4)$$

is the Hubble function. $\Omega_{\text{DM}} = 0.26$, $\Omega_{\text{m}} = 0.31$ and $\Omega_{\Lambda} = 0.69$ [5] are the energy densities of dark matter, matter and vacuum energy in units of the critical density $\rho_{\text{c},0}$, respectively, and $H_0 = 68 \text{ km s}^{-1} \text{ Mpc}^{-1}$ [5] is the present-day Hubble parameter. At sub-GeV energies, the attenuation factor $e^{-\tau}$ quantifying the Universe's opacity to photons is very close to unity, while above photon energies of $E_\gamma \gtrsim 0.1\text{--}1 \text{ TeV}$, it introduces significant suppression [78]. The sum runs over all final states f producing photons, multiplying each partial width $\Gamma_{\text{DM} \rightarrow f}$ with the corresponding energy spectrum $dN^{(f)}/dE_\gamma$, evaluated at the redshifted energy $(1+z)E_\gamma$. For practical purposes, the integration region can be limited to redshifts $0 < z < 100$, as the high-energy photons most relevant for detection come from lower redshifts.

The second contribution to the photon flux at Earth, due to decays in the Milky Way halo, is [80]

$$\frac{d\Phi_{\text{MW}}}{dE_\gamma d\Omega}(\psi) = \frac{1}{4\pi} \sum_f \left(\frac{\Gamma_{\text{DM} \rightarrow f}}{m_{\text{DM}}} \frac{dN^{(f)}}{dE_\gamma} \right) \mathcal{J}(\psi). \quad (2.5)$$

This flux is anisotropic; its magnitude depends on the viewing angle ψ relative to the Galactic Center and the galactic plane. The astrophysical J-factor in the direction ψ for decays is given by

$$\mathcal{J}(\psi) = \int_0^\infty ds \rho_{\text{MW}}(r(s, \psi)). \quad (2.6)$$

The dark matter density distribution of the Milky Way, $\rho_{\text{MW}}(r)$, is integrated along the line of sight s , taking into account the position of the solar system $r_\odot = 8.33 \text{ kpc}$ away from the Galactic Center. A popular choice for the dark matter density distribution is the NFW profile [9],

$$\rho_{\text{MW}}(r) = \frac{\rho_0}{\frac{r}{r_s} \left(1 + \frac{r}{r_s}\right)^2}, \quad (2.7)$$

with scale radius $r_s = 24.42 \text{ kpc}$, and normalized such that the local dark matter density is $\rho_{\text{MW}}(r_\odot) = 0.3 \text{ GeV cm}^{-3}$. Compared to the case of annihilating dark matter, where the appropriate integrand is proportional to the density distribution squared, the dependence of

the expected flux on the choice of halo profile ρ_{MW} is significantly weaker for a decay scenario. To obtain the observed photon flux, one finally needs to integrate the differential flux over the solid angle under observation $\Delta\Omega$. A compilation of integrated J-factors can be found in the literature [78]. For the calculation of the expected photon flux from dark matter decay in section 5.2, an integrated J-factor of $(4\pi) \times \mathcal{J}_{\text{MW}}^{(\text{ave})} = 1.69 \times 10^{22} \text{ GeV cm}^{-2}$ was used.

Whether one hopes to detect dark matter through its decay products in particle fluxes at Earth or through its signatures in direct detection or collider experiments, what is common to all three approaches is their reliance on there being some form of interaction between dark and visible matter, other than their effect on spacetime curvature. So far, there has not been a conclusive dark matter signal in any of the mentioned experiments. Nevertheless, the data allow one to constrain the strength of interactions between the dark and visible sector from above.

2.3 Dark matter production in the early Universe

If dark matter is indeed abundant in the Universe today, it must have been produced by some mechanism in the early Universe. If the dark matter particle couples to the visible sector, it is possible to calculate its expected abundance from thermodynamical considerations [4]. A scalar singlet dark matter candidate ϕ [81, 82], for example, can interact with the standard model in a Lorentz and gauge invariant way already at the renormalizable level via the so-called Higgs portal $\lambda_{H\phi} \Phi^\dagger \Phi \phi^2/2$, where Φ is the standard model Higgs doublet. For appropriate values of the coupling constant $\lambda_{H\phi}$, this allows for dark matter pair production in the early Universe through intermediate Higgs bosons and can lead to the traditional freeze-out scenario [4, 83].

Here, the dark matter abundance Y_{DM} initially traces its equilibrium value, as interactions with the thermal bath happen frequently enough (*cf.* figure 2.1). As the temperature drops and the dark matter particles become non-relativistic, their equilibrium abundance experiences exponential suppression. If their coupling to the thermal bath was strong enough, this suppression would continue until the dark matter abundance was virtually zero. However, as the Universe expands as it cools, interactions with the visible sector become rarer and rarer, until they cannot maintain equilibrium any longer: at some point Hubble expansion suppresses number-changing processes sufficiently for the dark matter abundance to freeze out and remain constant. The weaker dark matter couples to the thermal bath, the earlier it drops out of equilibrium, leading to a higher present-day number density. Consistency with the observed dark matter density parameter $\Omega_{\text{DM}} h^2 = 0.12$ [5] translates into a lower limit on the strength of the interaction responsible for freeze-out. In the context of traditional WIMP scenarios, a curious numerical coincidence occurs: if dark matter particles are predominantly pair-produced through 2-to-2 scattering processes, their present-day abundance is approximately given by

$$\Omega_{\text{DM}} h^2 \simeq \frac{3 \times 10^{-27} \text{ cm}^3 \text{ s}^{-1}}{\langle \sigma v \rangle} [6], \quad (2.8)$$

with $\langle \sigma v \rangle$ the thermally averaged scattering cross section. This value hints at a dark matter particle with weak-scale interactions, which would put it in experimental range of direct detection and collider experiments. In fact, for many models, the latest generation of these experiments has already cut deep into arguably the most interesting parts of parameter space. In particular, the Higgs portal coupling of the scalar singlet is under tension with data from dark matter direct detection experiments across a wide mass range. A scalar singlet WIMP with $m_\phi \simeq 60 \text{ GeV}$ and $\lambda_{H\phi} \simeq 10^{-3}$ remains a possibility, however [84, 85]. The freeze-out scenario itself, meanwhile, is applicable to many other dark matter scenarios, as are variants of it [86].

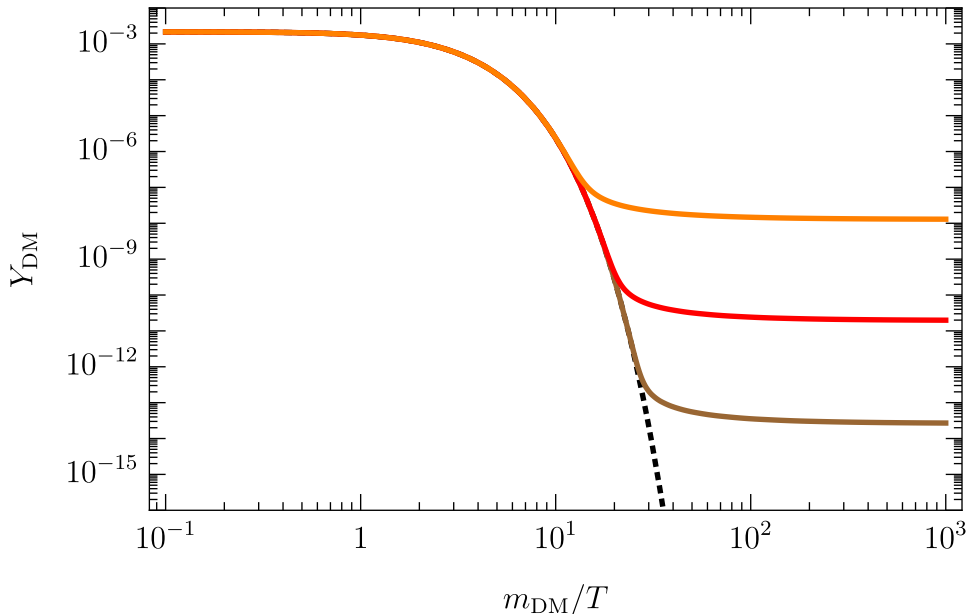


Figure 2.1: *Dark matter freeze-out production.* The dark matter abundance Y_{DM} traces its equilibrium value (dotted black line) until dark matter particles become so diluted that they cannot scatter efficiently anymore. This happens at a freeze-out temperature that depends on the strength of the coupling between the dark matter particle and the thermal bath. The continuous lines show the actual dark matter abundance for weaker, moderate and stronger coupling (orange, red and brown lines, respectively).

An alternative scenario for dark matter production is the freeze-in mechanism [31], which is especially applicable to dark matter candidates with couplings much smaller than those of a WIMP. For such a feebly interacting massive particle (FIMP), interactions between the particle in question and the standard model thermal bath are assumed to be so weak that the two never reach thermal equilibrium. Instead, one assumes a vanishing initial number density, as illustrated in figure 2.2. The particle abundance is then built up gradually as the Universe cools and expands, until Hubble expansion suppresses interactions and the particle abundance freezes in and remains constant. In this case, in contrast to the freeze-out scenario, the present-day relic abundance is proportional to the interaction cross section rather than inversely proportional to it: the larger the coupling to the thermal bath, the longer dark matter can be produced before interactions become inefficient. For a scalar singlet dark matter candidate, the correct relic abundance can be achieved through a Higgs portal of order $\lambda_{H\phi} \simeq 10^{-11}$ [87].

Generally speaking, whether a dark matter abundance is created via freeze-out or freeze-in depends primarily on the strength of its coupling to the standard model thermal bath. Starting in the freeze-in regime, *i.e.* with a vanishing initial population, for a fixed dark matter mass, the expected present-day abundance first grows with increasing coupling strength and eventually reaches the observed value $\Omega_{\text{DM}} h^2 \simeq 0.12$. Further increasing the coupling leads to an overproduction of dark matter and the model is in conflict with observations. However, as the coupling strength approaches that of a WIMP, interactions are strong enough to bring dark matter into thermal equilibrium with the standard model. Therefore, the freeze-out scenario applies and the present-day dark matter abundance decreases again with increasing coupling. Eventually, the observed value is reproduced a second time. For even larger couplings, dark matter is un-

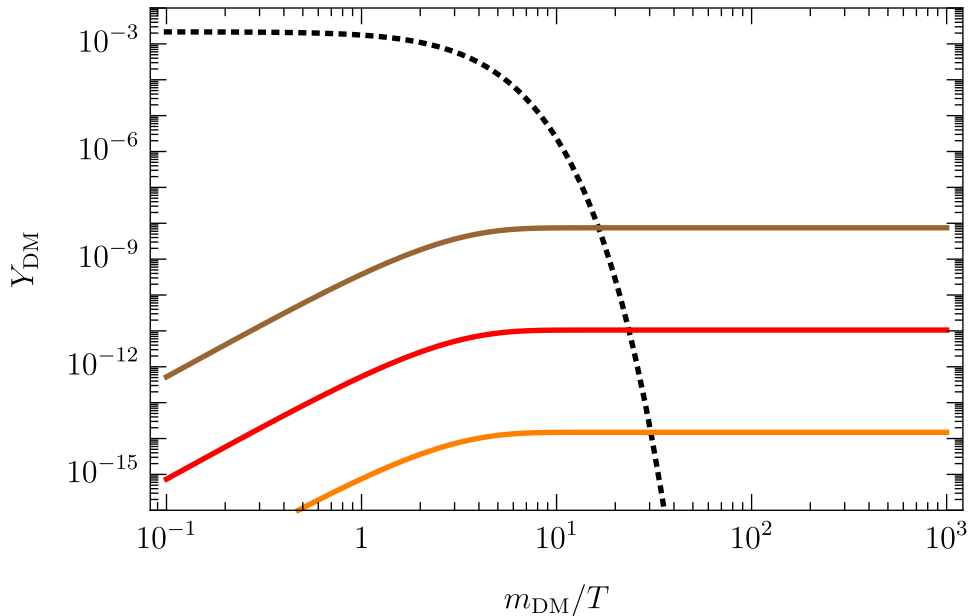


Figure 2.2: *Dark matter freeze-in production. Starting from a vanishing initial dark matter abundance, a relic density is built up gradually until interactions with the thermal bath cannot keep up with the Hubble expansion anymore. Up to this point, the dark matter abundance lies far below its equilibrium value (dotted black line). The continuous lines show the actual dark matter abundance for weaker, moderate and stronger coupling (orange, red and brown lines, respectively).*

derproduced and can only make up a part of the density parameter $\Omega_{\text{DM}} h^2$ [31]. Of course, this simplified overview cannot replace a detailed calculation of the present-day abundance in a given dark matter model, based on the appropriate Boltzmann equations [4]. For example, coannihilation processes can change this abundance drastically [30], as can dark matter self-interactions [32]. In section 6.2, dark matter production through a non-minimal coupling to gravity will be discussed in detail.

2.4 Dark matter stability

One of the most intriguing properties of dark matter is its longevity [34]. According to our current understanding of cosmology, structure formation at early cosmic times is highly sensitive to the presence of a cold dark matter component in the cosmic fluid [5]. At present times, we observe the effects of dark matter on the dynamics of galaxies [8] as well as galaxy clusters [11]. Therefore, if dark matter is mostly made up of one kind of particle, it needs to have a lifetime at least as long as the age of the universe,

$$\tau_{\text{DM}} \gtrsim \tau_{\text{Uni}} \simeq 4 \times 10^{17} \text{ s}. \quad (2.9)$$

From a theory perspective, such a large value hints at some symmetry being in place to protect dark matter against decay [34]. There are examples for this in the visible sector, where only very few particles are comparably stable: the electron is protected against decay by the conservation of electric charge, while the lightest neutrino species owes its stability to Lorentz symmetry.

In the dark sector, in contrast, one usually introduces an appropriate symmetry by hand. A popular choice is a global \mathbb{Z}_2 , under which some (or all) of the dark sector particles are odd, while the visible-sector fields are even,

$$\mathbb{Z}_2: \quad X_{\text{d}} \rightarrow -X_{\text{d}}, \quad X_{\text{vis}} \rightarrow X_{\text{vis}}, \quad (2.10)$$

in analogy to R-parity in supersymmetry. The lightest \mathbb{Z}_2 -odd particle φ is then the dark matter candidate. Its stability follows from the fact that any vertex linear in φ only leads to decays containing heavier particles in the final state. They are therefore forbidden at zero temperature and the dark matter particle is absolutely stable. (In the special case of a minimal dark sector, where the only \mathbb{Z}_2 -odd field is the dark matter candidate itself, no such vertices arise in the first place.) Alternatively, a dark gauge symmetry may be responsible for stabilizing dark matter against decay [41, 42], especially if the dark matter candidate is embedded in an extended hidden sector. In this case, its stability follows analogously to that of the electron. A third possibility exists for very light dark matter candidates, such as the axion [88, 37, 89, 38]. Its low mass, together with its small couplings to visible sector, means that it is stable on cosmological timescales, even without a protecting symmetry in place. As a last option, dark matter might be “accidentally” stable, similarly to the case of the proton within the standard model. If the dark matter field is part of a high-dimensional gauge multiplet [39, 90, 91], standard model gauge symmetries forbid renormalizable interactions leading to dark matter decay. In this case, the particle content and symmetries of the visible sector are indirectly responsible for the long lifetime of the dark matter particle. Analogously, if dark matter resides within a high-dimensional Lorentz representation, there are very limited options for renormalizable interactions with the standard model, leading to a naturally stable dark matter particle [40].

From a phenomenological perspective, a dark matter candidate that is not absolutely stable has a distinct advantage: the fact that it decays opens up new ways of detecting it experimentally, at least in principle [92, 93, 80, 94]. Given the fact that in the standard model, baryon and lepton number are accidental symmetries that might well be broken at higher energies [35, 36], it seems plausible that a global \mathbb{Z}_2 symmetry stabilizing dark matter against decay might likewise be broken by some ultraviolet dynamics. At low energies, this would manifest itself in the presence of \mathbb{Z}_2 -breaking effective operators in the Lagrangian. *A priori*, the scale $\Lambda_{\mathbb{Z}_2}$ at which these interactions become strong is not known. A case can be made, however, for identifying $\Lambda_{\mathbb{Z}_2}$ with the Planck scale: firstly, even if dark matter does not partake in any gauge or Yukawa interactions with the visible sector at all, we know that it interacts gravitationally. Therefore, if new dynamics are to spoil the \mathbb{Z}_2 , $\Lambda_{\mathbb{Z}_2} \simeq \bar{M}_{\text{P}}$ is the most conservative choice. Secondly, quantum gravity is not expected to conserve global symmetries anyway, on very general grounds [43, 44]. Therefore, also conceptually the appearance of \mathbb{Z}_2 -breaking operators at the Planck scale is anticipated [46, 45, 47, 48].

2.5 Dark and visible matter in curved spacetime

Under the assumption that the multitude of observations connected to the dark matter puzzle cannot be explained by unknown dynamics of baryonic matter only, some extension of the standard model of particle physics by a so-called “dark”, or “hidden”, sector will ultimately be necessary. In the spirit of effective field theory (EFT), at any given energy scale, the total action describing gravity, dark and ordinary matter, and their interactions in curved spacetime specified by the metric $g_{\mu\nu}$, will contain a sum of effective Lagrangians

$$\mathcal{S} = \int d^4x \sqrt{-g} (\mathcal{L}_{\text{grav}} + \mathcal{L}_{\text{vis}} + \mathcal{L}_{\text{d}}), \quad (2.11)$$

where $g = \det(g_{\mu\nu})$. Our best description of the gravitational sector is the theory of general relativity [95]. Its field equations follow from the Einstein-Hilbert Lagrangian

$$\mathcal{L}_{\text{grav}} = \mathcal{L}_{\text{EH}} \equiv -\frac{R}{2\kappa^2}, \quad (2.12)$$

with R the Ricci scalar and $\kappa = \bar{M}_{\text{P}}^{-1} = \sqrt{8\pi G} \simeq (2.435 \times 10^{18} \text{ GeV})^{-1}$ the inverse reduced Planck mass. As a contraction of the Riemann tensor, the Ricci scalar can be constructed from the Christoffel symbols,

$$R = g^{\mu\nu} R_{\mu\nu} = g^{\mu\nu} g_{\rho}^{\sigma} R_{\mu\sigma\nu}^{\rho} \quad (2.13)$$

$$= g^{\mu\nu} g_{\rho}^{\sigma} \left(\partial_{\sigma} \Gamma_{\mu\nu}^{\rho} + \Gamma_{\lambda\sigma}^{\rho} \Gamma_{\mu\nu}^{\lambda} - \{\sigma \leftrightarrow \nu\} \right), \quad (2.14)$$

which, in turn, can be computed from the metric,

$$\Gamma_{\mu\nu}^{\rho} = \frac{1}{2} g^{\rho\sigma} \left(\partial_{\mu} g_{\sigma\nu} + \partial_{\nu} g_{\mu\sigma} - \partial_{\sigma} g_{\mu\nu} \right). \quad (2.15)$$

The Lagrangian (2.12) leads to Einstein's field equations relating spacetime curvature in 1+3 dimensions to its matter content [96],

$$R_{\mu\nu} - \frac{1}{2} R g_{\mu\nu} = \kappa^2 T_{\mu\nu}, \quad (2.16)$$

where the energy-momentum tensor $T_{\mu\nu}$ receives contributions from both the dark and the visible sector. Classical general relativity has passed a variety of experimental tests with flying colors [97]. In the Λ CDM framework, there seems to be no need to extend this theory with additional fields or interactions, *i.e.* add more terms to (2.12). (In an alternative approach, there are attempts to dispense with dark matter altogether, trying to accommodate the various observations attributed to it by modifying the gravitational Lagrangian instead [10, 98, 99].)

Concerning the other three known fundamental interactions, at energies around the electroweak scale $\Lambda_{\text{EW}} \simeq v = 246 \text{ GeV}$, the visible sector is accurately described by the standard model of particle physics [1],

$$\mathcal{L}_{\text{vis}}^{(\text{EW})} = \mathcal{L}_{\text{SM}} \equiv \mathcal{T}_F + \mathcal{T}_f + \mathcal{T}_H - \mathcal{V}_H + \mathcal{L}_Y, \quad (2.17)$$

where \mathcal{L}_Y contains the Yukawa interactions, \mathcal{V}_H is the Higgs potential, and \mathcal{T}_i are the kinetic terms of gauge bosons, fermions and scalars,

$$\mathcal{T}_F = \sum_F \left(-\frac{1}{4} g^{\mu\nu} g^{\rho\sigma} F_{\mu\rho}^a F_{\nu\sigma}^a \right), \quad (2.18)$$

$$\mathcal{T}_f = \sum_f \left(\frac{i}{2} \bar{f} \overleftrightarrow{\not{D}} f \right), \quad (2.19)$$

$$\mathcal{T}_H = g^{\mu\nu} (D_{\mu} \Phi)^{\dagger} (D_{\nu} \Phi). \quad (2.20)$$

(The gauge-fixing terms and ghost Lagrangian have been omitted here for clarity, see *e.g.* [100].) In the first line above, the sum runs over the squares of the standard model field-strength tensors $F_{\mu\nu}^a = G_{\mu\nu}^a, W_{\mu\nu}^a, B_{\mu\nu}$, corresponding to the gauge group $\text{SU}(3)_c \times \text{SU}(2)_L \times \text{U}(1)_Y$, which are defined in terms of the gauge fields F_{μ}^a as

$$G_{\mu\nu}^a = \partial_{\mu} G_{\nu}^a - \partial_{\nu} G_{\mu}^a + g_s f^{abc} G_{\mu}^b G_{\nu}^c, \quad (2.21)$$

$$W_{\mu\nu}^a = \partial_{\mu} W_{\nu}^a - \partial_{\nu} W_{\mu}^a + g \epsilon^{abc} W_{\mu}^b W_{\nu}^c, \quad (2.22)$$

$$B_{\mu\nu} = \partial_{\mu} B_{\nu}^a - \partial_{\nu} B_{\mu}^a. \quad (2.23)$$

Here, f^{abc} and ϵ^{abc} are the $SU(3)_c$ and $SU(2)_L$ group structure constants, respectively, and g_s, g the gauge couplings. In (2.19), the sum is performed over all standard model fermion species f — lefthanded quark and lepton doublets Q_L and ℓ_L , and righthanded up- and down-type quarks u_R, d_R and leptons e_R . Summation over all three particle generations is implied. The antisymmetrized derivative is

$$A \overleftrightarrow{\nabla} B = A(\nabla B) - (\nabla A) B, \quad (2.24)$$

and the slashed derivative operator is defined as

$$\overline{\nabla} = \gamma^a e_a^\mu \nabla_\mu, \quad (2.25)$$

with γ^a a Dirac gamma matrix, e_a^μ a vierbein and $\nabla_\mu f = (D_\mu - \frac{i}{4} e_\nu^b (\partial_\mu e^{\nu c}) \sigma_{bc}) f$. Here, D_μ is the gauge-covariant derivative and $\sigma_{bc} = \frac{i}{2} [\gamma_b, \gamma_c]$ are the generators of Lorentz transformations in the spinor representation. The gauge covariant derivative for a lefthanded Quark doublet reads

$$D_\mu Q_L = \left(\partial_\mu - i g_s G_\mu^a T^a - i g W_\mu^i \frac{\sigma^i}{2} - i g' Y B_\mu \right) Q_L, \quad (2.26)$$

with T^a , $(\sigma^i/2)$ and Y the group generators of $SU(3)_c$, $SU(2)_L$ and $U(1)_Y$, respectively, and g' the $U(1)_Y$ gauge coupling. Gauge covariant derivatives of the other fermion fields contain the terms corresponding to their gauge charges, which are given in table 2.1. The scalar kinetic

	$SU(3)_c$	$SU(2)_L$	$U(1)_Y$
Q_L	3	2	1/6
ℓ_L	1	2	-1/2
u_R	3	1	2/3
d_R	3	1	-1/3
e_R	1	1	-1
Φ	1	2	1/2

Table 2.1: Standard model matter content with corresponding gauge charges.

term (2.20) contains the standard model ‘‘Higgs’’ $SU(2)_L$ doublet

$$\Phi = \begin{pmatrix} \varphi_3 + i \varphi_4 \\ \varphi_1 + i \varphi_2 \end{pmatrix} \quad (2.27)$$

with four real degrees of freedom. Its gauge covariant derivative contains minimal coupling with the $SU(2)_L$ and $U(1)_Y$ gauge bosons, according to table 2.1. The scalar potential is

$$\mathcal{V}_H = -\mu^2 \Phi^\dagger \Phi + \lambda (\Phi^\dagger \Phi)^2, \quad (2.28)$$

with $\mu^2 > 0$. The electroweak gauge group is broken to the electromagnetic $U(1)_{em}$, and three of the four gauge bosons acquire mass [101, 102, 103]. In the unitary gauge, the Higgs doublet is

$$\Phi = \frac{1}{\sqrt{2}} \begin{pmatrix} 0 \\ v + H \end{pmatrix}, \quad (2.29)$$

with $v = \mu/\sqrt{\lambda} = 246$ GeV its vacuum expectation value and H the physical Higgs field. The massive charged W bosons are $W_\mu^\pm = (W_\mu^1 \mp iW_\mu^2)/\sqrt{2}$, and the mass eigenstates of the electrically neutral components of the $SU(2)_L$ and $U(1)_Y$ gauge bosons are given by the linear combination

$$\begin{pmatrix} Z_\mu \\ A_\mu \end{pmatrix} = \begin{pmatrix} \cos \theta_W & -\sin \theta_W \\ \sin \theta_W & \cos \theta_W \end{pmatrix} \begin{pmatrix} W_\mu^3 \\ B_\mu \end{pmatrix} \quad (2.30)$$

with θ_W the Weinberg angle. The Yukawa term \mathcal{L}_Y , finally, couples the standard model fermions to the Higgs doublet,

$$\mathcal{L}_Y = -Y_{ij}^{(e)} \bar{\ell}_{L,i} \Phi e_{R,j} - Y_{ij}^{(d)} \bar{Q}'_{L,i} \Phi d'_{R,j} - Y_{ij}^{(u)} \bar{Q}'_{L,i} \tilde{\Phi} u'_{R,j} + \text{h.c.}, \quad (2.31)$$

where i, j run over the three standard model fermion generations, while $SU(2)_L$ indices are suppressed in this notation. $Y^{(f)}$ are the Yukawa matrices, ℓ_L (e_R) the lefthanded (righthanded) lepton $SU(2)_L$ doublets (singlets). The lefthanded (righthanded) quark fields Q'_L (d'_R, u'_R) are given in the interaction basis. They are related to the mass eigenstates by unitary transformations

$$q'_{R,i} = U_{R,ij}^{(q)} q_{R,j}. \quad (2.32)$$

In the coupling to up-type quarks u'_R , the Higgs field appears in the combination

$$\tilde{\Phi} = i\sigma^2 \Phi^*, \quad (2.33)$$

with σ^2 the second Pauli spin matrix. In the unitary gauge, the Yukawa Lagrangian is simply

$$\mathcal{L}_Y = -\left(\bar{u}_i M_{ij}^{(u)} u_j + \bar{d}_i M_{ij}^{(d)} d_j + \bar{e}_i M_{ij}^{(e)} e_j\right) \left(1 + \frac{H}{v}\right), \quad (2.34)$$

with diagonal mass matrices

$$M^{(u)} = \text{diag}(m_u, m_c, m_t), \quad M^{(d)} = \text{diag}(m_d, m_s, m_b), \quad M^{(e)} = \text{diag}(m_e, m_\mu, m_\tau). \quad (2.35)$$

A consistent set of Feynman rules for the standard model can be found, for example, in [100].

At lower energies, heavy particles such as the heavier fermions and electroweak gauge bosons can be integrated out. For the purpose of this thesis, below energies of around 700 MeV, the visible sector is well described by an effective Lagrangian containing light leptons, photons, neutrinos, and pions, the lightest degrees of freedom of the hadronic spectrum. Kaons cannot be pair-produced at these energies; therefore, $SU(2)$ chiral perturbation theory is sufficient for the purpose of describing dark matter decay in this regime. The visible-sector effective Lagrangian is

$$\mathcal{L}_{\text{vis}}^{(\text{IR})} = \mathcal{L}_\pi + \mathcal{T}_F + \mathcal{T}_f + \mathcal{L}_{m_f}. \quad (2.36)$$

Here, \mathcal{T}_F and \mathcal{T}_f are defined analogously to the standard model case. However, the gauge kinetic term now only contains the photon field, since the weak gauge bosons have been integrated out and the strong interaction is in its confinement regime, while the sum over fermion species includes only neutrinos, electrons and muons. The pion Lagrangian is given by the leading terms of chiral perturbation theory [104],

$$\mathcal{L}_\pi = \frac{f_\pi^2}{4} g^{\mu\nu} \text{Tr}[(D_\mu U)^\dagger (D_\nu U)] + \frac{f_\pi^2 m_\pi^2}{2} \text{Tr}[U^\dagger + U], \quad (2.37)$$

where $f_\pi = 93$ MeV is the pion decay constant. The matrix U is constructed from the pion fields π^a ,

$$U = \exp(i \sigma^a \pi^a / f_\pi), \quad (2.38)$$

with $a = 1, 2, 3$, and σ^a the Pauli spin matrices. Its covariant derivative is

$$D_\mu U = \partial_\mu U + i e A_\mu [Q, U], \quad (2.39)$$

where $Q = \text{diag}(2/3, -1/3, -1/3)$ and A_μ is the photon field. Likewise, the gauge covariant derivative in the fermion kinetic term

$$\mathcal{T}_f = \sum_{f=e,\mu,\{\nu_j\}} \left(\frac{i}{2} \bar{f} \overleftrightarrow{\nabla} f \right) \quad (2.40)$$

now only involves the electromagnetic coupling. The fermion mass term

$$\mathcal{L}_{m_f} = - \sum_{f=e,\mu} m_f \bar{f} f, \quad (2.41)$$

finally, is a remnant of the standard model Higgs mechanism at low energies.

In analogy to the visible matter, the dark sector is expected to be described by some effective Lagrangian \mathcal{L}_d that can in principle contain multiple new fields and interactions, as well as couplings to the visible sector. A special case of this general framework is the minimal scenario, where the dark matter particle is the only additional degree of freedom with regards to the standard model. Another is the “next-to-minimal” case introducing a dark matter candidate as well as a mediator linking the dark and the hidden sector via interactions. Scenarios of the latter kind are commonly referred to as simplified models [105]. These kind of models were originally designed in the context of collider searches for new physics [106]. Their analysis provides a middle ground between comprehensive, yet highly model-dependent studies of specific ultraviolet (UV)-complete models [107], and more universal investigations of effective theories [108] (that may, however, be limited in their applicability to high-energy collider experiments [109]). In such simplified models, the mediator can be charged under the standard model gauge group, since on general grounds, non-gravitational interactions between the two sectors cannot be ruled out. Indeed, in the popular WIMP scenario, such a coupling is explicitly needed to bring the dark matter into thermal contact with the visible sector bath in the early Universe (*cf.* section 2.3), and a multitude of direct detection, indirect detection and collider experiments around the world are actively trying to find evidence for it [6], as outlined in section 2.1. The precise form of this coupling, however, is highly model-dependent, and in a worst-case scenario for astroparticle physics, the dark matter candidate could be decoupled from the visible sector except through gravity. Regardless of the specific makeup of an extended dark sector, however, one can typically still identify one particle which accounts for most (or all) of the measured present-day dark matter abundance, with additional degrees of freedom being subdominant. (This expectation somewhat mirrors the situation in the visible sector: baryonic matter is mostly hydrogen [4].) Analyses of models with multi-component dark matter [110, 111] can be found in the literature, but are not subject of this work.

Chapter 3

Theories with non-minimal coupling to gravity

In the conventional, minimal coupling scenario, the leading gravitational interactions take the form of graviton exchange between particles. These can be described in the linearized gravity approach $g_{\mu\nu} = \bar{g}_{\mu\nu} + 2\kappa h_{\mu\nu}$, where the metric tensor is expanded around a classical background [96]. The leading interaction between the graviton field $h_{\mu\nu}$ and any type of matter takes the form [112]

$$\mathcal{L}_{\text{int},h}^{(1)} = -\kappa h_{\mu\nu} T_{\text{m}}^{\mu\nu}, \quad (3.1)$$

i.e. the graviton couples to matter through its energy-momentum tensor $T_{\text{m}}^{\mu\nu}$. This type of coupling does not spoil dark matter stability: since the energy-momentum tensor is derived from the matter Lagrangian $\mathcal{L}_{\text{d}} + \mathcal{L}_{\text{vis}}$, any stabilizing symmetry present in non-gravitational interactions remains intact.

The aim of this thesis is to discuss instead the effect of non-minimal gravitational interactions on dark matter stability, based on the investigations published as [50, 51, 52], extending the discussion in [49]. As discussed in section 2.4, astronomical observations require the dark matter particle to be very long-lived, but not necessarily absolutely stable. If dark matter decay is induced by some unknown dynamics at very large energies, one expects to be able to encode these dynamics through effective operators at low energies. As the dark matter lifetime seems to be very large, the suppression scale of these effective operators should be correspondingly high. In fact, it might lie at the Planck scale, hinting at a gravitational origin of dark matter decay [45, 46, 47, 48, 113, 114, 115]. In other words, the exceptional longevity, but not absolute stability, of the dark matter particle could be due to the minute, yet non-vanishing, strength of gravitational interactions. This requires the global symmetry that is responsible for dark matter stability in the absence of gravity to be explicitly broken by non-minimal gravitational interactions. For the remainder of this thesis, this symmetry is assumed to be a \mathbb{Z}_2 for concreteness. In the Lagrangian formalism, the first three terms of

$$\mathcal{S} = \int d^4x \sqrt{-g} (\mathcal{L}_{\text{grav}} + \mathcal{L}_{\text{vis}} + \mathcal{L}_{\text{d}} + \mathcal{L}_{\xi}) \quad (3.2)$$

conserve this global \mathbb{Z}_2 symmetry stabilizing dark matter, while the last term \mathcal{L}_{ξ} explicitly breaks it. Concerning the origin of this symmetry breaking, this thesis will take an agnostic position. In the spirit of effective field theory, given a set of fields and symmetries, together with a cutoff scale for the theory, the leading effects of the unknown short-distance physics

can be encapsulated in effective operators. Therefore, even without a UV-complete theory of quantum gravity, one can examine its impact on dark matter stability under the assumption that it violates the stabilizing global symmetry.

Dark matter decay through Planck mass-suppressed effective operators has been discussed in the literature [45, 47, 48, 113, 114, 115, 116]. For a scalar dark matter candidate S , \mathbb{Z}_2 -breaking effective interactions with visible-sector particles can be found already at mass dimension five, *e.g.*

$$\frac{S}{M_{\text{P}}} F^{\mu\nu} F_{\mu\nu}, \quad \frac{S}{M_{\text{P}}} \bar{\ell}_{\text{L}} \Phi e_{\text{R}}, \quad \frac{S}{M_{\text{P}}} (\Phi^\dagger \Phi)^2. \quad (3.3)$$

Generally speaking, any gauge invariant dimension-four operator $\mathcal{O}_{\text{vis}}^{(4)}$ can be coupled to the dark matter field in this way, if S is a gauge singlet itself. The Wilson coefficients of these operators, however, are in principle uncorrelated, and can only be constrained independently from each other. In the present work, in contrast, dark matter decay is assumed to arise from a non-minimal coupling between the dark matter field and gravity itself. As will be shown below, this still leads to effective operators like the ones above, inducing decay into standard model particles. However, as they all arise from a single operator in the Jordan frame formulation of the theory, their Wilson coefficients are correlated. This way, the number of free parameters is greatly reduced, and the framework gains in predictivity.

3.1 Non-minimal coupling to gravity

Concretely, the subject under discussion are operators of the form

$$\mathcal{L}_\xi = -\xi R_{\mu\nu} f^{\mu\nu}(\{X_{\text{d}}\}, \{X_{\text{vis}}\}), \quad (3.4)$$

coupling the Ricci curvature tensor $R_{\mu\nu}$ to a tensorial, \mathbb{Z}_2 -breaking, function $f^{\mu\nu}$ of dark and visible sector fields $X_{\text{d}}, X_{\text{vis}}$ with coupling strength ξ . In general, many such gauge- and Lorentz-invariant effective operators exist. (Of course, also \mathbb{Z}_2 -conserving non-minimal gravitational interactions may appear; these are, however, irrelevant for dark matter decay.) As for all effective theories, the dominant effects are encoded in the lowest-dimensional of these operators. Thus, for a given combination of dark matter and mediator fields, dark matter stability will in general be controlled by only one or two terms in the Lagrangian. The precise form of these leading operators depends on the spin and gauge charges of the fields involved. From a systematic standpoint, the following general statements can be made:

- On dimensional grounds, renormalizable non-minimal interactions are only possible for scalar fields S_k , in the form of couplings to the trace of the Ricci tensor,

$$\mathcal{L}_\xi^{(d=4)} = -R \sum_{i,j} (\xi_{S,i} M_S S_i + \xi_{S,ij} S_i S_j), \quad (3.5)$$

with M_S a mass scale and $\xi_{S,i}$ and $\xi_{S,ij}$ dimensionless couplings. Due to symmetry, the combination $(S_i S_j)$ has to be a CP -even, \mathbb{Z}_2 -odd gauge singlet. The first $(\xi_{S,i})$ type of scalar operator is allowed if the scalar field S_i is a CP -even, \mathbb{Z}_2 -odd singlet itself and will be discussed in section 4.1. In other words, a dimension-four non-minimal coupling to the Ricci tensor is only possible for a gauge singlet scalar, or if there exist at least two scalar fields with identical gauge quantum numbers.

- Since the standard model contains only one scalar field, the only renormalizable non-minimal operator connecting the dark and visible sector directly is the cross-coupling between the Higgs field and a second $SU(2)_L$ doublet,

$$-\xi_{\Phi\eta} R \left(\Phi^\dagger \eta + \eta^\dagger \Phi \right), \quad (3.6)$$

where, analogously to the Higgs field,

$$\eta = \left(\begin{array}{c} \eta^+ \\ \frac{1}{\sqrt{2}} (\eta^0 + i A^0) \end{array} \right). \quad (3.7)$$

In the presence of an additional global \mathbb{Z}_2 symmetry that precludes Yukawa interactions of this second doublet, this scenario is a straightforward extension of the “inert” doublet model, and is the subject of section 4.2. (For details on its non-gravitational phenomenology see *e.g.* [117, 118].)

- Fermions cannot be coupled to the Ricci curvature at dimension four or less. The leading non-renormalizable non-minimal effective operator

$$-\frac{R}{M_f} \xi_{f,ij} (\bar{f}_i f_j + \bar{f}_j f_i) \quad (3.8)$$

can, however, be generated through a scalar mediator S of mass m_S with a dimension-three non-minimal coupling to gravity ($\xi_S M_S S R$) and a Yukawa interaction ($y_{ij} S \bar{f}_i f_j$) with the fermions. In the limit where the scalar is much heavier than the fermions, the couplings and mass scales are related via $\xi_{f,ij}/M_f \simeq (-y_{ij} \xi_S M_S)/m_S^2$.

- At dimension six, one additionally finds

$$-\frac{R}{M_f^2} \xi_{Sf,ij} (\bar{f}_i S f_j + \bar{f}_j S^* f_i), \quad (3.9)$$

with S a scalar field. As the dimension-five operator (3.8), this term can be generated through an additional intermediate scalar field. Details on this scenario will be presented in section 4.3.

- Gauge bosons can only appear in the Lagrangian through their field-strength tensors or in gauge covariant derivatives of other particles. Schematically, the lowest-dimensional operators involving the field-strength tensors are

$$-R \xi_{V,ij}^{(1)} V_i^{\mu\nu} V_{j\mu\nu}, \quad -R_{\mu\nu} \xi_{V,ij}^{(2)} V_i^\mu{}_\rho V_j^{\rho\nu}, \quad -R^\rho{}_{\sigma\mu\nu} \xi_{V,ij}^{(3)} V_{i\rho}{}^\sigma V_j^{\mu\nu}, \quad (3.10)$$

which, at first sight, only differ in their Lorentz structure. The standard model contains one abelian gauge field B^μ . Therefore, the minimal setup of adding only one field to the standard model corresponds to $i = 1, 2$, with $V_1^{\mu\nu}$ the dark matter candidate field-strength tensor and $V_2^{\mu\nu} = B^{\mu\nu}$ [119]. While interesting from a phenomenological perspective, these types of interactions cannot be generated via renormalizable scalar interactions at higher energies, in contrast to the fermion scenario. They are thus less motivated in the sense of a possible ultraviolet completion of the effective theory. In the simplest scenarios, attempting to generate the first, kinetic mixing-type coupling via intermediate scalars or fermions introduces an identical interaction in flat spacetime, *i.e.*, without the coupling to the Ricci scalar. Decays mediated by this flat-spacetime kinetic mixing operator $\epsilon_{ij} V_i^{\mu\nu} V_{j\mu\nu}$

will always dominate over the Planck-mass suppressed ones from non-minimal coupling to gravity. Moreover, the second and third operator involve the Ricci and Riemann tensors, respectively. These Lorentz structures cannot be generated via intermediate scalar fields, since up to dimension four, these can only couple to the Ricci scalar.

- In the presence of an additional fermion f charged under the dark gauge symmetry, one also finds non-minimal operators of the form

$$-R \xi_{V_i}^{(1)} \bar{f} \overleftrightarrow{D}_i f, \quad -R_{\mu\nu} \xi_{V_i}^{(2)} \bar{f} \left(\gamma^\mu \overleftrightarrow{D}_i + \gamma^\nu \overleftrightarrow{D}_i^\mu \right) f, \quad (3.11)$$

where $D_i^\mu f = (\nabla^\mu + i g_i V_i^\mu) f$. These operators are of mass dimension six. In contrast to the ones in (3.10), however, they require the presence of the additional fermion field f in the hidden sector. In this case, and as long as $m_{V_i} > 2 m_f$, also non-gravitational decays of the vector V_i are possible through the f kinetic term. In that case, due to their inherent Planck-mass suppression, decays arising from the non-minimal terms of (3.11) are of less phenomenological significance.

Classically, the Ricci tensor is a measure of spacetime curvature. Therefore, naively one would expect a non-minimal coupling proportional to this quantity to describe an interaction that is sensitive to the amount of curvature at the interaction region, and vanishes in the flat-space limit. In reality, the situation is more subtle. In the linearized gravity expansion, the Riemann tensor and its contractions take the form of infinite sums over effective operators containing increasing powers of the graviton field, with two derivatives each, *e.g.*

$$R = \kappa (2 \partial^\mu \partial^\nu h_{\mu\nu} - 2 \partial^2 h) + \mathcal{O}(\kappa^2 \partial^2 h^2). \quad (3.12)$$

Therefore, operators of the form (3.4) seem to introduce a number of vertices connecting a specific combination of matter quantum fields with gravitons. This would constitute a breakdown of the weak equivalence principle, as the matter fields in question would couple differently to gravity than fields that couple only minimally. This can easiest be seen for the simplest scenario of a single scalar singlet field ϕ with a linear coupling to the Ricci scalar,

$$-\xi R M \phi. \quad (3.13)$$

Inserting (3.12) into (3.13), it is evident that the lowest-dimensional operator induced by this term is actually a dimension-four kinetic mixing term between the scalar singlet and the graviton field. Thus, to diagonalize the quadratic Lagrangian and to ensure the validity of the weak equivalence principle, a field transformation has to be performed on both the matter fields and the metric tensor, resulting in a theory with particle interactions that are independent of classical spacetime curvature.

3.2 Weyl transformation

Widely studied in the literature on extended theories of gravity and non-minimally coupled matter fields [99], such a field redefinition of the metric tensor goes by the name of Weyl transformation. If the non-minimal operator (3.4) is proportional to the Ricci scalar, *i.e.*, if the coupling function $f^{\mu\nu}$ is proportional to the metric tensor $g^{\mu\nu}$, this transformation can be performed simultaneously to all orders in ξ . For illustration, consider a theory with a non-minimally

coupled dark matter candidate φ in the so-called Jordan frame formulation with metric $g_{\mu\nu}$,

$$\mathcal{S} = \int d^4x \sqrt{-g} \left(-\frac{R}{2\kappa^2} - \xi R f(\varphi) + \mathcal{L}_\varphi(g_{\mu\nu}) + \mathcal{L}_{\text{vis}}(g_{\mu\nu}) \right) \quad (3.14)$$

$$= \int d^4x \sqrt{-g} \left(-\frac{R}{2\kappa^2} \Omega^2(\varphi) + \mathcal{L}_\varphi(g_{\mu\nu}) + \mathcal{L}_{\text{vis}}(g_{\mu\nu}) \right), \quad (3.15)$$

where any dependence of f on other dark or visible sector fields has been suppressed in the notation. In the last line, the Einstein-Hilbert action and the non-minimal coupling have been combined into the Weyl factor

$$\Omega^2(\varphi) = 1 + 2\kappa^2 \xi f(\varphi). \quad (3.16)$$

If one now performs a Weyl transformation $g_{\mu\nu} \rightarrow \hat{g}_{\mu\nu}$, where

$$\hat{g}_{\mu\nu} = \Omega^2(\varphi) g_{\mu\nu}, \quad (3.17)$$

the geometric quantities $\sqrt{-g}$ and R transform as

$$\sqrt{-\hat{g}} = \Omega^4 \sqrt{-g}, \quad \hat{R} = \Omega^{-2} R - 6\Omega^{-3} \hat{g}^{\mu\nu} \hat{\nabla}_\mu \hat{\nabla}_\nu \Omega, \quad (3.18)$$

and yield the Einstein frame action

$$\mathcal{S} = \int d^4x \sqrt{-\hat{g}} \left(-\frac{\hat{R}}{2\kappa^2} + \frac{3}{\kappa^2} \hat{g}^{\mu\nu} \frac{\hat{\nabla}_\mu \Omega \hat{\nabla}_\nu \Omega}{\Omega^2} + \Omega^{-4} \mathcal{L}_\varphi(\Omega^{-2} \hat{g}_{\mu\nu}) + \Omega^{-4} \mathcal{L}_{\text{vis}}(\Omega^{-2} \hat{g}_{\mu\nu}) \right) \quad (3.19)$$

$$= \int d^4x \sqrt{-\hat{g}} \left(-\frac{\hat{R}}{2\kappa^2} + \frac{3}{\kappa^2} \hat{g}^{\mu\nu} \frac{\hat{\nabla}_\mu \Omega \hat{\nabla}_\nu \Omega}{\Omega^2} + \hat{\mathcal{L}}_\varphi(\hat{g}_{\mu\nu}) + \hat{\mathcal{L}}_{\text{vis}}(\hat{g}_{\mu\nu}) \right). \quad (3.20)$$

The non-minimal coupling to gravity vanishes when formulating the theory in the Einstein frame: the Einstein-Hilbert term appears in isolation again, and the Einstein-frame graviton field $\hat{h}_{\mu\nu}$, defined as the quantum excitation of the metric $\hat{g}_{\mu\nu}$, couples minimally to all particle species, in accordance with the equivalence principle. On the other hand, there are two changes to the matter Lagrangian: for the fields contained in f , the second term in (3.19) may modify their kinetic terms and introduce derivative couplings between them. Additionally, the matter Lagrangian now has to be expressed in terms of the Einstein frame metric tensor, which explicitly depends on the dark matter field φ through the Weyl factor $\Omega^2(\varphi)$. If the visible sector is described by the standard model Lagrangian (2.17), for example, then

$$\hat{\mathcal{L}}_{\text{vis}}^{(\text{EW})} = \hat{\mathcal{T}}_F + \frac{1}{\Omega^3} \hat{\mathcal{T}}_f + \frac{1}{\Omega^2} \hat{\mathcal{T}}_H + \frac{1}{\Omega^4} (\mathcal{L}_Y - \mathcal{V}_H), \quad (3.21)$$

where the different powers of the prefactor arise due to the different Lorentz structures of the individual terms. The Yukawa interactions and Higgs potential do not depend on the metric tensor at all, so $\hat{\mathcal{L}}_Y = \mathcal{L}_Y$ and $\hat{\mathcal{V}}_H = \mathcal{V}_H$. The dark sector Lagrangian transforms correspondingly, as would a different visible sector Lagrangian, *e.g.* an effective Lagrangian for lower energies, such as (2.36). Expanding, as the final step, the Weyl factor Ω around unity,

$$\Omega^n \simeq 1 + n\kappa^2 \xi f(\varphi) + \mathcal{O}(\kappa^4 \xi^2 f^2(\varphi)), \quad (3.22)$$

i.e. treating the contribution from the non-minimal coupling as a small perturbation, one can explicitly read off point interactions between the dark matter field and the standard model degrees of freedom,

$$\widehat{\mathcal{L}}_{\text{int},\xi}^{(1)} = -2\kappa^2 \xi \left. \frac{\partial f}{\partial \varphi} \right|_{\varphi=0} \varphi \left(\frac{3}{2} \widehat{\mathcal{T}}_f + \widehat{\mathcal{T}}_H + 2(\mathcal{L}_Y - \mathcal{V}_H) \right). \quad (3.23)$$

As evident already in (3.21), a tree-level coupling to the kinetic term of gauge bosons is absent, due to its Lorentz structure.

On the other hand, if the non-minimal coupling is only proportional to the Ricci tensor rather than scalar, as for the $\xi^{(2)}$ -coupling of a vector field in (3.10), the Weyl transformation can only be performed order-by-order in ξ . In this case, the Jordan-frame action reads

$$\mathcal{S} = \int d^4x \sqrt{-g} \left(-\frac{R}{2\kappa^2} - \xi R_{\mu\nu} f^{\mu\nu}(\varphi) + \mathcal{L}_\varphi(g_{\mu\nu}) + \mathcal{L}_{\text{vis}}(g_{\mu\nu}) \right). \quad (3.24)$$

To “transform away” the non-minimal coupling to the Ricci tensor, what is needed is a transformation of the (inverse) metric tensor $g^{\mu\nu} \rightarrow \widehat{g}^{\mu\nu}$ that can be expressed as a power series in the parameter ξ ,

$$\widehat{g}^{\mu\nu} = g^{\mu\nu} + \xi \delta g^{\mu\nu} + \mathcal{O}(\xi^2). \quad (3.25)$$

Under this change of metric, the action transforms as $\mathcal{S} \rightarrow \mathcal{S} + \delta\mathcal{S}$, where

$$\delta\mathcal{S} = \int d^4x \left(-\frac{1}{2\kappa^2} \xi \frac{\delta(\sqrt{-g} R)}{\delta g^{\mu\nu}} - \xi^2 \frac{\delta(\sqrt{-g} R_{\rho\sigma} f^{\rho\sigma}(\varphi))}{\delta g^{\mu\nu}} + \xi \frac{\delta(\sqrt{-g} (\mathcal{L}_\varphi + \mathcal{L}_{\text{vis}}))}{\delta g^{\mu\nu}} \right) \delta g^{\mu\nu}. \quad (3.26)$$

The second term is of order ξ^2 and can be omitted, while the first, gravitational, term reads

$$\delta\mathcal{S}_{\text{grav}} = \int d^4x \sqrt{-g} \left(-\frac{1}{2\kappa^2} \right) \xi \left(R_{\mu\nu} - \frac{1}{2} R g_{\mu\nu} \right) \delta g^{\mu\nu} + \mathcal{O}(\xi^2). \quad (3.27)$$

By definition, in the Einstein frame the gravitational sector is minimal and takes the Einstein-Hilbert form. Therefore, the change in the gravitational action has to cancel the non-minimal operator,

$$\delta\mathcal{S}_{\text{grav}} \stackrel{!}{=} \int d^4x \sqrt{-g} \xi R_{\mu\nu} f^{\mu\nu}(\varphi), \quad (3.28)$$

which yields a tensor equation for $\delta g^{\mu\nu}$,

$$\left(R_{\mu\nu} - \frac{1}{2} R g_{\mu\nu} \right) \delta g^{\mu\nu} = -2\kappa^2 R_{\mu\nu} f^{\mu\nu}(\varphi). \quad (3.29)$$

With the ansatz $\delta g^{\mu\nu} = c_1 (f^{\rho\sigma} g_{\rho\sigma}) g^{\mu\nu} + c_2 f^{\mu\nu}$, one finds $c_2 = -2\kappa^2$, $c_1 = \kappa^2$ as a solution, so to first order in ξ , the infinitesimal Weyl transformation into the Einstein frame is given by

$$\delta g^{\mu\nu} = \kappa^2 \left((g_{\rho\sigma} f^{\rho\sigma}(\varphi)) g^{\mu\nu} - 2 f^{\mu\nu}(\varphi) \right). \quad (3.30)$$

Carrying out the transformation of the matter part of the action, one can directly read off the interaction vertices to order ξ ,

$$\sqrt{-\widehat{g}} \widehat{\mathcal{L}}_{\text{int},\xi}^{(1)} = \xi \frac{\delta(\sqrt{-g} (\mathcal{L}_\varphi + \mathcal{L}_{\text{vis}}))}{\delta g^{\mu\nu}} \delta g^{\mu\nu}. \quad (3.31)$$

It is worth noting that

$$\frac{-2}{\sqrt{-g}} \frac{\delta(\sqrt{-g} \mathcal{L}_{\text{vis}})}{\delta g^{\mu\nu}} = T_{\mu\nu}^{(\text{vis})}, \quad (3.32)$$

so

$$\widehat{\mathcal{L}}_{\text{int},\xi}^{(1)} = -\frac{1}{2} \xi T_{\mu\nu}^{(\text{vis})} (\kappa^2 (g_{\rho\sigma} f^{\rho\sigma}(\varphi)) g^{\mu\nu} - 2 \kappa^2 f^{\mu\nu}(\varphi)), \quad (3.33)$$

i.e. the dark matter candidate couples to the energy-momentum tensor of the visible sector fields, just like the graviton. Of course, for a non-minimal coupling proportional to the Ricci scalar, $f^{\mu\nu}(\varphi) = g^{\mu\nu} f(\varphi)$, the expression (3.33) reduces to the previous result (3.23). Here, $\delta g^{\mu\nu} = 2 \kappa^2 f(\varphi) g^{\mu\nu}$, and the dark matter couples to the trace of the visible sector energy-momentum tensor.

Finally, for non-minimal operators proportional to the Riemann tensor, such as the $\xi^{(3)}$ -coupling in the vector scenario (3.10), one cannot perform a Weyl transformation into the Einstein frame at all. Under a change of metric, the gravitational action always transforms as (3.27). Therefore, one cannot cancel a non-minimal coupling proportional to the (uncontracted) Riemann tensor through a Weyl transformation as in (3.28).

To summarize, in the Jordan frame formulation, the non-minimal coupling to gravity is explicit. If one identified the metric fluctuations $h_{\mu\nu}$ with physical gravitons, this construction would introduce a violation of the weak equivalence principle. Furthermore, $h_{\mu\nu}$ does not have a canonical kinetic term for a massless spin-2 particle. In contrast, this thesis is concerned with the Weyl-transformed theory that identifies the Einstein frame metric excitation $\widehat{h}_{\mu\nu}$ with the physical graviton field. In the Einstein frame, gravity couples minimally to all particle species and the graviton kinetic term has its canonical form. The non-minimal coupling instead leads to universal interactions between the non-minimally coupled fields and the remaining matter content of the theory. At the Lagrangian level, these interactions proceed through the energy-momentum tensor of the fields in question. This framework can be seen as a special case of a more general effective theory for dark matter interactions: since all couplings between the dark and visible sector arise from a single term in the Jordan frame action, the Wilson coefficients of vertices involving different visible sector particles are all correlated. The dark matter candidate couples with universal strength to all forms of matter via their energy-momentum tensor, and it does so independently of classical spacetime curvature.

3.3 Modification of the electroweak vacuum

Apart from its implications for dark matter stability, the presence of a non-minimal coupling to gravity in the Lagrangian has a number of other phenomenological consequences. Perhaps the most obvious change compared to a minimally coupled theory is a modification of the scalar potential, best visible after performing the Weyl transformation into the Einstein frame. Considering as an example a scalar singlet dark matter candidate ϕ together with the standard model (the scenario discussed in section 4.1), one starts with the Jordan-frame potential

$$\mathcal{V}(\phi, \Phi) = \mathcal{V}_H(\Phi) + \mathcal{V}_\phi(\phi) \quad (3.34)$$

$$= -\mu^2 \Phi^\dagger \Phi + \lambda (\Phi^\dagger \Phi)^2 + \frac{\mu_\phi^2}{2} \phi^2 + \frac{\lambda_\phi}{4} \phi^4 + \frac{\lambda_{H\phi}}{2} \phi^2 \Phi^\dagger \Phi. \quad (3.35)$$

Parametrizing the Higgs field as

$$\Phi = \frac{1}{\sqrt{2}} \begin{pmatrix} 0 \\ \varphi \end{pmatrix}, \quad (3.36)$$

one obtains

$$\mathcal{V}(\phi, \varphi) = -\frac{\mu^2}{2}\varphi^2 + \frac{\lambda}{4}\varphi^4 + \frac{\mu_\phi^2}{2}\phi^2 + \frac{\lambda_\phi}{4}\phi^4 + \frac{\lambda_{H\phi}}{4}\phi^2\varphi^2, \quad (3.37)$$

in terms of the physical Higgs and dark matter fields φ and ϕ in the Jordan frame. After the Weyl transformation, the Einstein frame potential reads

$$\widehat{\mathcal{V}}(\phi, \varphi) = \Omega^{-4}(\phi)\mathcal{V}(\phi, \varphi). \quad (3.38)$$

Thus, in principle there can be a shift away from the standard model ground state. Indeed, minimizing this potential yields

$$\langle \varphi \rangle = v - (\xi M \kappa)^2 (\kappa v)^2 \lambda \lambda_{H\phi} \frac{v^4}{\left(2\mu_\phi^2 + \lambda_{H\phi} v^2\right)^2} v + \mathcal{O}\left((\xi M \kappa)^3\right), \quad (3.39)$$

$$\langle \phi \rangle = -(\xi M \kappa) (\kappa v) \lambda \frac{2v^2}{2\mu_\phi^2 + \lambda_{H\phi} v^2} v + \mathcal{O}\left((\xi M \kappa)^3\right), \quad (3.40)$$

with $v = \mu/\sqrt{\lambda}$, as usual. The standard model Higgs vacuum expectation value receives a correction of order ξ^2 , while the dark matter scalar obtains a vacuum expectation value $\mathcal{O}(\xi)$. Due to the additional suppression by powers of $(\kappa v) \simeq 10^{-16}$, these contributions are negligible unless $(\xi M \kappa) \gtrsim 10^{16}$. For the sake of a discussion of $\mathcal{O}(\xi)$ processes, these corrections can be neglected, as due to the form of the non-minimal coupling term (4.4), any occurrence of the dark matter field ϕ introduces an additional power of ξ . Thus, for the remainder of this thesis, the approximation

$$\langle \varphi \rangle \simeq v, \quad (3.41)$$

$$\langle \phi \rangle \simeq 0 \quad (3.42)$$

suffices. This is even more true for the other dark matter scenarios under discussion: in the scalar doublet case (4.24), for example, the mass scale M is effectively replaced by the Higgs vacuum expectation value v , so the suppression is even larger.

3.4 A note on the cosmological constant

To observe the effect of the non-minimal coupling on the cosmological constant, one starts with the Jordan-frame action

$$\mathcal{S} = \int d^4x \sqrt{-g} \left(-\frac{R}{2\kappa^2} \Omega^2 + \Lambda + \mathcal{L}_m \right), \quad (3.43)$$

where $\Omega^2(\varphi) = 1 + 2\kappa^2 \xi f(\varphi)$, and \mathcal{L}_m describes the matter sector of the theory. A transformation into the Einstein frame yields

$$\mathcal{S} = \int d^4x \sqrt{-\widehat{g}} \left(-\frac{\widehat{R}}{2\kappa^2} + \frac{3}{\kappa^2} \frac{\left(\widehat{\nabla}_\mu \Omega\right)^2}{\Omega^2} + \frac{\Lambda}{\Omega^4} + \widehat{\mathcal{L}}_m \right), \quad (3.44)$$

and for the specific case of a scalar singlet, $\Omega^2(\varphi = \phi) = 1 + 2\kappa^2 \xi M \phi$. Expanding all terms involving the scalar singlet up to quadratic order, one obtains $\widehat{\mathcal{L}}_\phi = \widehat{\mathcal{L}}_\phi^{(2)} + \mathcal{O}(\phi^3)$, where

$$\widehat{\mathcal{L}}_\phi^{(2)} = \frac{1}{2} (\partial_\mu \phi)^2 (1 + 6\xi^2 \kappa^2 M^2) - \left(\frac{m_\phi^2}{2} - 12\kappa^4 \xi^2 M^2 \Lambda \right) \phi^2 - 4\kappa^2 \xi M \Lambda \phi + \Lambda. \quad (3.45)$$

Now, the first step is to normalize the kinetic term via $\widetilde{\phi} = \sqrt{1 + 6\xi^2 M^2 \kappa^2} \phi$, as in (4.8). This rescaling of the scalar field introduces modifications to the other terms in the Lagrangian, proportional to the non-minimal coupling parameter. As a second step, one can remove the term linear in the scalar field by a constant shift. Then, the scalar field Lagrangian reads

$$\widehat{\mathcal{L}}_\phi^{(2)} = \frac{1}{2} (\partial_\mu \widehat{\phi})^2 - \frac{m_{\widetilde{\phi}}^2}{2} \widehat{\phi}^2 + \widehat{\Lambda}, \quad (3.46)$$

where the Einstein frame scalar field, its mass and the cosmological constant are given by

$$\widehat{\phi} = \widetilde{\phi} + 4(\xi M \kappa) \frac{\sqrt{1 + 6\xi^2 M^2 \kappa^2} \kappa \Lambda}{m_\phi^2 - 24(\xi M \kappa)^2 (\kappa^2 \Lambda)}, \quad (3.47)$$

$$m_{\widetilde{\phi}}^2 = \frac{m_\phi^2 - 24(\xi M \kappa)^2 (\kappa^2 \Lambda)}{1 + 6\xi^2 M^2 \kappa^2}, \quad (3.48)$$

$$\widehat{\Lambda} = \Lambda + 8(\xi M \kappa)^2 \frac{\kappa^2 \Lambda^2}{m_\phi^2 - 24(\xi M \kappa)^2 (\kappa^2 \Lambda)}. \quad (3.49)$$

In light of the extremely small value of the cosmological constant $\Lambda \simeq (2.474 \times 10^{-12} \text{ GeV})^4$ determined by experiment [5], these modifications can be neglected. The Einstein-frame scalar field is taken to be $\widehat{\phi} = \widetilde{\phi}$.

Chapter 4

Dark matter decays from non-minimal coupling to gravity

The remainder of this thesis is concerned with the phenomenological consequences of the interactions of (3.33), as they lead to dark matter decay and annihilation processes that can, in principle, be relevant for dark matter production in the early Universe, leave observable imprints on the cosmic microwave background, and cause measurable fluxes of highly energetic standard model particles at Earth. As will be demonstrated momentarily, the non-minimal coupling to gravity can induce dark matter decay in one of two ways, as sketched in figure 4.1: either the dark matter candidate φ decays directly via n -point interactions, or one of the final-state particles in a \mathbb{Z}_2 -conserving process undergoes subsequent decay through the non-minimal coupling to gravity.

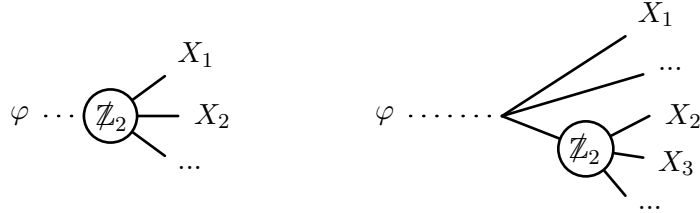


Figure 4.1: Dark matter decay through non-minimal coupling to gravity, after the Weyl transformation. The \mathbb{Z}_2 -breaking vertex is labelled in each case.

For illustration, consider the case of the standard model extended by a hidden sector composed of a fermionic gauge singlet χ and a Higgs-like scalar $SU(2)_L$ doublet η , both odd under a global \mathbb{Z}_2 transformation. The Lagrangian including the lowest-dimensional non-minimal operators linear in χ and η , respectively, reads

$$\begin{aligned} \mathcal{L} = & \mathcal{L}_{\text{SM}} + \bar{\chi} \left(\frac{i}{2} \overleftrightarrow{\not{\partial}} - m_\chi \right) \chi + (D_\mu \eta)^\dagger (D^\mu \eta) - \mathcal{V}(\eta, \Phi) - y \left(\bar{\ell}_L \tilde{\eta} \chi + \bar{\chi} \tilde{\eta}^\dagger \ell_L \right) \\ & + \mathcal{L}_{\text{EH}} - R \left(\xi_1 \left(\eta^\dagger \Phi + \Phi^\dagger \eta \right) + \frac{\xi_2}{M^2} \left(\bar{\ell}_L \tilde{\Phi} \chi + \bar{\chi} \tilde{\Phi}^\dagger \ell_L \right) + \frac{\xi_3}{M^2} \left(\bar{\ell}_L \tilde{\eta} \chi + \bar{\chi} \tilde{\eta}^\dagger \ell_L \right) \right). \end{aligned} \quad (4.1)$$

Here, the Yukawa-type interactions again contain the $SU(2)_L$ -contractions $(\tilde{\eta}, \tilde{\Phi}) = i \sigma^2 (\eta^*, \Phi^*)$. As the second line shows, while the scalar doublet can be linked to the Ricci scalar via a dimension-four operator, linear coupling of the fermion singlet only occurs at dimension six, through an effective operator with a cutoff scale M . The ξ_1 - and ξ_2 -terms break the \mathbb{Z}_2 symmetry

explicitly, while the ξ_3 -operator is \mathbb{Z}_2 -conserving. Being subdominant to the flat-spacetime Yukawa interaction in the first line, however, the latter plays no role in the decay phenomenology. Now, if $m_\eta < m_\chi$, only one of the neutral components of the scalar doublet (η^0, A^0) can be the dark matter, because the fermion singlet χ decays through the \mathbb{Z}_2 -conserving Yukawa interaction into $\eta^0 \nu_L$ or $\eta^+ e_L^-$. If η^0 is the dark matter, the ξ_1 -operator leads to dark matter decay through Planck-mass suppressed point interactions after the Weyl transformation, as sketched in the first diagram of figure 4.1. Due to the \mathbb{Z}_2 -breaking ξ_2 -term and the Yukawa interaction, η^0 can also decay via a virtual χ (corresponding to the second diagram), but this amplitude carries a relative suppression by $(\xi_2 y)/(\xi_1 M^2)$. If instead A^0 is the dark matter, it can convert into a η^0 under emission of a Z boson through the η kinetic term, and the η^0 can subsequently decay through ξ_1 . (A direct decay of A^0 is not possible due to its CP -odd nature.)

The situation is different if $m_\chi < m_\eta$ and the fermion is the dark matter candidate. Now, ξ_2 leads to direct decays into standard model final states. In addition, the dark matter particle may decay via a virtual η^0 , through a combination of the Yukawa- and ξ_1 -operators. These do not carry any M^2 suppression, so they can dominate over ξ_2 -induced decays. Indeed, for $m_\chi \ll m_\eta$, the ξ_1 -amplitude gives a contribution identical to that of the ξ_2 -operator, with the replacement $\xi_2/M^2 \rightarrow (-\xi_1 y)/m_\eta^2$, while in the near-degenerate scenario $m_\chi \lesssim m_\eta$, the ξ_1 -amplitude is further enhanced because of the presence of the scalar propagator. In summary, at energies below the effective theory cutoff M , in both scenarios ($m_\eta \gtrsim m_\chi$), dark matter decay proceeds predominantly through the renormalizable ξ_1 -operator. The CP -even scalar dark matter candidate decays through point interactions introduced by its direct coupling to the Ricci scalar, while the dominant effective fermionic operator can be understood as arising from the interactions of an intermediate scalar in the decoupling limit. The following sections provide a more detailed analysis of some specific dark matter scenarios, among them the two cases sketched above.

4.1 Scalar singlet dark matter

From a theoretical perspective, a scalar gauge singlet dark matter candidate [81, 82, 84] is probably the simplest possible ansatz to explain the dark matter puzzle. The classical action takes the form (3.2), with

$$\mathcal{L}_{\text{grav}} = -\frac{R}{2\kappa^2}, \quad (4.2)$$

$$\mathcal{L}_d = \frac{1}{2} g^{\mu\nu} (\partial_\mu \phi) (\partial_\nu \phi) - \mathcal{V}(\phi, \Phi), \quad (4.3)$$

$$\mathcal{L}_\xi = -\xi M R \phi, \quad (4.4)$$

and \mathcal{L}_{vis} given by (2.17) at energies above a few GeV, and by (2.36) below around 700 MeV. The potential

$$\mathcal{V}(\phi, \Phi) = \frac{1}{2} \mu_\phi^2 \phi^2 + \frac{1}{4} \lambda_\phi \phi^4 + \frac{1}{2} \lambda_{H\phi} \phi^2 \Phi^\dagger \Phi \quad (4.5)$$

contains all gauge and Lorentz invariant terms up to mass dimension four. After electroweak symmetry breaking, the tree-level mass of the scalar singlet is $m_\phi^{(0)} = \sqrt{\mu_\phi^2 + \lambda_{H\phi} v^2/2}$. As a stereotypical WIMP scenario, this model faces stringent constraints from direct detection, indirect detection and collider experiments as well as from relic abundance calculations. In fact, today most of the WIMP mass range is ruled out, leaving only a small window in the Higgs resonance region $57 \text{ GeV} \lesssim m_\phi^{(0)} \lesssim 62 \text{ GeV}$, with couplings of order $\lambda_{H\phi} \simeq 10^{-3}$ [84, 85].

However, masses above the TeV scale remain a possibility, as does a FIMP-like scalar singlet with $\lambda_{H\phi} \simeq 10^{-11}$ for masses between the GeV and TeV scales [87].

The scalar potential (4.5) conserves a global \mathbb{Z}_2 symmetry under which the scalar singlet is odd, $\phi \rightarrow -\phi$, while all standard model fields, including the Higgs doublet Φ , are even. That way, only the non-minimal coupling \mathcal{L}_ξ leads to dark matter decay. The resulting Weyl factor and leading interaction Lagrangian are given by (3.16) and (3.33), respectively, with $\varphi = \phi$ and $f^{\mu\nu}(\phi) = g^{\mu\nu} M \phi$.

In the scalar singlet case, one additional subtlety arises due to the fact that the non-minimal coupling $R\phi$ is of mass dimension three. In the Einstein frame action (3.19), there is an extra term resulting from expressing the Ricci scalar in terms of the new metric $\hat{g}_{\mu\nu}$. Upon Taylor expanding the Weyl factor, this term introduces a correction to the kinetic term,

$$\frac{3}{\kappa^2} \hat{g}^{\mu\nu} \frac{\hat{\nabla}_\mu \Omega \hat{\nabla}_\nu \Omega}{\Omega^2} = \frac{3}{\kappa^2} \hat{g}^{\mu\nu} \frac{(\partial_\phi \Omega)^2}{\Omega^2} (\partial_\mu \phi) (\partial_\nu \phi) \quad (4.6)$$

$$= \frac{1}{2} \hat{g}^{\mu\nu} (\partial_\mu \phi) (\partial_\nu \phi) (6 \xi^2 M^2 \kappa^2 + \mathcal{O}(\xi^3 M^3 \kappa^4 \phi)). \quad (4.7)$$

Therefore, a canonically normalized scalar field can be defined as

$$\hat{\phi} = \sqrt{1 + 6 \xi^2 M^2 \kappa^2} \phi. \quad (4.8)$$

With this redefinition taken into account, it is assumed to receive a physical mass m_ϕ through its potential. Its interactions with the visible sector are given by

$$\hat{\mathcal{L}}_{\text{int},\xi}^{(1)} = - \frac{\kappa^2 \xi M \hat{\phi}}{\sqrt{1 + 6 \xi^2 M^2 \kappa^2}} \hat{g}^{\mu\nu} T_{\mu\nu}^{(\text{vis})}, \quad (4.9)$$

with $T_{\mu\nu}^{(\text{vis})}$ the visible sector energy-momentum tensor defined in (3.32). For dark matter masses above the GeV scale, the latter follows from the standard model Lagrangian (2.17) and reads, in the unitary gauge,

$$\begin{aligned} T_{\mu\nu}^{(\text{SM})} &= \sum_F \left(-F^a{}_\mu{}^\rho F^a{}_{\nu\rho} + \frac{1}{4} g_{\mu\nu} F^{a\rho\sigma} F^a{}_{\rho\sigma} \right) + \sum_f \left(\frac{i}{4} \bar{f} \left(\gamma_\mu \overleftrightarrow{D}_\nu + \gamma_\nu \overleftrightarrow{D}_\mu \right) f - \frac{i}{2} g_{\mu\nu} \bar{f} \overleftrightarrow{D} f \right) \\ &+ g_{\mu\nu} \sum_f m_f \bar{f} f \left(1 + \frac{H}{v} \right) + (\partial_\mu H) (\partial_\nu H) - \frac{1}{2} g_{\mu\nu} (\partial_\rho H) (\partial^\rho H) + g_{\mu\nu} \mathcal{V}(H) \\ &+ (m_W^2 (W_\mu^+ W_\nu^- + W_\nu^+ W_\mu^-) + m_Z^2 Z_\mu Z_\nu) \left(1 + \frac{H}{v} \right)^2 \\ &- g_{\mu\nu} \left(m_W^2 W^{+\rho} W_\rho^- + \frac{m_Z^2}{2} Z^\rho Z_\rho \right) \left(1 + \frac{H}{v} \right)^2. \end{aligned} \quad (4.10)$$

The Feynman rules can be extracted either manually or in an automated fashion [120, 121]. The results, and details on the *FeynRules* implementation, can be found in appendices A.1 and B, respectively. The resulting decay rates can be computed using the standard formulae given in appendix D, or with the help of existing software packages [122], as demonstrated in appendix C. A somewhat unusual feature of (4.9) is the non-trivial dependence of the decay vertices on the non-minimal coupling parameter ξ , introduced by the field redefinition (4.8). While for small values of $(\xi M \kappa)$, the dependence is approximately linear, for $(\xi M \kappa) \gg 1$, the coupling between the scalar singlet and the energy-momentum tensor approaches the constant value $1/(\sqrt{6} \bar{M}_\text{P})$. This peculiar feature will be further addressed below.

As will be evident from the analysis in section 5.1, for the scalar singlet dark matter candidate, an extension to lower energies (*i.e.* lower dark matter masses) is of interest. At these energies, the strong coupling constant becomes non-perturbative, so the description of the strongly interacting sector via perturbative quantum chromodynamics (QCD) breaks down. Instead, chiral perturbation theory describes the dynamics of hadronic degrees of freedom, leading to the Lagrangian (2.36) for energies below 700 MeV. The individual parts of this Lagrangian transform straightforwardly under the Weyl transformation, according to their Lorentz structure. However, as presented in [52], additional modifications to this low-energy theory arise due to the heavy off-shell particles that have been integrated out (heavy fermions, the massive weak gauge bosons, as well as the Higgs boson). These can be encoded in the Wilson coefficients of four-fermion operators and the vacuum polarization of the photon field. Due to phase space suppression of the resulting decay rates, the former do not have a noticeable impact on the dark matter lifetime and will be omitted from the discussion. The latter effect modifies the photon wavefunction renormalization constant Z_3 in the gauge kinetic Lagrangian

$$\mathcal{T}_F = -\frac{1}{4} Z_3^{-1} g^{\mu\nu} g^{\rho\sigma} A_{\mu\rho} A_{\nu\sigma}. \quad (4.11)$$

All electrically charged particles that are heavier than the cutoff scale of 700 MeV contribute to this quantity, in the form of

$$Z_3^{-1}(E) \simeq 1 - \frac{e^2}{8\pi^2} \left(\sum_{i=t,b,c,\tau,W} \tilde{b}_i(E) \right), \quad \tilde{b}_i(E) = b_i \log \frac{E}{m_i}, \quad (4.12)$$

with $\tilde{b}_t(m_t) = \tilde{b}_c(m_c) = -16/9$, $\tilde{b}_b(m_b) = -4/9$, $\tilde{b}_\tau(m_\tau) = -4/3$, $\tilde{b}_W(m_W) = 7$ at the energy scale E equal to the particle mass in question, and e the electron charge. If there exist other charged particles at energies currently inaccessible to experiments, these will modify Z_3 analogously. However, for the purpose of this work, no assumptions about additional electromagnetically charged matter will be made and such contributions will be neglected. An additional shift in Z_3 arises due to light hadronic degrees of freedom other than the pions. Due to the non-perturbativity of the strong interaction at these energies, this hadronic contribution is difficult to calculate. However, it is not expected to dominate over the effect of all other degrees of freedom combined. It will therefore be omitted in the following discussion as well, introducing a theoretical uncertainty of $\mathcal{O}(1)$ on the precise value of Z_3 . In light of the constraints to be placed later on the non-minimal coupling of a dark matter candidate to gravity, this is an acceptable compromise between theoretical accuracy and computational complexity.

With these considerations in mind, one can perform the Weyl transformation into the Einstein frame. In contrast to the situation at higher energies, there is now a local coupling of the dark matter candidate to the electromagnetic field-strength tensor in the Einstein frame. This coupling is the low-energy manifestation of one-loop diagrams involving the integrated-out particles, as required by the matching procedure between the low-energy effective theory and the standard model description at the electroweak scale. Specifically, it arises because of the dependence of the photon wavefunction renormalization constant Z_3 on the particle masses m_i . Through the Weyl transformation, the kinetic and mass terms of these particles pick up a dependence on the Weyl factor Ω . For the W boson, for example,

$$\hat{\mathcal{L}}_W = -\frac{1}{4} \hat{g}^{\mu\nu} \hat{g}^{\rho\sigma} W_{\mu\rho} W_{\nu\sigma} + \frac{1}{2} \frac{m_W^2}{\Omega^2} \hat{g}^{\mu\nu} W_\mu W_\nu. \quad (4.13)$$

Since at low energies, the W mass is much larger than the momentum of the dark matter field, ϕ is effectively constant, leading to a ϕ -dependent mass $m_W/\Omega(\phi)$, as was argued in [123]

in the context of Higgs boson decays into diphotons. In fact, this is quite intuitive: a Weyl transformation rescales the infinitesimal length element

$$ds^2 = g_{\mu\nu} dx^\mu dx^\nu \rightarrow \Omega^2 g_{\mu\nu} dx^\mu dx^\nu = \Omega^2 ds^2 \quad (4.14)$$

and all dimensionful quantities, such as particle masses, with it. The heavy fermion masses pick up an identical rescaling factor. Since the photon wavefunction renormalization constant depends on the masses of the heavy particles through their coefficients $\tilde{b}_i(E)$, all these factors appear in the Lagrangian,

$$\hat{Z}_3^{-1}(E, m_i) = Z_3^{-1}\left(E, \frac{m_i}{\Omega}\right) \simeq 1 - \frac{e^2}{8\pi^2} \left(\sum_{i=t,b,c,\tau,W} b_i \log \frac{E\Omega}{m_i} \right). \quad (4.15)$$

Therefore, Taylor expanding $\Omega(\phi)$ leads to an effective vertex between the dark matter field and the squared photon field-strength tensor. Explicitly, the full interaction Lagrangian for the canonically normalized scalar singlet $\hat{\phi}$ reads

$$\begin{aligned} \hat{\mathcal{L}}_{\text{int},\xi}^{(1)} = & - \frac{2\kappa^2 \xi M \hat{\phi}}{\sqrt{1+6\xi^2 M^2 \kappa^2}} \left(\sum_{f=e,\mu,\{\nu_j\}} \left(\frac{3i}{2} \bar{f} \not{\partial} f - 2m_f \bar{f} f \right) - \sum_{f=e,\mu} \left(\frac{3e}{2} \bar{f} \not{A} f \right) \right. \\ & \left. + \frac{1}{2} (\partial_\mu \pi^a) (\partial^\mu \pi^a) - \frac{m_\pi^2}{2} \pi^a \pi^a + c_{\gamma\gamma} A_{\mu\nu} A^{\mu\nu} \right), \end{aligned} \quad (4.16)$$

where

$$c_{\gamma\gamma} = - \frac{e^2}{8\pi^2} \left(\sum_{i=t,b,c,\tau,W} b_i \right) = \frac{5e^2}{24\pi^2}. \quad (4.17)$$

The corresponding Feynman rules can be found in appendix A.2.

4.2 Scalar (inert) doublet dark matter

Another simple dark matter scenario consists in extending the standard model $\mathcal{L}_{\text{vis}} = \mathcal{L}_{\text{SM}}$ by a scalar $\text{SU}(2)_L$ doublet η that has the same quantum numbers as the Higgs field [124, 117]. In addition, a global \mathbb{Z}_2 symmetry is postulated under which η is odd, while all standard model fields are even. The presence of this symmetry precludes Yukawa couplings of the second doublet to fermions, as well as η taking on a non-vanishing vacuum expectation value. It is therefore rendered “inert” in the sense that it only couples to the standard model via the scalar potential

$$\mathcal{V}_\eta(\Phi, \eta) = \mu_2^2 |\eta|^2 + \lambda_2 |\eta|^4 + \lambda_3 |\Phi|^2 |\eta|^2 + \lambda_4 |\Phi^\dagger \eta|^2 + \frac{1}{2} \left(\lambda_5 (\Phi^\dagger \eta) (\Phi^\dagger \eta) + \text{h.c.} \right), \quad (4.18)$$

with Φ the standard model Higgs doublet. The full hidden sector lagrangian is given by

$$\mathcal{L}_d = g^{\mu\nu} (D_\mu \eta)^\dagger (D_\nu \eta) - \mathcal{V}_\eta(\Phi, \eta). \quad (4.19)$$

In the unitary gauge,

$$\Phi = \begin{pmatrix} 0 \\ \frac{1}{\sqrt{2}} (v + H) \end{pmatrix}, \quad \eta = \begin{pmatrix} \eta^+ \\ \frac{1}{\sqrt{2}} (\eta^0 + i A^0) \end{pmatrix}, \quad (4.20)$$

where after electroweak symmetry breaking, the masses of the additional scalars are [117]

$$m_{\eta^+}^2 = \mu_2^2 + \lambda_3 v^2/2, \quad (4.21)$$

$$m_{\eta^0}^2 = \mu_2^2 + (\lambda_3 + \lambda_4 + \lambda_5) v^2/2, \quad (4.22)$$

$$m_{A^0}^2 = \mu_2^2 + (\lambda_3 + \lambda_4 - \lambda_5) v^2/2. \quad (4.23)$$

While η^\pm are charged, either η^0 or A^0 is a viable dark matter candidate, depending on which of the two is lighter. This in turn depends on the values of the quartic couplings in the potential. Being an archetypical WIMP model, the correct dark matter abundance can be created via thermal freeze-out in the early Universe. A combination of direct and indirect detection constraints allows two mass regimes for the inert doublet model: either the dark matter particle is lighter than the W boson, or it falls into the high-mass regime where $m_{\text{DM}} \gtrsim 535 \text{ GeV}$ [117, 125]. In the latter case, obtaining the correct relic density with perturbative couplings requires that $m_{\text{DM}} \lesssim 20 \text{ TeV}$ [125].

The gravitational action in this scenario is, as before, given by (2.12). As anticipated above, the lowest-dimensional linear coupling to the Ricci tensor takes the form

$$\mathcal{L}_\xi = -\xi R \left(\eta^\dagger \Phi + \Phi^\dagger \eta \right) \quad (4.24)$$

$$= -\xi R (v + H) \eta^0. \quad (4.25)$$

It is worth noting that only the CP -even component η^0 obtains a direct coupling to the Ricci scalar. After a Weyl transformation with the factor

$$\Omega^2 = 1 + 2\kappa^2 \xi (v + H) \eta^0, \quad (4.26)$$

there are additional contributions to the H and η^0 kinetic terms, arising through terms analogous to (4.6). Specifically, they read

$$\begin{aligned} & \frac{3}{\kappa^2} \hat{g}^{\mu\nu} \frac{\hat{\nabla}_\mu \Omega \hat{\nabla}_\nu \Omega}{\Omega^2} \\ &= \frac{3}{\kappa^2} \hat{g}^{\mu\nu} \left(\frac{(\partial_{\eta^0} \Omega)^2}{\Omega^2} (\partial_\mu \eta^0) (\partial_\nu \eta^0) + \frac{2(\partial_{\eta^0} \Omega)(\partial_H \Omega)}{\Omega^2} (\partial_\mu \eta^0) (\partial_\nu H) + \frac{(\partial_H \Omega)^2}{\Omega^2} (\partial_\mu H) (\partial_\nu H) \right). \end{aligned} \quad (4.27)$$

In contrast to the scalar singlet case, however, the derivatives of the Weyl factor $\partial_{\eta^0} \Omega$, $\partial_H \Omega$ always introduce a factor of $(\xi v \kappa)$. Thus, any such contribution to the kinetic terms is negligible for non-minimal couplings smaller than $\xi \simeq M_{\text{P}}/v \simeq 10^{16}$. (Indeed, any non-minimal operator present in the Jordan-frame action appears in the Weyl factor Ω^2 and potentially modifies the scalar kinetic Lagrangian. In the scalar singlet scenario, for example, adding the term $-\xi' R \Phi^\dagger \Phi$ to (4.4), with Φ the standard model Higgs doublet, results in such a modification. Under the assumption $\xi M \gg \xi' v$, however, it is negligible.) Limiting oneself to smaller values of ξ , the Jordan- and Einstein-frame fields are practically identical, $\hat{\eta}^0 \simeq \eta^0$, $\hat{H} \simeq H$. The leading interactions between the CP -even scalar and the visible sector can then be read off from the interaction Lagrangian

$$\hat{\mathcal{L}}_{\text{int},\xi}^{(1)} = -\kappa^2 \xi (v + H) \eta^0 \hat{g}^{\mu\nu} T_{\mu\nu}^{(\text{SM})}, \quad (4.28)$$

with $T_{\mu\nu}^{(\text{SM})}$ given by (4.10), and are listed in appendix A.3. Decays of the CP -even component η^0 proceed directly through these vertices.

In contrast, if A^0 is the dark matter candidate, decay originates from the three-point interaction

$$\widehat{\mathcal{L}}_{\text{int},\eta}^{(1)} = \frac{g}{2c_W} Z^\mu (\eta^0 \partial_\mu A^0 - A^0 \partial_\mu \eta^0) \quad (4.29)$$

arising from the kinetic term in the Lagrangian \mathcal{L}_d . Here, c_W is the cosine of the Weinberg angle and g the $SU(2)_L$ gauge coupling. In the absence of gravity, this vertex does not lead to dark matter decay, since $m_{A^0} < m_{\eta^0}$. Through the \mathbb{Z}_2 -breaking non-minimal coupling to gravity, however, a virtual η^0 can subsequently decay via (4.28), and dark matter becomes unstable. The amplitudes for A^0 decay are identical to those for η^0 multiplied by the appropriate vertex and propagator factors and can be found in appendix A.3.

Compared to the scalar singlet case, the mass scale M is replaced by the standard model Higgs field $(v + H)$ for a scalar doublet dark matter candidate. This leads to a rescaling of the decay rates by v/M as well as to the presence of additional decay channels with Higgs bosons in the final state. The most striking difference, however, is the trivial dependence of the dark matter lifetime on the non-minimal coupling parameter ξ , as long as $\xi \lesssim 10^{16}$. Since the components of the scalar doublet are already very nearly canonically normalized in the Einstein frame, no field redefinition analogous to (4.8) needs to be made. As a result, the vertices are linear in ξ . The resulting decay phenomenology will be discussed in chapter 5.3.

4.3 Fermionic dark matter

In the spirit of keeping the dark sector minimal, one can also choose to extend the standard model by a single gauge-singlet Dirac fermion χ [126]. As before, the visible sector \mathcal{L}_{vis} is assumed to be described by the Lagrangian (2.17) at energies above a few GeV, while for the dark sector,

$$\mathcal{L}_d = \bar{\chi} \left(\frac{i}{2} \overleftrightarrow{\not{D}} - m_\chi \right) \chi - \mathcal{V}_\chi(\chi, \{X_{\text{vis}}\}), \quad (4.30)$$

where the covariant derivative is defined as in (2.17). \mathcal{V}_χ may contain interactions between the dark matter candidate and the standard model as long as they conserve a global \mathbb{Z}_2 symmetry under which $\chi \rightarrow -\chi$ and the visible sector fields are invariant. This ensures the stability of the fermion against decay as far as its non-gravitational interactions are concerned. The minimal standard model does not contain gauge singlet fermion fields. Albeit an extension with righthanded neutrinos is straightforward, in the spirit of minimality, the dark matter candidate χ is assumed to be the only additional fermion. In this case, no gauge invariant dimension-five fermion operator (3.8) can be constructed. Instead, the lowest-dimensional non-minimal operator coupling χ to the Ricci tensor is

$$\mathcal{L}_\xi = - \frac{\xi_j}{M^2} R \left(\bar{\ell}_{L,j} \tilde{\Phi} \chi + \bar{\chi} \tilde{\Phi}^\dagger \ell_{L,j} \right), \quad (4.31)$$

with $j = 1, 2, 3$ a generation index. In the unitary gauge, the corresponding Weyl factor reads

$$\Omega^2 = 1 + \sqrt{2} \kappa^2 \frac{\xi_j}{M^2} (v + H) (\bar{\nu}_{L,j} \chi + \bar{\chi} \nu_{L,j}), \quad (4.32)$$

and in the Einstein frame, the leading interaction Lagrangian is of mass dimension six:

$$\widehat{\mathcal{L}}_{\text{int},\xi}^{(1)} = - \frac{\kappa^2 \xi_j}{\sqrt{2} M^2} (v + H) (\bar{\nu}_{L,j} \chi + \bar{\chi} \nu_{L,j}) \widehat{g}^{\mu\nu} T_{\mu\nu}^{(\text{SM})}, \quad (4.33)$$

where $T^{(\text{SM})}$, as before, is the trace of the standard model energy-momentum tensor (4.10). The coupling is very similar to the scalar doublet scenario, the main difference being the presence of the lefthanded neutrino field. Accordingly, the decay amplitudes can be obtained straightforwardly by attaching a factor of

$$\frac{1}{2\sqrt{2}M^2} \bar{u}(p_\nu) (1 - \gamma_5) u(p_\chi) \quad (4.34)$$

to those of the scalar doublet (*cf.* appendix A.4). In contrast to the scalar case, however, the non-minimal coupling is non-renormalizable. A simple way to generate the dimension-six operator (4.31) via renormalizable interactions is to introduce one additional scalar $SU(2)_L$ doublet η with a non-minimal coupling to gravity

$$\mathcal{L}_{\xi,\eta} = -\xi_\eta R (\eta^\dagger \Phi + \Phi^\dagger \eta) \quad (4.35)$$

and Yukawa interactions linking the dark- and visible-sector fermion fields

$$\mathcal{L}_{Y,\eta} = -y_j (\bar{\ell}_{L,j} \tilde{\eta} \chi + \bar{\chi} \tilde{\eta}^\dagger \ell_{L,j}). \quad (4.36)$$

In a way, this setup of a fermionic dark matter candidate coupled to a scalar mediator is reminiscent of the visible sector, and has been extensively studied in the literature [127]. It is also precisely the hidden sector composition introduced as a first example in the beginning of chapter 4. Depending on the mass difference between the dark matter particle and the mediator, the observed relic abundance can be obtained through thermal freeze-out for masses between $40 \text{ GeV} \lesssim m_\chi \lesssim 10 \text{ TeV}$, in line with constraints mainly from indirect detection [127].

Performing a Weyl transformation on this ‘‘UV completion’’ results in the interaction vertices (4.28) between the CP -even neutral scalar η^0 and the visible sector presented in section 4.2. The dark matter candidate χ can decay through an intermediate η^0 , with the amplitude

$$i \mathcal{M}_\chi = \bar{u}(p_\nu) \frac{1 - \gamma_5}{2} u(p_\chi) \times \frac{y_j}{\sqrt{2}} \frac{1}{p_{\eta^0}^2 - m_{\eta^0}^2} \times i \mathcal{M}_{\eta^0}. \quad (4.37)$$

In the limit where the scalar decouples, $m_{\eta^0} \gg m_\chi$, the internal scalar line shrinks to a point interaction and one obtains the effective operator (4.33) by identifying

$$\frac{\xi_j}{M^2} = -\frac{\xi_\eta y_j}{m_{\eta^0}^2}. \quad (4.38)$$

In contrast, in the degenerate limit $m_{\eta^0} \lesssim m_\chi$, the presence of the scalar propagator in (4.37) leads to an enhanced decay rate when the η^0 is nearly on-shell.

4.4 Dark matter decay in simplified models

The previous sections mostly dealt with hidden sectors that each are minimal, in the sense that only a single new field was added to the standard model. (An exception was the extension of the fermion scenario with a scalar doublet as a way to generate the non-renormalizable interaction with the Ricci scalar.) In general, however, the dark sector may contain additional fields. As the next step in terms of complexity, so-called dark matter simplified models [106, 105] extend the standard model by a dark matter candidate as well as a mediator. They allow one to ‘‘resolve’’ the effective interaction between the dark and visible sector by explicitly including the intermediate

particle in their description, and therefore remain valid at center-of-mass energies approaching the mass of the mediator, where the EFT description starts to break down [109]. However, even in the presence of a mediator, dark matter typically still does not decay through non-gravitational interactions, as it is the lightest \mathbb{Z}_2 -odd particle in the hidden sector. The precise way a non-minimal coupling to gravity can spoil this stability depends on the composition of the dark sector in question, although some general statements can be made:

- As stressed already in section 3.1, only scalar fields can couple to the Ricci tensor at dimension four or lower. Thus, if one wishes to limit oneself to these operators up to mass dimension four, the fundamental \mathbb{Z}_2 -breaking non-minimal coupling to gravity can only occur through a scalar field. Note, however, that dark matter decay ultimately still proceeds through non-renormalizable terms in the Einstein frame Lagrangian.
- Of course, the presence of the Ricci scalar in the Einstein-Hilbert action as well as in the non-minimal operator will always introduce non-renormalizable interactions to the theory once gravity is “turned on.” Due to the non-renormalizable nature of gravity itself, these are unavoidable. However, one can at least understand the presence of additional mass scales, apart from the Planck mass, in the lowest-dimensional effective operators, as discussed for the fermion singlet scenario in section 4.3.
- If the dark matter field is a scalar S , there are two options. Either S is a gauge singlet, in which case it becomes unstable as described in section 4.1. Then, the presence of additional hidden sector fields has a negligible effect on the dark matter lifetime. If S instead carries non-zero charge under a gauge group, it remains stable against decay at the renormalizable level unless there exists a second scalar field with identical quantum numbers. In that case, a cross-coupling to the Ricci scalar is allowed by symmetry, as discussed in section 4.2 for the inert doublet model. If the dark matter field is charged under a dark gauge group instead of the standard model one, a second hidden sector scalar is needed to enable the cross-coupling. However, if both scalars are \mathbb{Z}_2 -odd, the resulting operator conserves the global symmetry and decay is likely to occur more rapidly through non-gravitational interactions.
- For a dark matter fermion, the situation is slightly more complex. In order to construct the dimension-five interaction term (3.8), one requires two fermion fields with identical or vanishing gauge charges. In that case, a third new field is needed to act as a mediator to the visible sector, *e.g.* the scalar that generates the non-minimal coupling at higher energies, *cf.* the discussion below (3.8). This points towards an extended hidden sector, going beyond the simplified-model approach. In contrast, the dimension-six operator (3.9) can be constructed using only a single dark sector fermion and standard model fields. An additional scalar mediator can connect the two sectors and generate the non-minimal operator, as shown in section 4.3. If instead two of the fields in (3.9) are \mathbb{Z}_2 -odd, the operator itself is \mathbb{Z}_2 -even and one does not need to invoke gravitational breaking of the symmetry to induce decay. Consequently, the decay rate is not expected to be Planck-mass suppressed.
- In the case of vector dark matter, decay through a non-minimal coupling to gravity can be described in an EFT framework, but the origin of the additional mass scales in the theory remains unspecified. In particular, as pointed out in section 3.1 already, the non-minimal operators for a vector field cannot be generated through dimension-four interactions alone. The presence of additional hidden sector fields does not change this picture.

In summary, with respect to the impact of non-minimal couplings to gravity on the dark matter lifetime, the scenarios presented in the previous sections exhaust the most interesting hidden-sector configurations.

Chapter 5

Decay phenomenology

As outlined in the previous section, a dark matter candidate that is stabilized against decay by a global symmetry may become unstable through non-minimal gravitational interactions. The dark matter lifetime τ_{DM} mainly depends on the strength of the “gravity portal” coupling ξ and on the dark matter mass m_{DM} . From the experimental side, however, τ_{DM} is not a free parameter — a variety of astronomical and cosmological bounds apply. The most trivial constraint results from the fact that in Λ CDM cosmology, dark matter is required to seed structure formation in the early Universe [5]. Since observations of galaxy and cluster dynamics [8, 11] show that dark matter is still abundant today, only a small fraction of the total abundance may have decayed over the history of the Universe. Therefore, if the various phenomena collectively called the dark matter puzzle are to be explained by a population of elementary particles, the lifetime of this particle has to exceed the age of the Universe,

$$\tau_{\text{DM}} \gtrsim \tau_{\text{Uni}} \simeq 4 \times 10^{17} \text{ s}. \quad (5.1)$$

However, thanks to tremendous experimental efforts over the last decades, depending on the dominant decay channels of the dark matter particle, additional constraints may apply that are many orders of magnitude stronger. More specifically, by measuring the differential particle fluxes of photons, neutrinos and antimatter arriving at Earth one can set limits on the presence of exotic components in these fluxes. To do that, one can in principle calculate the expected fluxes from astrophysical processes to obtain an estimate for the background, and then look for signals from dark matter decay in the measured flux. A more robust approach consists in refraining from making any assumptions about astrophysical backgrounds and simply requiring that, for a given dark matter scenario, the expected flux from dark matter decay or annihilation does not exceed the total measured flux. This second approach typically results in weaker limits on the parameters of the model, but does not introduce significant astrophysical uncertainties into the results. In either case, given the absence of conclusive signals for exotic components in the measured fluxes so far, one can set constraints on the dark matter lifetime.

For very heavy dark matter, the strongest limits on its lifetime come from observations of neutrino telescopes. For a dark matter particle with $m_{\text{DM}} \simeq 10^3\text{--}10^{15}$ GeV that decays into $\nu\bar{\nu}$ or $e^+e^-\nu$, observations of Super-Kamiokande [128], IceCube [129, 130, 75], AMANDA [131], Auger [132] and ANITA [133] require its lifetime to satisfy [134, 135]

$$\tau_{\text{DM}}^{(\nu)} \gtrsim 10^{25} \text{ s}. \quad (5.2)$$

At intermediate masses, measurements of gamma rays and antimatter fluxes yield complementary constraints. Agreement with data taken by the Large Area Telescope aboard the Fermi

satellite (Fermi-LAT) requires that a dark matter particle with $m_{\text{DM}} \simeq 0.1\text{--}30$ TeV has a lifetime of around [93]

$$\tau_{\text{DM}}^{(\gamma)} \gtrsim 10^{26}\text{--}10^{27} \text{ s}, \quad (5.3)$$

for two-body decays into e^+e^- , $\mu^+\mu^-$, $\tau^+\tau^-$, $b\bar{b}$, W^+W^- or $t\bar{t}$ final states. Meanwhile, the Alpha Magnetic Spectrometer (AMS) on the International Space Station has measured the positron [76] and antiproton [77] fluxes at Earth, enabling one to constrain the dark matter lifetime to [136, 28]

$$\tau_{\text{DM}}^{(\text{CR})} \gtrsim 10^{25}\text{--}10^{28} \text{ s} \quad (5.4)$$

for masses $m_{\text{DM}} \simeq 10\text{--}10^4$ GeV, depending on the particular two-body final state and chosen propagation model. For even lower dark matter masses down to around $m_{\text{DM}} \gtrsim 1$ MeV, measurements of the isotropic diffuse x-ray and gamma-ray spectra by INTEGRAL [137] and COMPTEL [138], EGRET [139] and Fermi-LAT [74], respectively, can be used to constrain the lifetime of a scalar dark matter candidate decaying through a gravity portal to

$$\tau_{\text{DM}}^{(\gamma)} \gtrsim 10^{24}\text{--}10^{26} \text{ s}, \quad (5.5)$$

as will be shown explicitly below.

5.1 Scalar singlet dark matter above the GeV scale

The observations of cosmic-ray and gamma-ray experiments have strong implications for the scalar singlet dark matter scenario introduced in section 4.1. Focussing at first on dark matter masses above the GeV scale, it is evident from the interaction Lagrangian (4.9) that, already at tree level, two-, three-, and four-body decays can occur, if kinematically allowed. Due to the structure of these effective operators apparent from (3.23), the two-body decays arise from the standard model kinetic and mass terms, to which an external dark matter leg is attached multiplicatively. Three- and four-body decays, in contrast, arise from standard model interaction terms. A list of all tree-level decay channels can be found in table 5.1. The right column shows

Decay mode	Asymptotic scaling
$\phi \rightarrow HH, WW, ZZ$	m_ϕ^3
$\phi \rightarrow f\bar{f}$	$m_\phi m_f^2$
$\phi \rightarrow HHH$	$m_\phi v^2$
$\phi \rightarrow WWH, ZZH$	m_ϕ^5/v^2
$\phi \rightarrow f\bar{f}H$	$m_\phi^3 m_f^2/v^2$
$\phi \rightarrow f'\bar{f}'W, f'\bar{f}'Z$	m_ϕ^5/v^2
$\phi \rightarrow f\bar{f}\gamma, q\bar{q}G$	m_ϕ^3
$\phi \rightarrow HHHH$	m_ϕ^3
$\phi \rightarrow WWHH, ZZHH$	m_ϕ^7/v^4

Table 5.1: Tree-level decay modes of the scalar singlet dark matter candidate. Where applicable, m_f is the mass of the final-state fermion, while $v = 246$ GeV is the Higgs vacuum expectation value.

the asymptotic dependence of the corresponding partial width on the dark matter mass, in the limit of massless final-state particles. Throughout this section, $\phi \equiv \widehat{\phi}$ refers to the canonically normalized, Einstein-frame scalar field. The hat has been dropped for conciseness. A universal prefactor

$$\frac{(\xi M \kappa)^2}{1 + 6(\xi M \kappa)^2} \frac{1}{\overline{M}_{\text{P}}^2} \equiv \frac{\bar{\xi}^2}{\overline{M}_{\text{P}}^2} \quad (5.6)$$

arising from the non-minimal coupling to gravity has been omitted in table 5.1, as have appropriate phase-space factors. As evident from the right column, decays into massive W and Z bosons have a strong dependence on the dark matter mass. More precisely, it is the longitudinal polarization states of these particles that carry an m_ϕ^2/v^2 enhancement over the transversal modes. This also explains the different scaling of the $f\bar{f}\gamma$ and $q\bar{q}G$ partial rates compared to the $f'\bar{f}'W$ and $f\bar{f}Z$ ones. The dependence of the $f\bar{f}$ and $f\bar{f}H$ channels on the fermion mass has two reasons. The $\phi f\bar{f}$ vertex is proportional to the equation of motion of the fermion field. Therefore, for on-shell fermions, it scales linearly with m_f . The $\phi f\bar{f}H$ vertex, on the other hand, is proportional to the standard model Yukawa terms, which are proportional to m_f/v . In general, decays with higher final-state particle multiplicity have a stronger dependence on the dark matter mass, which results from the higher dimensionality of the phase-space integral. (Details on the computation can be found in appendix D.)

The two-body decay rates can be calculated analytically:

$$\Gamma_{\phi \rightarrow HH} = \frac{\bar{\xi}^2}{32\pi} \frac{m_\phi^3}{\overline{M}_{\text{P}}^2} (1 + 2x_H)^2 (1 - 4x_H)^{1/2}, \quad (5.7)$$

$$\Gamma_{\phi \rightarrow WW} = \frac{\bar{\xi}^2}{16\pi} \frac{m_\phi^3}{\overline{M}_{\text{P}}^2} (1 - 4x_W + 12x_W^2) (1 - 4x_W)^{1/2}, \quad (5.8)$$

$$\Gamma_{\phi \rightarrow ZZ} = \frac{\bar{\xi}^2}{32\pi} \frac{m_\phi^3}{\overline{M}_{\text{P}}^2} (1 - 4x_Z + 12x_Z^2) (1 - 4x_Z)^{1/2}, \quad (5.9)$$

$$\Gamma_{\phi \rightarrow f\bar{f}} = \frac{\bar{\xi}^2}{8\pi} N_c^{(f)} \frac{m_\phi^3}{\overline{M}_{\text{P}}^2} x_f (1 - 4x_f)^{3/2}, \quad (5.10)$$

where $x_i = m_i^2/m_\phi^2$, $N_c^{(f)}$ is the color factor for fermion f , and $f = e, \mu, \tau, u, d, s, c, b, t$. In general, the phase-space integral for three or more massive final-state particles can only be evaluated numerically, *e.g.* through the procedure described in appendix D. However, in the limit where the scalar singlet is much heavier than any of the final-state particles, the following expressions give excellent approximations to the decay rates into three or four particles:

$$\Gamma_{\phi \rightarrow q\bar{q}G} \simeq \frac{\bar{\xi}^2}{4\pi^2} \alpha_s \frac{m_\phi^3}{\overline{M}_{\text{P}}^2}, \quad (5.11)$$

$$\Gamma_{\phi \rightarrow f_i \bar{f}_j W} \simeq \frac{3\bar{\xi}^2}{4\sqrt{2}(4\pi)^3} N_c^{(f_i)} |U_{ij}|^2 \frac{m_\phi^5 G_{\text{F}}}{\overline{M}_{\text{P}}^2}, \quad (5.12)$$

$$\Gamma_{\phi \rightarrow f\bar{f}Z} \simeq \frac{3\bar{\xi}^2}{2\sqrt{2}(4\pi)^3} N_c^{(f)} (g_{f,V}^2 + g_{f,A}^2) \frac{m_\phi^5 G_{\text{F}}}{\overline{M}_{\text{P}}^2}, \quad (5.13)$$

$$\Gamma_{\phi \rightarrow WWHH} \simeq \frac{\bar{\xi}^2}{15(8\pi)^5} \frac{m_\phi^7}{\overline{M}_{\text{P}}^2 v^4}, \quad (5.14)$$

$$\Gamma_{\phi \rightarrow ZZHH} \simeq \frac{\bar{\xi}^2}{30(8\pi)^5} \frac{m_\phi^7}{\overline{M}_{\text{P}}^2 v^4}. \quad (5.15)$$

Here, $\alpha_s = g_s^2/(4\pi)^2$ is the “fine-structure constant” of the strong interaction, $G_F = 1/(\sqrt{2}v^2)$ is Fermi’s weak interaction constant, the vector and pseudovector couplings of the weak interaction are $g_{f,V} = t_3^{(f)}/2 - Q_f \sin^2 \theta_W$ and $g_{f,A} = t_3^{(f)}/2$, respectively, and for quarks (leptons), U_{ij} is the Cabibbo-Kobayashi-Maskawa (Pontecorvo-Maki-Nakagawa-Sakata) matrix relating the weak to the mass eigenstates. The rate $\Gamma_{\phi \rightarrow f_i \bar{f}_j W}$ is the combination of the partial widths for $\phi \rightarrow f_i \bar{f}_j W^+$ and its complex conjugate $\phi \rightarrow f_j \bar{f}_i W^-$. The remaining channels from table 5.1 have branching fractions below 5 % and are not given explicitly here. All partial widths for the scalar singlet scenario have been determined both semi-analytically (following appendix D) and in an automated fashion (appendices B and C) [51] and are shown in figure 5.1. For this figure,

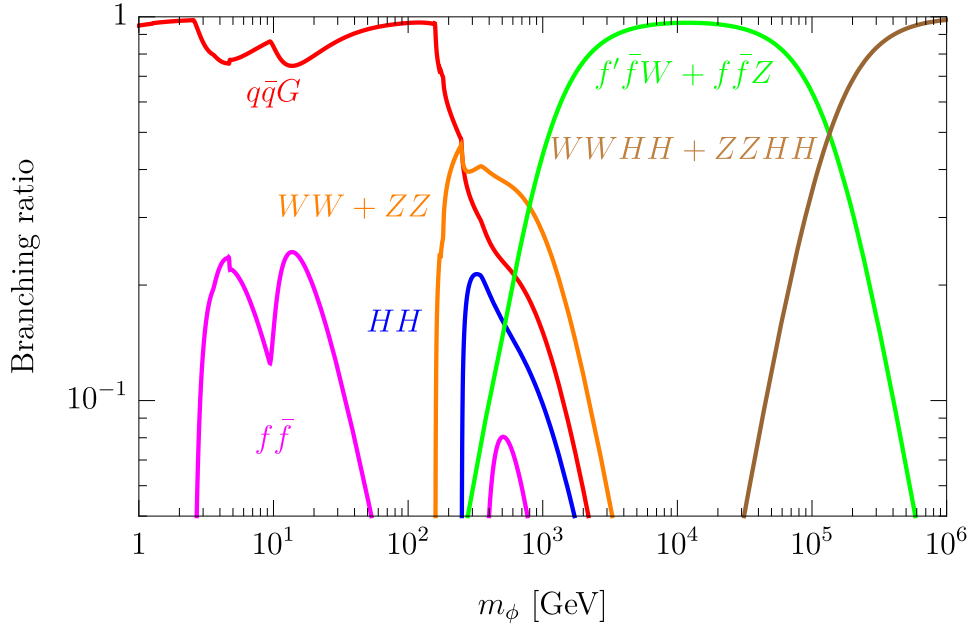


Figure 5.1: Branching ratios in the scalar singlet scenario as a function of the dark matter mass, at a fixed value of $(\xi M \kappa)$. Decay channels with branching fractions below 5 % are not shown.

an arbitrary fixed value of $(\xi M \kappa)$ was chosen, since all partial rates carry the same dependence on the non-minimal coupling parameter. Below the electroweak scale, only two- and three-body decays with fermion-antifermion pairs in the final state are kinematically allowed. Compared to decays into a quark-antiquark pair and a gluon $q\bar{q}G$, the $f\bar{f}\gamma$ partial widths are suppressed by the ratio of the couplings α/α_s as well as a smaller color factor. The $f\bar{f}$ decays without a gauge boson in the final state, on the other hand, feature a factor m_f^2/m_ϕ^2 in their partial widths (5.10) and are thus only important close to threshold (figure 5.1 shows this behavior at $m_\phi \simeq 2m_c, 2m_b, 2m_t$). Above dark matter masses equal to twice the W boson mass, decays into (longitudinal) electroweak gauge bosons start to dominate the total rate. Due to phase-space suppression, the three-body $f'\bar{f}W$ and $f\bar{f}Z$ decays take over at around 1 TeV, while the four-body channels $WWHH$ and $ZZHH$ dominate at masses above $m_\phi \gtrsim 10^5$ GeV. Generically, at energies significantly above the electroweak scale, additional exclusive final states open up kinematically, modifying the branching fractions and total rate [140, 141, 142, 143]. In this mass region, the first-order results given in this chapter are therefore subject to corrections. This applies equally to the scalar doublet and fermion scenarios discussed in sections 5.3 and 5.4, respectively.

Of course, the unstable standard model particles produced in decays of the scalar singlet subsequently decay further. In principle, starting from the set of branching fractions for a scalar singlet dark matter candidate of a given mass, one could then follow the complete decay chain and compute the energy spectra of the produced electrons, photons, neutrinos and protons. Under certain astrophysical assumptions, these energy spectra could be translated into particle fluxes expected at Earth and directly compared with experimental data, as outlined at the beginning of chapter 5. The non-observation of excesses over astrophysical backgrounds in these fluxes of photons, neutrinos and cosmic rays could then be translated into bounds on the dark matter lifetime $\tau_{\text{DM}}^{(\gamma,\nu,\text{CR})}$, the relative strength of which would depend strongly on the dark matter mass. In a computationally simpler approach, one could compare the partial widths of the scalar singlet into different tree-level final states with published bounds individually, and then derive a limit on the total rate by weighing these bounds according to their branching ratios. However, for obvious reasons, the bounds that can be found in the literature mostly apply to two- or three-body final states [135, 134, 93, 136, 28] and do not include somewhat exotic channels like $\phi \rightarrow WWHH$. Therefore, in order to obtain a rough, but robust, estimate of the constraints set on the non-minimally coupled scalar singlet scenario through gamma-ray, neutrino and cosmic-ray observations, in [50, 51] the following approach was pursued: given the typical strength of observational lower limits on the dark matter lifetime of around $10^{25}\text{--}10^{28}$ s for masses $m_{\text{DM}} \simeq 1\text{--}10^{15}$ GeV (*cf.* the beginning of chapter 5), one can reasonably work with a mass-independent limit of $\tau_{\text{DM}} \gtrsim 10^{24}$ s across this entire mass range.

At any given value for the dark matter mass, the total width of the scalar singlet ϕ is determined by a small number of partial widths. An approximate lower estimate of the total rate reads

$$\Gamma_{\phi} \gtrsim \frac{\bar{\xi}^2}{8\pi} \frac{m_{\phi}^3}{M_{\text{P}}^2} \times \begin{cases} 2n_q \frac{\alpha_s}{\pi}, & m_{\phi} \simeq 1\text{--}200 \text{ GeV}, \\ 1 + 2n_q \frac{\alpha_s}{\pi}, & m_{\phi} \simeq 0.2\text{--}1 \text{ TeV}, \\ \frac{3}{(2\pi)^2} \frac{m_{\phi}^2}{v^2}, & m_{\phi} \simeq 1\text{--}100 \text{ TeV}, \\ \frac{1}{10(8\pi)^4} \frac{m_{\phi}^4}{v^4}, & m_{\phi} \gtrsim 100 \text{ TeV}, \end{cases} \quad (5.16)$$

with n_q the number of quark flavors that are kinematically accessible. In contrast to the rate given in [50, 51], the full dependence on the non-minimal coupling ($\xi M \kappa$) has been reintroduced. In figure 5.2, this expression for the total rate is compared to the lower bound on the dark matter lifetime from the age of the universe, $\tau_{\text{DM}} \gtrsim 4 \times 10^{17}$ s, as well as the constraint from gamma-ray, neutrino and cosmic-ray experiments discussed above. Figure 5.3, in turn, shows the upper bound on the non-minimal coupling from demanding that the dark matter lifetime exceed 10^{24} s. Figure 5.2 shows the non-trivial scaling of the total rate (5.16) with the non-minimal coupling parameter introduced by the field redefinition (4.8). For low values, $(\xi M \kappa) \ll 1$, the lifetime $\tau_{\phi} = \Gamma_{\phi}^{-1}$ scales as $(\xi M \kappa)^{-2}$, while for $(\xi M \kappa) = 1$, the corresponding prefactor in (5.16) evaluates to $1/7$, and in the limit $(\xi M \kappa) \rightarrow \infty$, it approaches $1/6$, independently of the exact value of the non-minimal coupling. In this limit, the mixing between the Jordan-frame metric and the scalar is maximal. Phenomenologically, the dark matter lifetime cannot be shortened significantly by assuming a non-minimal coupling larger than unity. A scalar singlet non-minimally coupled to gravity with a mass $m_{\phi} \simeq 1$ GeV requires a non-minimal coupling smaller than $(\xi M \kappa) \lesssim 0.017$ for its lifetime to exceed the age of the Universe. To satisfy $\tau_{\phi} \gtrsim 10^{24}$ s, the upper bound on the coupling from figure 5.3 is $(\xi M \kappa) \lesssim 1.1 \times 10^{-5}$. At larger dark matter masses, the bounds become even stronger. For example, fixing the dark matter mass to $m_{\phi} = 1$ TeV means that only a coupling smaller than $(\xi M \kappa) \lesssim 1.9 \times 10^{-10}$ will not result in observable contributions to gamma-ray, neutrino or cosmic-ray fluxes. These kind of

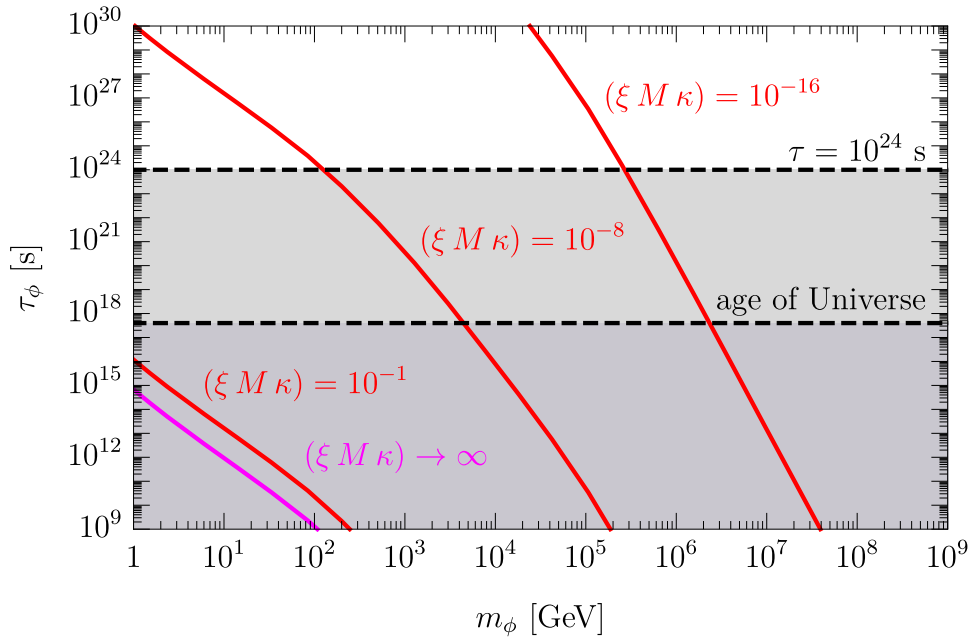


Figure 5.2: *The total lifetime of the scalar singlet dark matter candidate, for different values of the non-minimal coupling $(\xi M \kappa)$. Also shown are the observational constraints from the age of the Universe and the non-observation of exotic contributions to gamma-ray, neutrino or cosmic-ray fluxes at Earth, respectively.*

numbers hint at some mechanism suppressing the non-minimal coupling to gravity. Either the mass scale M lies significantly below the Planck scale κ^{-1} , or the dimensionless coupling ξ needs to be much smaller than unity. One way to achieve this is to postulate that ϕ is charged under a gauge symmetry. In this case, any non-minimal operator linear in the dark matter field will contain additional fields to form a gauge singlet. This will be the case in section 5.3 discussing the inert doublet scenario.

5.2 Low-mass scalar singlet dark matter

Figures 5.2 and 5.3 show that for a scalar singlet dark matter candidate, experimental bounds on the non-minimal coupling parameter remain strong even in the low-mass region around a GeV. Therefore, it makes sense to extend the discussion of the previous section to even lower masses. The main difference at these energy scales is the visible sector matter content, described now by the Lagrangian (2.36). As demonstrated in section 4.1, this leads to the interaction terms (4.16). Mirroring the analysis of the previous section, one can explicitly compute the partial widths of a low-mass scalar singlet dark matter candidate. Among hadronic final states, the discussion will be limited to the $\pi^+\pi^-$ and $\pi^0\pi^0$ channels. Decays into more than two pions do occur, and their partial widths can be determined by expanding (2.37) to higher orders. However, the energy spectra of final-state particles in multibody decays are typically softer, and thus the strongest observational constraints can usually be derived on the basis of two-body decays. Explicitly, the

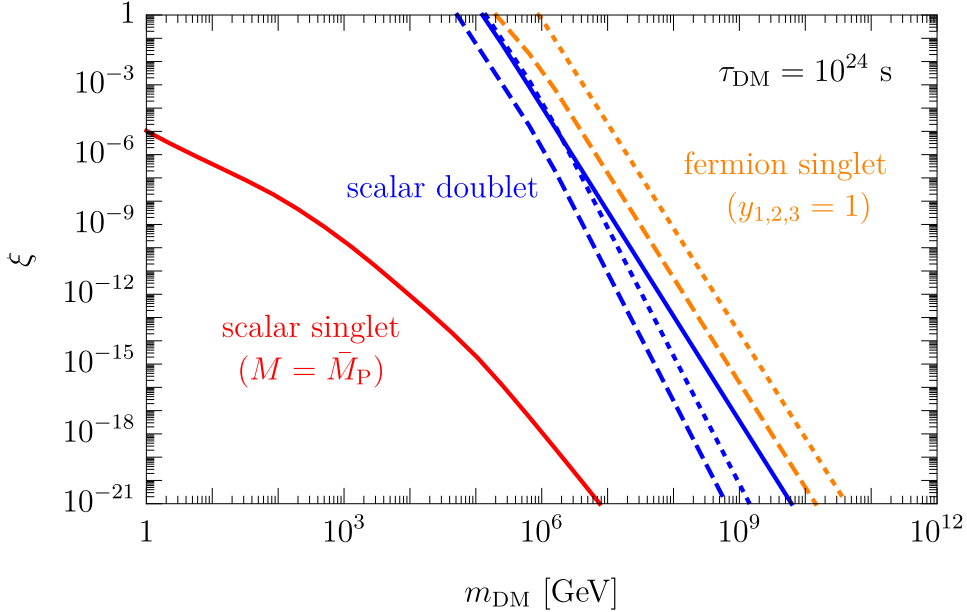


Figure 5.3: *Experimental upper bound on the non-minimal coupling parameter resulting from the requirement that the dark matter lifetime exceed 10^{24} s, for the scalar singlet candidate (red) as well as the scalar doublet (blue) and fermion singlet (orange) discussed in sections 5.3 and 5.4, respectively. Regions above the curves are excluded. For the scalar doublet, the continuous line corresponds to the CP-even component, while the dashed (dotted) line refers to the CP-odd component with $m_{\eta^0} = m_{A^0}$ ($5 m_{A^0}$). For the fermion singlet, the dashed (dotted) line corresponds to $m_{\eta^0} = m_\chi$ ($5 m_\chi$).*

rates for a scalar singlet decaying into pairs of pions read

$$\Gamma_{\phi \rightarrow \pi^+ \pi^-} = \frac{\bar{\xi}^2}{16\pi} \frac{m_\phi^3}{\bar{M}_P^2} (1 + 2x_{\pi^+})^2 (1 - 4x_{\pi^+})^{1/2}, \quad (5.17)$$

$$\Gamma_{\phi \rightarrow \pi^0 \pi^0} = \frac{\bar{\xi}^2}{32\pi} \frac{m_\phi^3}{\bar{M}_P^2} (1 + 2x_{\pi^0})^2 (1 - 4x_{\pi^0})^{1/2}, \quad (5.18)$$

analogously to the decay into a pair of Higgs bosons (5.7) at higher energies, while the rates for $\phi \rightarrow e^+ e^-$, $\phi \rightarrow \mu^+ \mu^-$ take the form (5.10). As in the previous section, the hat is dropped on the canonically normalized scalar field in the Einstein frame, $\phi \equiv \hat{\phi}$, the modified non-minimal coupling $\bar{\xi}$ is given by (5.6), and $x_i = m_i^2/m_\phi^2$. The three-body decays $\phi \rightarrow e^+ e^- \gamma$ and $\phi \rightarrow \mu^+ \mu^- \gamma$ with hard photons emitted directly from the vertex occur with the rate

$$\Gamma_{\phi \rightarrow f \bar{f} \gamma} = \frac{\bar{\xi}^2}{16\pi^2} \alpha \frac{m_\phi^3}{\bar{M}_P^2} g(x_f), \quad (5.19)$$

where

$$g(x) = (1 + 2x + 24x^2) \sqrt{1 - 4x} - 12x^2 (3 - 4x) \log\left(\frac{1 - 2x + \sqrt{1 - 4x}}{2x}\right). \quad (5.20)$$

Far from threshold, as $x \rightarrow 0$, $g(x)$ approaches unity. Finally, the scalar singlet can also decay into a pair of photons. At order α , this process receives contributions both from the effective

vertex in (4.16) and from loop diagrams involving charged particles. The full expression reads

$$\Gamma_{\phi \rightarrow \gamma\gamma} = \frac{\bar{\xi}^2}{16\pi} \frac{m_\phi^3}{\bar{M}_P^2} \left| F_\ell \left(\frac{m_\phi^2}{4m_e^2} \right) + F_\ell \left(\frac{m_\phi^2}{4m_\mu^2} \right) + F_\pi + c_{\gamma\gamma} \right|^2, \quad (5.21)$$

where the leptonic loop factor is given by

$$F_\ell(x) = \frac{e^2}{8\pi^2} x^{-2} (x + (x-1)f(x)), \quad (5.22)$$

with

$$f(x) = \begin{cases} \arcsin^2 \sqrt{x}, & x \leq 1, \\ -\frac{1}{4} \left(\log \frac{1+\sqrt{1-x^{-1}}}{1-\sqrt{1-x^{-1}}} - i\pi \right)^2, & x > 1. \end{cases} \quad (5.23)$$

The pion loop F_π will be neglected, as will the contributions of heavy hadrons within $c_{\gamma\gamma}$, as justified in section 4.1. In principle, decays into pairs of neutrinos also occur. As they are proportional to the neutrino mass squared, however, they are strongly suppressed at energies above the neutrino mass scale. Decays into a higher number of neutrinos, *e.g.* via intermediate vector bosons, $\phi \rightarrow Z^* Z^* \rightarrow \nu\bar{\nu}\nu\bar{\nu}$, do not carry this chiral suppression, but it was found numerically that they still cannot compete with the partial rates listed here explicitly. Figure 5.4 shows the partial widths of the relevant channels for $m_\phi \simeq 0.4\text{--}700$ MeV. At higher energies, the

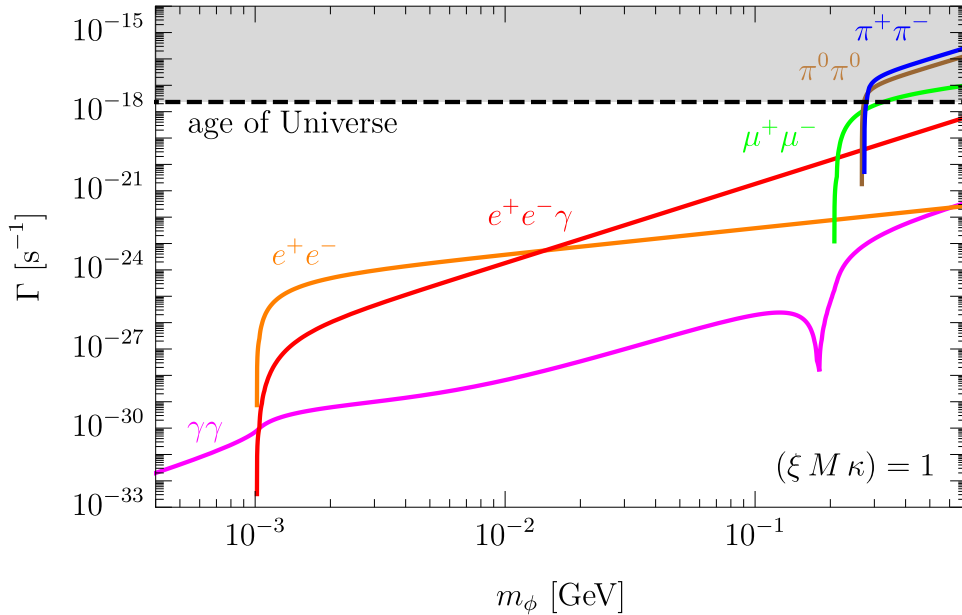


Figure 5.4: Partial widths of the scalar singlet at low dark matter masses, as well as the constraint on the total dark matter width derived from the age of the Universe.

description of pion physics through the chiral Lagrangian (2.37) breaks down and the formalism introduced here can no longer be used. The scaling of all partial rates with the non-minimal coupling is the same as in the high-mass scenario; notably, the rates cannot be arbitrarily enhanced by taking $(\xi M \kappa) \gg 1$. Similar to the situation at higher dark matter masses, two-body decays tend to dominate the total rate close to their respective kinematic thresholds. Between the

electron and muon resonances, the three-body decay $e^+e^-\gamma$ is important. (The corresponding channel involving muons, $\mu^+\mu^-\gamma$, is dwarfed by the partial rates for decay into pion pairs and does not appear on the figure.) Decays into pairs of photons are only relevant below the electron threshold. As figure 5.4 shows, for a non-minimal coupling of order unity, dark matter masses above twice the pion mass are excluded on the basis that a significant fraction of the primordial dark matter abundance would have decayed by now. At lower masses, the dark matter lifetime exceeds the age of the Universe. However, as in the previous section, stronger constraints can be derived from the absence of decay signals in the high-energy particle fluxes arriving at Earth.

Specifically, as demonstrated in [52], one can confront the expected differential photon flux from a decaying scalar singlet with observations of the isotropic diffuse gamma-ray and x-ray background. Decays into $\gamma\gamma$, $f\bar{f}\gamma$ and $\pi^0\pi^0$ final states result in especially relevant contributions to the prompt photon flux. The differential energy spectra for these channels read

$$\frac{dN_\gamma^{(\gamma\gamma)}}{dy_\gamma} = 2\delta\left(y_\gamma - \frac{1}{2}\right), \quad (5.24)$$

$$\frac{dN_\gamma^{(f\bar{f}\gamma)}}{dy_\gamma} = \frac{24}{g(x_f)} (1 + 2x_f - 2y_\gamma) y_\gamma \sqrt{1 - \frac{4x_f}{1 - 2y_\gamma}}, \quad (5.25)$$

$$\frac{dN_\gamma^{(\pi^0\pi^0)}}{dy_\gamma} = \frac{8}{\sqrt{1 - 4x_{\pi^0}}} \Theta(y_\gamma - y_-) \Theta(y_+ - y_\gamma), \quad (5.26)$$

where $y_\gamma = E_\gamma/m_\phi$, $y_\pm = (1 \pm \sqrt{1 - 4x_{\pi^0}})/4$, $g(x)$ was given in 5.20, and $\Theta(x)$ is the Heaviside step function. The first channel, relevant for dark matter masses below the electron threshold, produces monochromatic photons. These would be especially easy to differentiate from astrophysical backgrounds, which typically show a very smooth spectrum that can be well described by an inverse power law [93]. Dark matter decays into $\pi^0\pi^0$, on the other hand, result in a “gamma-ray box” [144] in the spectrum, since neutral pions decay into a pair of photons with a branching fraction of $\text{BR}(\pi^0 \rightarrow \gamma\gamma) \simeq 0.988$ [1]. This box will dominate the photon energy spectrum for dark matter masses above the pion threshold, $m_\phi \simeq 270\text{--}700$ MeV. (At these masses, the only other relevant decay mode, into charged pions, mainly produces electrons and neutrinos [1].) Finally, between the electron and pion thresholds, decays into $e^+e^-\gamma$ also produce hard photons. A detailed calculation of the resulting photon flux expected at Earth along the lines of [80, 78, 93] can be performed as described in section 2.2. Figure 5.5 shows this differential flux for three different dark matter masses, $m_\phi = 5, 50, 500$ MeV, together with the isotropic diffuse x-ray and gamma-ray background measured by INTEGRAL [137] and COMPTEL [138], EGRET [139] and Fermi-LAT [74], respectively.

For this figure, a non-minimal coupling of $(\xi M \kappa) = 1$ was assumed. For the photon flux, the contributions from $\gamma\gamma$, $e^+e^-\gamma$ and $\pi^0\pi^0$ were summed over, and the fluxes from the Milky Way halo, approximated by a Navarro-Frenk-White profile [9], and from cosmological dark matter were added (details can be found in section 2.2.) As a crude surrogate for detector response, a flat 10 % energy resolution was assumed across the entire energy range. As evident from the figure, above dark matter masses of a few MeV, the expected flux from dark matter decay alone would exceed the total measured isotropic diffuse photon spectrum, for a non-minimal coupling of order unity. Furthermore, the spectrum always features a sharp falloff close to the dark matter mass which would be easily detectable on top of smooth astrophysical backgrounds. Put another way, the absence of such spectral features in the measured fluxes implies stringent bounds on the value of the non-minimal coupling. Figure 5.6 shows the experimental upper limit on $(\xi M \kappa)$ from demanding that, in each individual energy bin of the data plotted in figure 5.5, the expected photon flux from dark matter decay alone does not exceed the total measured

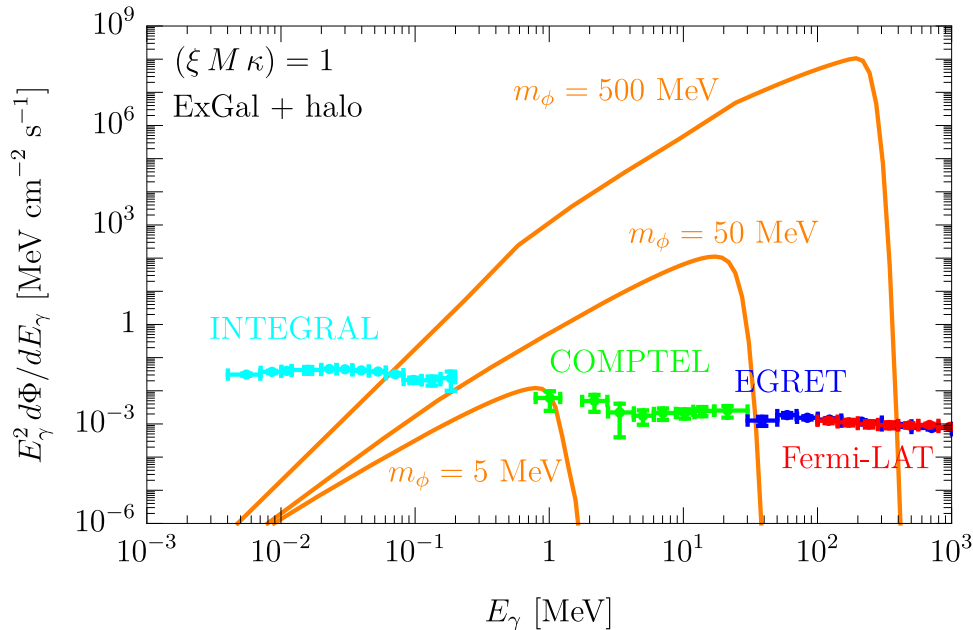


Figure 5.5: *Differential photon flux times energy squared from dark matter decay as a function of energy. Also shown are measurements of the isotropic diffuse x-ray and gamma-ray backgrounds. For this figure, the non-minimal coupling was set to unity, $(\xi M \kappa) = 1$.*

flux by more than twice the size of the experimental error, roughly corresponding to a two-sigma excess. Shaded areas are excluded. For this figure, the reported energy resolution of each experiment [145, 146, 147] was taken into account. As was the case for larger dark matter masses, the dark matter lifetime scales non-trivially with the non-minimal coupling (5.6). Therefore, in the limit $(\xi M \kappa) \rightarrow \infty$, the rates are only larger by a factor 7/6 compared to the case $(\xi M \kappa) = 1$. If this maximal value for the decay rate is allowed by the data, the experimental bounds lose all sensitivity to the non-minimal coupling, as can be seen around $m_\phi \simeq 2$ MeV in figure 5.6. Below the electron threshold, the expected spectral feature from dark matter decay into a pair of photons would be most striking. However, due to the loop suppression of this channel, the resulting photon flux is too low to be detectable in INTEGRAL data. Also shown in the figure is the CMB bound discussed in section 6.1.

5.3 Scalar (inert) doublet dark matter

The decay phenomenology of the CP -even component of the scalar doublet is very similar to that of the scalar singlet discussed in the previous section. Comparing the interaction Lagrangian (4.28) with that of the singlet (4.9), the mass scale M is identified with the standard model Higgs field plus its vacuum expectation value. Due to the presence of the Higgs field in the non-minimal operator, additional decay modes exist for the scalar doublet, with up to five particles in the final state. Table 5.2 lists all tree-level decay channels and their asymptotic scaling with the dark matter mass m_{η^0} . A common factor of $\xi^2 v^2 / \bar{M}_P^4$ has been omitted from the table. If the CP -odd component A^0 is the dark matter candidate, m_{η^0} has to be replaced by m_{A^0} in the right column, and an additional factor $(m_{A^0}/m_Z)^2$ appears in each channel, corresponding to the additional longitudinal Z boson in each final state. (For dark matter masses below m_Z , the Z is virtual.) Furthermore, strictly speaking, the resulting scaling with the dark

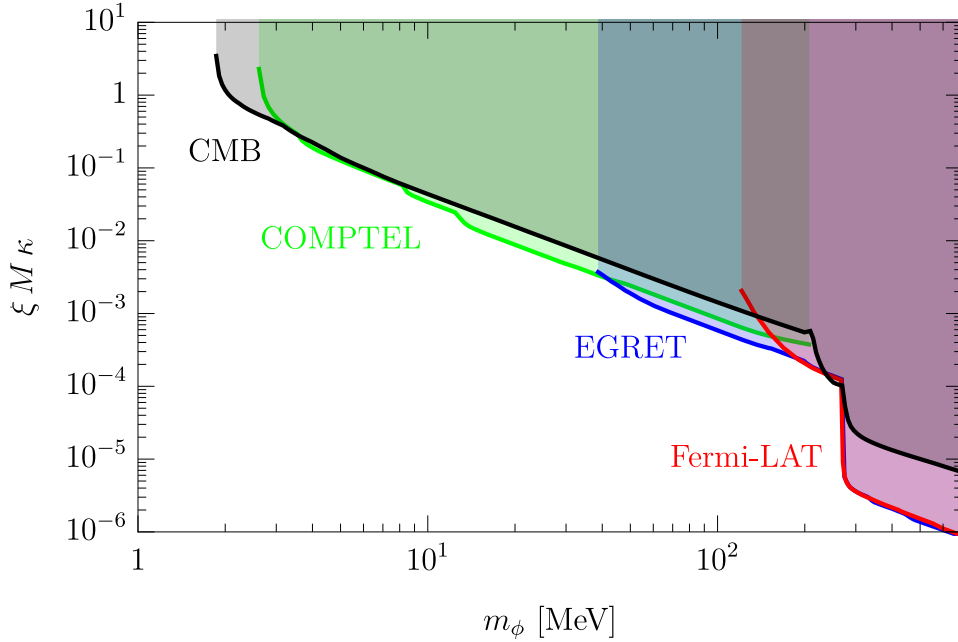


Figure 5.6: *Experimental constraints on the non-minimal coupling parameter in the low-mass scalar singlet scenario, from the absence of exotic excesses in the isotropic diffuse gamma-ray background and from CMB data.*

matter mass m_{A^0} applies only in the degenerate limit where both components of the doublet have similar mass, $m_{\eta^0} \simeq m_{A^0}$. In the decoupling limit, $m_{\eta^0} \gg m_{A^0}$, an additional suppression factor of $(m_{A^0}/m_{\eta^0})^4$ arises, as the propagator of the intermediate η^0 effectively shrinks to a point. Just as for the scalar singlet, decays into longitudinal vector bosons are expected to dominate the total rate once they are kinematically accessible.

The two-body partial widths of η^0 can be obtained by rescaling the corresponding rates for ϕ , (5.7) to (5.10), by a factor of $v^2/\bar{M}_\text{P}^2 \simeq 10^{-32}$. The same is true for the $\eta^0 \rightarrow q\bar{q}G, f\bar{f}\gamma, f'\bar{f}'W$ and $\phi \rightarrow f\bar{f}Z$ channels [51]. The decay modes $\eta^0 \rightarrow WWHH, ZZHH$ never contribute significantly to the total rate. Instead, the following channels are relevant:

$$\Gamma_{\eta^0 \rightarrow f_i \bar{f}_j WH} \simeq \frac{3\sqrt{2}\xi^2}{160(4\pi)^5} N_c^{(f_i)} |U_{ij}|^2 \frac{m_{\eta^0}^7 G_F}{\bar{M}_\text{P}^4}, \quad (5.27)$$

$$\Gamma_{\eta^0 \rightarrow f \bar{f} ZH} \simeq \frac{3\sqrt{2}\xi^2}{80(4\pi)^5} N_c^{(f)} (g_{f,V}^2 + g_{f,A}^2) \frac{m_{\eta^0}^7 G_F}{\bar{M}_\text{P}^4}, \quad (5.28)$$

$$\Gamma_{\eta^0 \rightarrow WWHHH} \simeq \frac{2\xi^2}{75(8\pi)^7} \frac{m_{\eta^0}^9}{\bar{M}_\text{P}^4 v^4}, \quad (5.29)$$

$$\Gamma_{\eta^0 \rightarrow ZZHHH} \simeq \frac{\xi^2}{75(8\pi)^7} \frac{m_{\eta^0}^9}{\bar{M}_\text{P}^4 v^4}, \quad (5.30)$$

in the limit of large dark matter masses compared to the electroweak scale. In terms of notation, the same conventions apply as in the scalar singlet case. Explicit computation of all partial widths of the CP -even scalar doublet result in the branching ratios shown in figure 5.7, which are again independent of the value of the non-minimal coupling ξ . The picture is very similar to that of figure 5.1, the only difference being the behavior at dark matter masses above around

Decay mode	Asymptotic scaling
$\eta^0 \rightarrow HH, WW, ZZ$	$m_{\eta^0}^3$
$\eta^0 \rightarrow f\bar{f}$	$m_{\eta^0} m_f^2$
$\eta^0 \rightarrow HHH$	$m_{\eta^0} v^2$
$\eta^0 \rightarrow WWH, ZZH$	$m_{\eta^0}^5/v^2$
$\eta^0 \rightarrow f\bar{f}H$	$m_{\eta^0}^3 m_f^2/v^2$
$\eta^0 \rightarrow f'\bar{f}'W, f\bar{f}Z$	$m_{\eta^0}^5/v^2$
$\eta^0 \rightarrow f\bar{f}\gamma, q\bar{q}G$	$m_{\eta^0}^3$
$\eta^0 \rightarrow HHHH$	$m_{\eta^0}^3$
$\eta^0 \rightarrow WWHH, ZZHH$	$m_{\eta^0}^7/v^4$
$\eta^0 \rightarrow f\bar{f}HH$	$m_{\eta^0}^5 m_f^2/v^4$
$\eta^0 \rightarrow f'\bar{f}'WH, f\bar{f}ZH$	$m_{\eta^0}^7/v^4$
$\eta^0 \rightarrow f\bar{f}\gamma H, q\bar{q}GH$	$m_{\eta^0}^5/v^2$
$\eta^0 \rightarrow HHHHH$	$m_{\eta^0}^5/v^2$
$\eta^0 \rightarrow WWHHH, ZZHHH$	$m_{\eta^0}^9/v^6$

Table 5.2: Tree-level decay modes of the CP -even scalar doublet dark matter candidate. Where applicable, m_f is the mass of the final-state fermion, while $v = 246$ GeV is the Higgs vacuum expectation value. If the CP -odd component A^0 is the dark matter candidate, $m_{\eta^0} \rightarrow m_{A^0}$ and an additional factor $m_{A^0}^2/m_Z^2$ arises for all partial widths, together with an additional Z boson in the final state. In the decoupling limit $m_{A^0} \ll m_{\eta^0}$, the rates are further multiplied by $(m_{A^0}/m_{\eta^0})^4$.

10^4 GeV. Even though the $WWHH$ and $ZZHH$ channels have the same $m_{\eta^0}^7$ -dependence on the dark matter mass as the $f'\bar{f}'WH$ and $f\bar{f}ZH$ ones (*cf.* table 5.2), the much larger number of fermionic degrees of freedom results in an enhancement of the latter. At even larger dark matter masses, $m_{\eta^0} \gtrsim 10^5$ GeV, the five-body decays $\eta^0 \rightarrow WWHHH, ZZHHH$ take over due to their enhanced phase-space factor.

As argued during the discussion of the scalar singlet scenario in section 5.1, a full analysis of the decay phenomenology of the scalar doublet at any given dark matter mass would require computing the total expected flux of photons, neutrinos, electrons and protons from dark matter decay. These fluxes could then be compared to the measured fluxes of these particles at Earth. As before, a rough estimate of the experimental bounds on the scalar doublet scenario set in this way can be obtained by summing over all partial widths and comparing the total lifetime of η^0 to the age of the Universe as well as a typical mass-independent limit $\tau_{\text{DM}} \gtrsim 10^{24}$ s. The total decay rate of the CP -even scalar doublet is approximately given by [51]

$$\Gamma_{\eta^0} \gtrsim \frac{\xi^2}{8\pi} \frac{m_{\eta^0}^3 v^2}{M_{\text{P}}^4} \times \begin{cases} 2n_q \frac{\alpha_s}{\pi}, & m_{\eta^0} \simeq 1\text{--}200 \text{ GeV}, \\ 1 + 2n_q \frac{\alpha_s}{\pi}, & m_{\eta^0} \simeq 0.2\text{--}1 \text{ TeV}, \\ \frac{3}{(2\pi)^2} \frac{m_{\eta^0}^2}{v^2}, & m_{\eta^0} \simeq 1\text{--}10 \text{ TeV}, \\ \frac{3}{5(4\pi)^4} \frac{m_{\eta^0}^4}{v^4}, & m_{\eta^0} \simeq 10\text{--}100 \text{ TeV}, \\ \frac{1}{25(8\pi)^6} \frac{m_{\eta^0}^6}{v^6}, & m_{\eta^0} \gtrsim 100 \text{ TeV}, \end{cases} \quad (5.31)$$

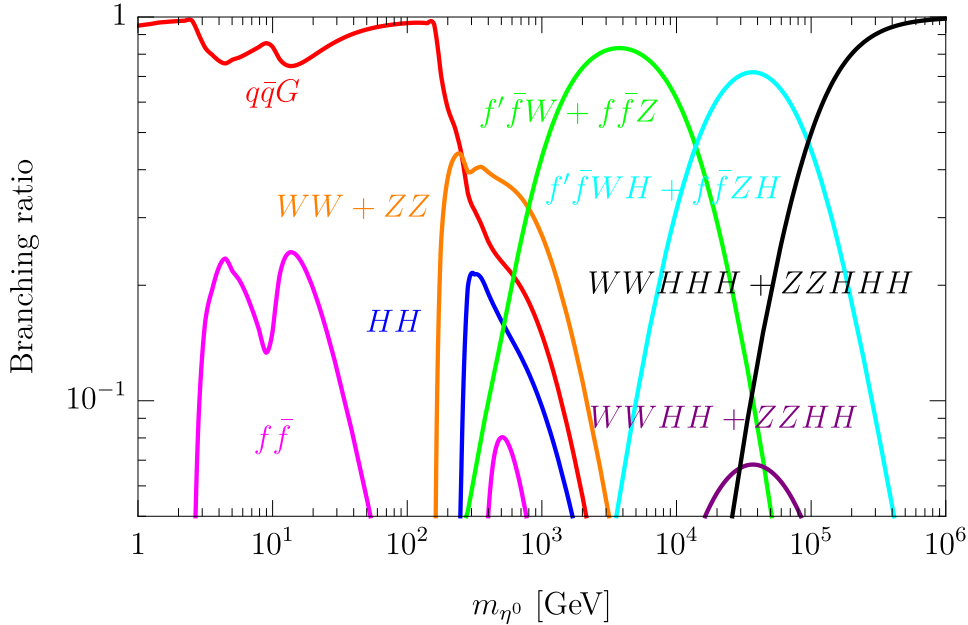


Figure 5.7: Branching ratios in the scalar doublet scenario as a function of the dark matter mass, at a fixed value of ξ . Decay channels with branching fractions below 5 % are not shown.

in analogy to the scalar singlet. The relative v^2/\bar{M}_P^2 suppression of the rate means that for similar values of the non-minimal coupling parameter ξ , the scalar doublet is much more long-lived than the scalar singlet. This can be seen on figure 5.8, which shows the lifetime of the CP -even scalar doublet for different values of the non-minimal coupling, together with the age of the Universe and the bound $\tau_{\text{DM}} \gtrsim 10^{24}$ s. The resulting constraints on the non-minimal coupling ξ can be found in figure 5.3. For a non-minimal coupling of order unity and a dark matter mass above 700 TeV, the dark matter lifetime is shorter than the age of the Universe. Moreover, the scalar doublet decays too quickly to be in agreement with observations for dark matter masses $m_{\eta^0} \gtrsim 100$ TeV. Compared to the scalar singlet, the scalar doublet is protected against decay via non-minimal coupling to gravity to some extent through its non-vanishing gauge charge, as it restricts the explicit form of the non-minimal operator (4.24) to include the Higgs doublet.

If the CP -odd component of the scalar doublet A^0 is the dark matter candidate, its decay phenomenology can be derived completely analogously. The modification of the decay amplitudes for A^0 was already discussed in section 4.2 and is given explicitly in appendix A.3. The resulting changes to table 5.2 are summarized in its caption. If the dark matter mass m_{A^0} lies either significantly below or significantly above the Z pole, the modification of the partial rates is universal and the branching ratios do not change notably from the CP -even case. The total lifetime of the CP -odd scalar doublet A^0 is compared to the age of the Universe and the flat estimate for an experimental bound, $\tau_{\text{DM}} \gtrsim 10^{24}$ s, in figure 5.9, for two different values of the mediator mass m_{η^0} . Figure 5.3 shows the resulting limit on the non-minimal coupling parameter ξ . For dark matter masses above m_Z , the presence of an additional longitudinal Z boson in the final state means that the total decay rate for the CP -odd component is slightly larger than in the CP -even case. This translates into somewhat stronger limits on the non-minimal coupling parameter. A coupling of order unity, for example, requires the dark matter mass to lie below 50 TeV in order to be consistent with observations, *cf.* figure 5.9.

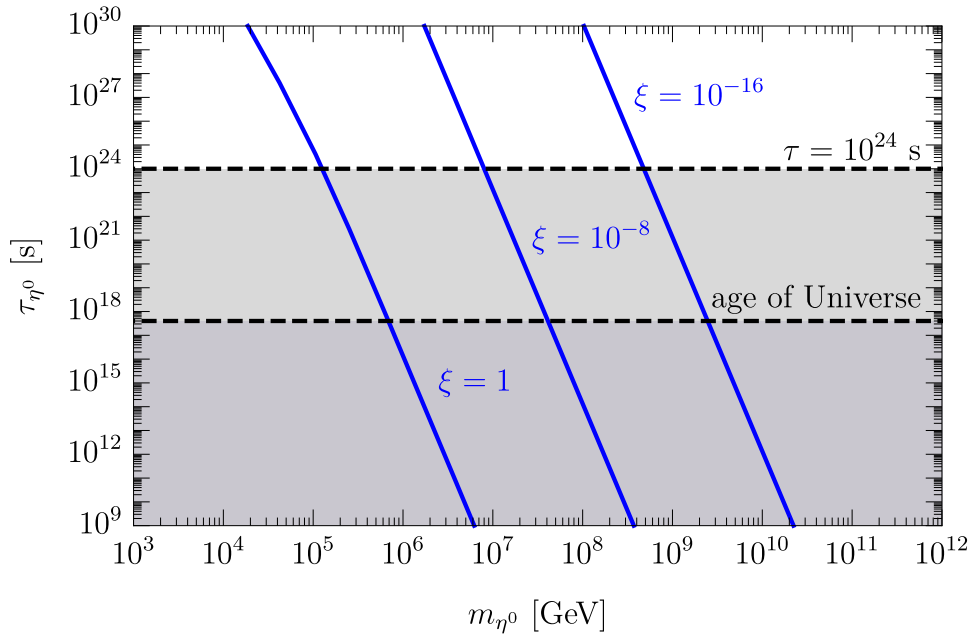


Figure 5.8: The total lifetime of the CP -even scalar doublet dark matter candidate, for different values of the non-minimal coupling ξ . Also shown are the observational constraints from the age of the Universe and the non-observation of exotic contributions to gamma-ray, neutrino or cosmic-ray fluxes at Earth, respectively.

However, this statement only holds with respect to the exclusive final states considered. With the aim of capturing the effects of all new point interaction vertices introduced through the non-minimal coupling, the analysis for the CP -even component considers up to five-body decays, while for the CP -odd one, also six-body final states have to be taken into account. Of course, in either scenario, additional final-state radiation of standard model particles can occur, if allowed kinematically, opening up decay modes with much higher particle multiplicity. At energies above the TeV scale, copious amounts of final-state radiation are expected to lead to logarithmic corrections to the decay rates [140, 141, 142, 143] and alter the resulting particle spectra [148]. A detailed study of the difference in total width of the CP -even and CP -odd components for this mass regime, however, is outside the scope of this thesis. Below the Z threshold, the situation is somewhat clearer. The vertex (4.29) is proportional to the weak gauge coupling; if there is no compensation by the phase-space factor, this leads to an overall suppression in all partial widths. Therefore, the bounds on the CP -even scenario are stronger in this mass region. In figure 5.3, however, this regime falls into a region where the data cannot constrain the non-minimal coupling to be less than unity, and is therefore not shown. Figure 5.9 also shows the dependence of the total lifetime on the ratio between the masses of the two components of the scalar doublet. A heavy mediator η^0 leads to a suppression of all partial rates by $(m_{A^0}/m_{\eta^0})^4$ and weakens the limit on the non-minimal coupling accordingly, cf. figure 5.3.

5.4 Fermionic dark matter

As outlined in section 4.3, a fermion singlet is another popular dark matter candidate. The interaction Lagrangian (4.33) leads to the same decay channels as for the scalar doublet, with

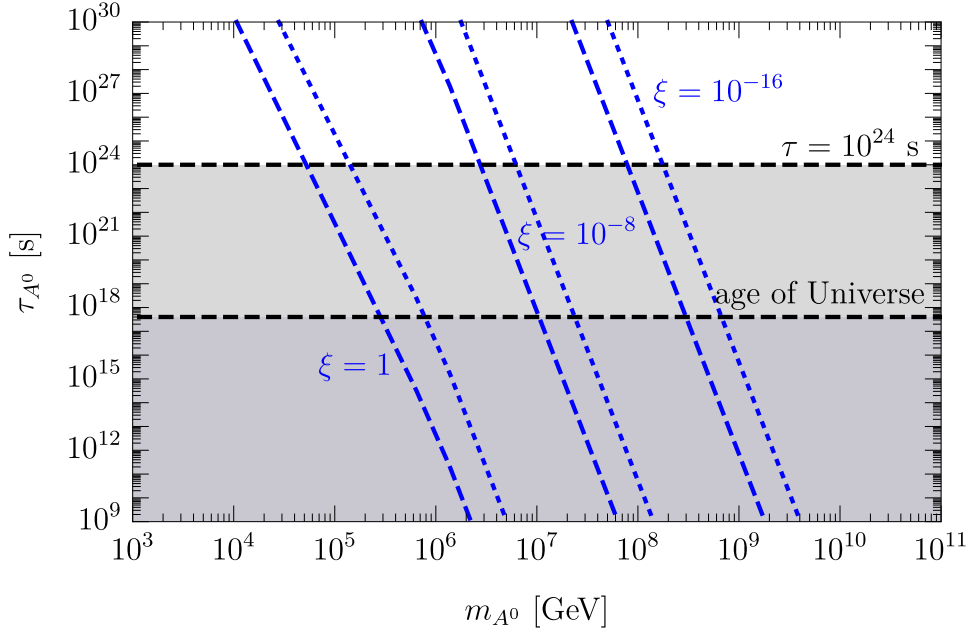


Figure 5.9: The total lifetime of the CP-odd scalar doublet dark matter candidate, for different values of the non-minimal coupling ξ . Dashed and dotted lines correspond to a mediator mass of $m_{\eta^0} = m_{A^0}, 5m_{A^0}$, respectively. Also shown are the observational constraints from the age of the Universe and the non-observation of exotic contributions to gamma-ray, neutrino or cosmic-ray fluxes at Earth.

an additional neutrino in each final state. Table 5.3 lists all tree-level decay modes. The right column shows the asymptotic dependence of the individual partial widths on the dark matter mass m_χ . A common prefactor $\xi^2 v^2 M^{-4} \bar{M}_P^{-4}$ as well as phase-space factors have been omitted. The partial rates for three-body decays can be given analytically:

$$\Gamma_{\chi \rightarrow HH\nu} \simeq \frac{\xi^2}{15(16\pi)^3} \frac{m_\chi^7 v^2}{M^4 \bar{M}_P^4} g_1(x_H), \quad (5.32)$$

$$\Gamma_{\chi \rightarrow WW\nu} \simeq \frac{2\xi^2}{15(16\pi)^3} \frac{m_\chi^7 v^2}{M^4 \bar{M}_P^4} g_2(x_W), \quad (5.33)$$

$$\Gamma_{\chi \rightarrow ZZ\nu} \simeq \frac{\xi^2}{15(16\pi)^3} \frac{m_\chi^7 v^2}{M^4 \bar{M}_P^4} g_2(x_Z), \quad (5.34)$$

$$\Gamma_{\chi \rightarrow f\bar{f}\nu} \simeq \frac{2\xi^2}{3(16\pi)^3} N_c^{(f)} \frac{m_\chi^7 v^2}{M^4 \bar{M}_P^4} x_f g_3(x_f), \quad (5.35)$$

where the same notation conventions as in the scalar singlet case apply [51]. The rates for all three neutrino flavors have been added, and $\xi^2 \equiv \sum_j \xi_j^2$. The phase-space functions $g_{1,2,3}$ are

Decay mode	Asymptotic scaling
$\chi \rightarrow HH\nu, WW\nu, ZZ\nu$	m_χ^7
$\chi \rightarrow f\bar{f}\nu$	$m_\chi^5 m_f^2$
$\chi \rightarrow HHH\nu$	$m_\chi^5 v^2$
$\chi \rightarrow WWH\nu, ZZH\nu$	m_χ^9/v^2
$\chi \rightarrow f\bar{f}H\nu$	$m_\chi^7 m_f^2/v^2$
$\chi \rightarrow f'\bar{f}'W\nu, f\bar{f}Z\nu$	m_χ^9/v^2
$\chi \rightarrow f\bar{f}\gamma\nu, q\bar{q}G\nu$	m_χ^7
$\chi \rightarrow HHHH\nu$	m_χ^7
$\chi \rightarrow WWHH\nu, ZZHH\nu$	m_χ^{11}/v^4
$\chi \rightarrow f\bar{f}HH\nu$	$m_\chi^9 m_f^2/v^4$
$\chi \rightarrow f'\bar{f}'WH\nu, f\bar{f}ZH\nu$	m_χ^{11}/v^4
$\chi \rightarrow f\bar{f}\gamma H\nu, q\bar{q}GH\nu$	m_χ^9/v^2
$\chi \rightarrow HHHHH\nu$	m_χ^9/v^2
$\chi \rightarrow WWHHH\nu, ZZHHH\nu$	m_χ^{13}/v^6

Table 5.3: Tree-level decay modes of the fermion singlet dark matter candidate. Where applicable, m_f is the mass of the final-state fermion, while $v = 246 \text{ GeV}$ is the Higgs vacuum expectation value.

given by

$$g_1(x) = (1 + 7x - 44x^2 + 810x^3 - 1260x^4)(1 - 4x)^{1/2} - 120x^3(5 - 17x + 21x^2)\log f(x), \quad (5.36)$$

$$g_2(x) = (1 - 13x + 156x^2 + 450x^3 - 540x^4)(1 - 4x)^{1/2} - 120x^3(5 - 9x + 9x^2)\log f(x), \quad (5.37)$$

$$g_3(x) = (1 - 22x - 42x^2 + 36x^3)(1 - 4x)^{1/2} + 24x^2(3 - 4x + 3x^2)\log f(x), \quad (5.38)$$

where

$$f(x) = \frac{1 - 2x + (1 - 4x)^{1/2}}{2x}. \quad (5.39)$$

Partial widths for decay modes with more than three particles in the final state can only be computed numerically. If the dark matter mass lies above the electroweak scale, the relevant

ones can be approximated by [51]

$$\Gamma_{\chi \rightarrow q\bar{q}G\nu} \simeq \frac{\xi^2}{25(4\pi)^4} \alpha_s \frac{m_\chi^7 v^2}{M^4 \bar{M}_P^4}, \quad (5.40)$$

$$\Gamma_{\chi \rightarrow f_i \bar{f}_j W\nu} \simeq \frac{\xi^2}{20(8\pi)^5} N_c^{(f_i)} |U_{ij}|^2 \frac{m_\chi^9}{M^4 \bar{M}_P^4}, \quad (5.41)$$

$$\Gamma_{\chi \rightarrow f\bar{f}Z\nu} \simeq \frac{\xi^2}{10(8\pi)^5} N_c^{(f)} (g_{f,V}^2 + g_{f,A}^2) \frac{m_\chi^9}{M^4 \bar{M}_P^4}, \quad (5.42)$$

$$\Gamma_{\chi \rightarrow f_i \bar{f}_j WH\nu} \simeq \frac{\sqrt{2}\xi^2}{175(8\pi)^7} N_c^{(f_i)} |U_{ij}|^2 \frac{m_\chi^{11} G_F}{M^4 \bar{M}_P^4}, \quad (5.43)$$

$$\Gamma_{\chi \rightarrow f\bar{f}ZH\nu} \simeq \frac{2\sqrt{2}\xi^2}{175(8\pi)^7} N_c^{(f)} (g_{f,V}^2 + g_{f,A}^2) \frac{m_\chi^{11} G_F}{M^4 \bar{M}_P^4}, \quad (5.44)$$

$$\Gamma_{\chi \rightarrow WWHHH\nu} \simeq \frac{\xi^2}{6300(8\pi)^9} \frac{m_\chi^{13}}{v^4 M^4 \bar{M}_P^4}, \quad (5.45)$$

$$\Gamma_{\chi \rightarrow ZZHHH\nu} \simeq \frac{\xi^2}{12600(8\pi)^9} \frac{m_\chi^{13}}{v^4 M^4 \bar{M}_P^4}, \quad (5.46)$$

while the remaining modes listed in table 5.3 have branching ratios below 5 % throughout the entire mass range under discussion. Figure 5.10 shows the branching fractions of the fermion singlet dark matter candidate for a fixed value of ξ^2/M^4 . They are very similar to those of the

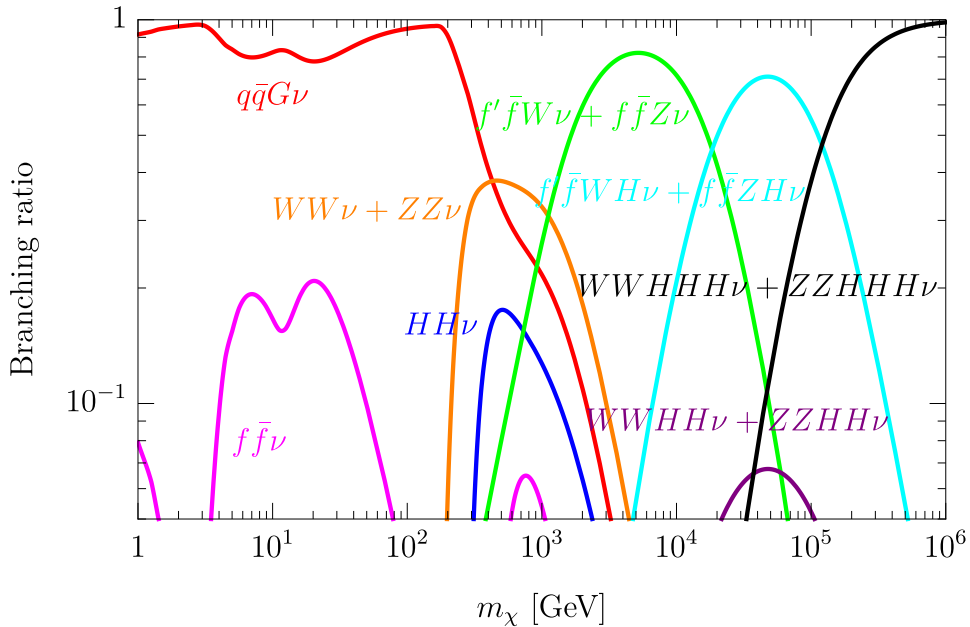


Figure 5.10: Branching ratios in the fermion singlet scenario as a function of the dark matter mass, at a fixed value of ξ^2/M^4 . Decay channels with branching fractions below 5 % are not shown.

scalar doublet (*cf.* section 5.3), the biggest difference being the extra neutrino emitted in every dark matter decay. As before, at any given dark matter mass, only a handful of decay modes are responsible for most dark matter decays. Therefore, the total width of the fermion singlet

can be approximated as [51]

$$\Gamma_\chi \gtrsim \frac{4\xi^2}{15(16\pi)^3} \frac{m_\chi^7 v^2}{M^4 M_{\text{P}}^4} \times \begin{cases} \frac{12}{5} n_q \frac{\alpha_s}{\pi}, & m_\chi \simeq 1\text{--}200 \text{ GeV}, \\ 1 + \frac{12}{5} n_q \frac{\alpha_s}{\pi}, & m_\chi \simeq 0.2\text{--}1 \text{ TeV}, \\ \frac{3}{8\pi^2} \frac{m_\chi^2}{v^2}, & m_\chi \simeq 1\text{--}10 \text{ TeV}, \\ \frac{6}{35(4\pi)^4} \frac{m_\chi^4}{v^4}, & m_\chi \simeq 10\text{--}100 \text{ TeV}, \\ \frac{1}{140(8\pi)^6} \frac{m_\chi^6}{v^6}, & m_\chi \gtrsim 100 \text{ TeV}, \end{cases} \quad (5.47)$$

in analogy to expressions (5.16) and (5.31) for the scalar dark matter candidates. What is immediately evident is the additional M^{-4} suppression compared to the scalar doublet scenario. This results from the fact that the lowest-dimensional effective operator for a fermion singlet allowed by symmetry (4.31) is of mass dimension six. As the effective theory is only valid at energies below M , a non-minimally coupled fermion is generically longer-lived by a factor M^4/m_{DM}^4 compared to a scalar dark matter candidate of the same mass. As the dark matter mass approaches the cutoff scale of the effective theory, one needs to specify an ultraviolet completion. In the model introduced in section 4.3, a heavy scalar doublet η is responsible for generating (4.31) through renormalizable interactions, and the cutoff scale M is related to the scalar mass via (4.38). The partial widths of the fermion singlet in this extended theory can be computed straightforwardly according to (4.37).

The total decay rate of the fermion singlet is compared with observational bounds in figure 5.11, both in the degenerate limit where $m_{\eta^0} \simeq m_\chi$ and for $m_{\eta^0} = 5 m_\chi$, where the effective theory description applies. For the plot, the Yukawa couplings of the scalar doublet η to the three neutrino species is set to unity, $y_{1,2,3} = 1$. Figure 5.3, in turn, shows the upper bound on the value of the non-minimal coupling parameter ξ resulting from the requirement that the lifetime is $\tau_\chi \gtrsim 10^{24}$ s. In the degenerate limit $m_{\eta^0} \simeq m_\chi$, a non-minimal coupling of order unity is in agreement with observations for dark matter masses below 200 TeV. In contrast, for a very heavy dark matter candidate of mass 10^9 GeV, the dimensionless non-minimal coupling needs to be significantly smaller, $\xi \lesssim 10^{-16}$. Increasing the mass of the scalar mediator weakens the bounds on ξ , as the dark matter lifetime scales roughly as $m_{\eta^0}^4/m_\chi^4$ away from threshold. Similar to the case of the scalar doublet dark matter candidate, the experimental bounds on the non-minimal coupling of the fermion singlet are significantly weaker than those on the scalar singlet scenario. The decay rates are suppressed by several powers of both the Planck mass and the cutoff scale of the effective operator. This suppression is only overcome for very heavy dark matter candidates.

5.5 Higher-order corrections

A few remarks have to be made concerning the role of higher-order corrections to the decay rates computed in this chapter. Through the non-minimal coupling to gravity, a number of new interaction vertices are introduced that contain up to seven fields, depending on the spin of the dark matter particle. Computing two-body decays at lowest order in perturbation theory is straightforward. However, already for the three-body decays of the scalar singlet dark matter candidate, there is some non-trivial interference with its two-body channels. Fundamentally, this behavior is due to the multiplicative structure of the non-minimal coupling, which induces decay vertices that are proportional to the product of the gravity portal coupling and standard model parameters.

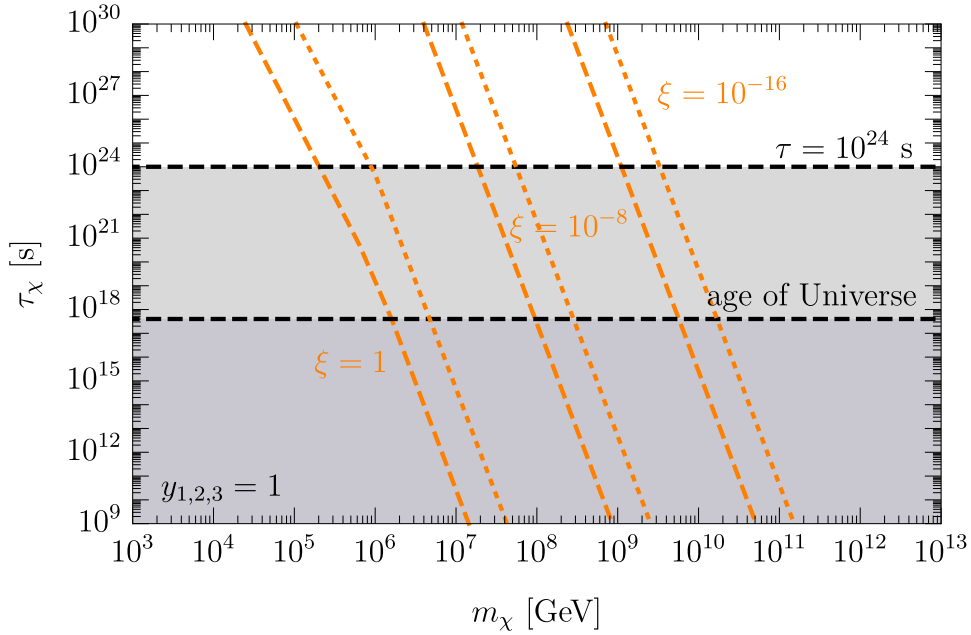


Figure 5.11: The total lifetime of the fermion singlet dark matter candidate, for different values of the non-minimal coupling ξ . The dashed (dotted) line corresponds to a mediator mass of $m_{\eta^0} = m_\chi$ ($5m_\chi$). Also shown are the observational constraints from the age of the Universe and the non-observation of exotic contributions to gamma-ray, neutrino or cosmic-ray fluxes at Earth, respectively.

As an example, consider the decay $\phi \rightarrow f\bar{f}\gamma$. As illustrated in figure 5.12, at order $\xi^2 \alpha$, this decay proceeds through both the point-interaction vertex directly and through the three-particle vertex $f\bar{f}\phi$ with final-state photons emitted from the external legs. Moreover, for photon

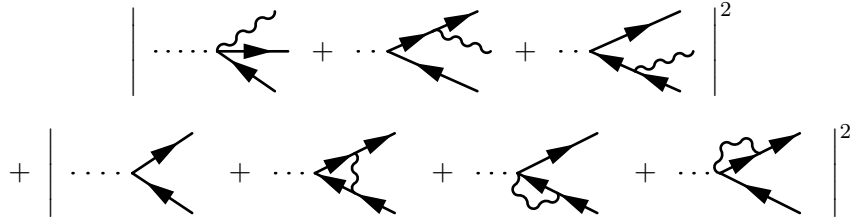


Figure 5.12: Decay of the scalar singlet dark matter candidate at order $\xi^2 \alpha$.

energies below the detector threshold, the three-body final state cannot be distinguished from the two-body decay into fermions only. Therefore, there is further interference from the one-loop diagrams for the process $\phi \rightarrow f\bar{f}$. In practice, however, the bremsstrahlung diagrams, as well as the one-loop corrections to the two-body decay can be neglected: as all these diagrams are proportional to the $f\bar{f}\phi$ vertex, they carry a suppression by the fermion mass compared to the four-point vertex. Numerical checks show that while their contribution is comparable at energies around the kinematic threshold, for higher energies the decay rate is dominated by the point-interaction term. (This is also to be expected from figure 5.4, where the rates for $\phi \rightarrow f\bar{f}$ and $\phi \rightarrow f\bar{f}\gamma$ are computed from the four-point vertices only.) Moreover, from a phenomenological perspective, the astrophysical gamma-ray flux decreases roughly with the photon energy squared, cf. figure 5.5. Thus, one is primarily interested in hard photons, which again mostly originate

from the point-interaction term. The bremsstrahlung diagrams are responsible for the soft photon spectrum instead, as illustrated in figure 5.13, since in this kinematic region, the fermion propagator is nearly on shell. A similar behavior is found for the decay modes with massive

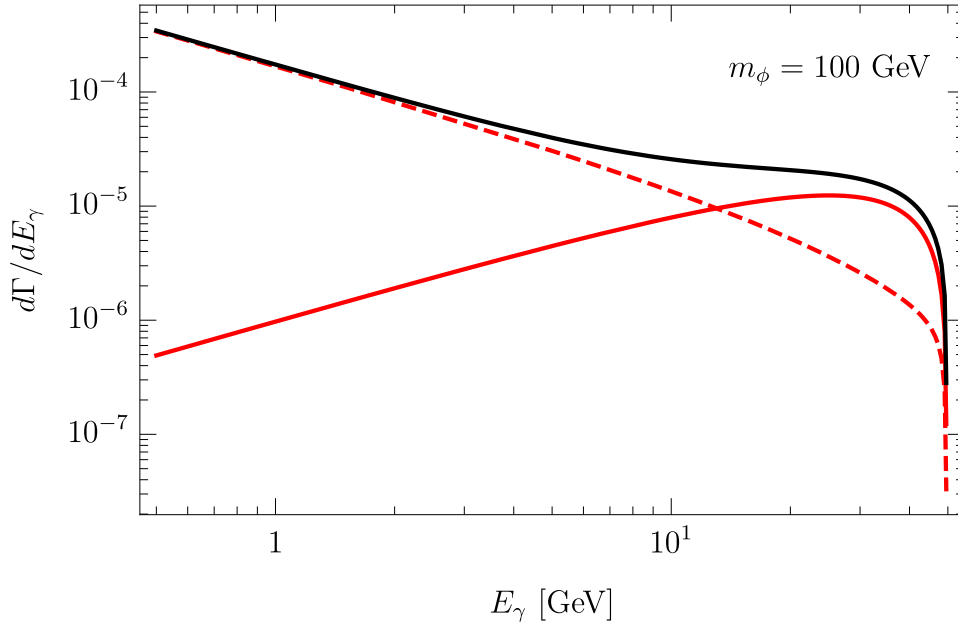


Figure 5.13: Photon spectrum for the decay $\phi \rightarrow b\bar{b}\gamma$. The solid (dashed) red line shows the spectrum of the point-interaction vertex (the bremsstrahlung diagrams) only, the black line shows the total spectrum including diagram interference.

gauge bosons in the final state: also here, the rate is dominated by the single point-interaction diagram soon above threshold, and the remaining diagrams can be omitted to speed up the numerical computations.

A somewhat different picture emerges for the decay into three Higgs bosons. Here, the contribution of diagrams with final-state Higgs radiation outweighs the single four-point vertex. This is due to the E^2 -scaling of the $HH\phi$ vertex compared to the $HHH\phi$ interaction (*cf.* appendix (A.1)), leading to a partial width that scales like $\Gamma_{\phi \rightarrow HHH} \propto m_\phi^3$ when including all diagrams, in contrast to the entry in table 5.1. The final-state Higgs radiation, however, can also be interpreted as a correction to the lowest-order $\phi \rightarrow HH$ rate, which already shows the m_ϕ^3 scaling. The impact of diagram interference is again minimal, due to the different mass scaling of the two types of diagrams. Finally, multi-body decays into final states with two gauge bosons also receive contributions from a large number of diagrams, *e.g.* two-body decays into off-shell Higgs bosons or vector bosons and three-body decays with final-state radiation. Numerical checks show that including all diagrams in the computation of the partial width leads to relative changes in the rate of at most order unity. The scaling of the partial rate with the dark matter mass remains the same as the one reported in table 5.1, however, and the increase in accuracy comes at the cost of significantly increased computational effort. In keeping with the exploratory nature of the calculations of chapter 5, the accuracy achieved by considering the single point-interaction vertex only for each partial rate is deemed sufficient, for each of the dark matter scenarios discussed.

Chapter 6

Constraints from cosmology

Chapter 5 discussed potential signals in present-day particle fluxes at Earth of a non-minimally coupled dark matter candidate. Complementary information can be gained by studying the impact of such a dark matter particle on other observables throughout cosmic history. The next sections will discuss its effect on the cosmic microwave background as well as the possibility of producing dark matter in the early Universe through a non-minimal coupling to gravity.

6.1 Constraints from the cosmic microwave background

The cosmic microwave background presents a unique observational window into the early Universe. Emitted around redshift $z \simeq 1100$, when protons and electrons in the primordial plasma had finally cooled down enough to form neutral hydrogen atoms, it provides a detailed snapshot of the cosmic matter distribution at a time when the Universe was only a few hundred thousand years old [4]. As a powerful probe of the thermal history of our Universe, it tests the Λ CDM cosmological model and any modifications or extensions of it. More specifically, any exotic source of energy injection during the cosmic dark ages (between recombination and reionization of the cosmic fluid) would modify both the CMB blackbody spectrum and its anisotropy spectrum [149, 150, 151, 152]. Dark matter annihilations or decays during this period, for example, would produce highly energetic particles that could subsequently decay into stable standard model degrees of freedom. These, in turn, would heat, excite and ionize the neutral hydrogen gas, altering the thermal history of our Universe and the CMB data with it. In the literature, the impact of injecting high-energy photons, electrons and positrons into the cosmic fluid has been studied extensively [153, 154], and also the smaller effect of protons and antiprotons has been quantified [155]. More recently, a set of interpolation tables has been provided that describe in detail the impact of photons, electrons and positrons created at arbitrary redshift, taking into account delayed absorption as well as redshift-dependent absorption efficiency of the intergalactic medium [156]. These tables allow one to robustly estimate the effect of any conventional model of annihilating or decaying dark matter on the cosmic microwave background. As there is currently no evidence for any additional energy injection during the cosmic dark ages, the precise measurements by the Planck satellite [5] allow one to place stringent bounds on dark matter annihilation or decay.

Interestingly, the distortion of the CMB anisotropy spectrum typically has the same shape for different dark matter models [157, 158]. Therefore, to good approximation, the impact of a generic model can be encoded by a single number measuring the overall normalization of this distortion. Once this normalization factor has been computed for a fixed reference model and the corresponding experimental bound on the dark matter lifetime or scattering cross section

has been found, one can robustly estimate the constraint on any other model by computing a “detectability parameter” g_{eff} that rescales the bound appropriately, as demonstrated in [157, 158] based on principal component analysis. Comparing the results of this approximation with exact bounds derived via a Markov Chain Monte Carlo (MCMC) procedure for a variety of benchmark points, it was found that the deviation lies within 10 % [157].

The detectability parameter g_{eff} , in turn, is determined in the following way: first, both the reference model and the dark matter model under discussion are decomposed into weighted sums of basis injection models. These injection models are characterized by a fixed particle species (photons or electron-positron pairs), injected with a fixed energy E , at a fixed redshift z . Then, the overall effect of each of the two models on the cosmic microwave background can be determined by reweighing the coefficients of these sums by an efficiency function $f_i(\tau_{\text{DM}}, E)$, where $i = \gamma, e$, that describes the impact of the injected particles, depending on the lifetime of the decaying dark matter particle τ_{DM} and the injection energy E . The detectability parameter g_{eff} of the dark matter model under discussion, finally, is simply the ratio of the two overall normalization constants.

In practice, as the first step, one has to compute the energy spectrum of electrons, positrons and photons produced through dark matter decay or annihilations. This corresponds to taking the continuum limit in the decomposition of the dark matter model into basis injection models. As discussed in section 5.2, for a sub-GeV scalar singlet dark matter candidate with a non-minimal coupling to gravity, the relevant tree-level decay modes are those into $\gamma\gamma$, e^+e^- , $e^+e^-\gamma$, $\mu^+\mu^-$, $\mu^+\mu^-\gamma$, $\pi^0\pi^0$ and $\pi^+\pi^-$. To obtain the electron and photon energy spectra for the latter four channels, subsequent decays of the muons and pions produced in the initial process have to be taken into account, *e.g.* through the procedure discussed in appendix E. Then, for a fixed dark matter mass m_ϕ , the total energy spectrum of particle $i = \gamma, e$ (where e corresponds to either an electron or a positron) is given by the sum over all relevant final states f , weighted by their branching ratios,

$$\frac{dN_i}{dE}(m_\phi, E) = \sum_f \left(\text{BR}(\phi \rightarrow f) \Big|_{m_\phi} \times \left(\frac{dN_i}{dE} \right)_f(m_\phi, E) \right). \quad (6.1)$$

Next, the relative impact of electron-positron pairs and photons at different energies on the cosmic microwave background is taken into account by convolving the spectra with the effective-detectability functions $f_i(\tau_{\text{DM}}, E)$ supplied together with [156],

$$g_i(m_\phi) = \int_{m_i}^{m_\phi/2} dE \frac{E}{m_\phi} \frac{dN_i}{dE}(m_\phi, E) f_i(10^{25} \text{ s}, E). \quad (6.2)$$

If the lifetime of the dark matter candidate exceeds the age of the Universe, the dependence of the detectability functions f_i on τ_{DM} is only minor. Therefore, a constant value of 10^{25} s can be plugged into the above expression, in light of the bounds on τ_{DM} derived below. In [157], the precise effect of injecting electron-positron pairs or photons at several fixed benchmark values for their kinetic energy was determined based on the MCMC approach. Planck 2015 data [5] was then used to place the corresponding lower bounds on the dark matter lifetime. For example, for a decaying dark matter particle injecting electron-positron pairs of 100 MeV kinetic energy each, $\tau_{\text{DM}} \gtrsim 2.31 \times 10^{25}$ s, while for dark matter decaying into pairs of photons, $\tau_{\text{DM}} \gtrsim 0.35 \times 10^{25}$ s, at 95 % confidence level [157]. An estimate of the bound on the non-minimally coupled scalar singlet scenario can be found by rescaling these limits appropriately,

$$\tau_\phi(m_\phi) \gtrsim 10^{25} \text{ s} \times \left(2.31 \times \frac{g_e(m_\phi)}{g_e^{(\text{ref})}} + 0.35 \times \frac{g_\gamma(m_\phi)}{g_\gamma^{(\text{ref})}} \right), \quad (6.3)$$

where the detection efficiency parameters of the reference models are

$$g_e^{(\text{ref})} = g_e(201 \text{ MeV}) \Big|_{\phi \rightarrow e^+e^-}, \quad g_\gamma^{(\text{ref})} = g_\gamma(200 \text{ MeV}) \Big|_{\phi \rightarrow \gamma\gamma}, \quad (6.4)$$

corresponding to injection of monoenergetic electron-positron or photon pairs, respectively. Given the expressions for the partial widths of the scalar singlet listed in section 5.2, one can translate this experimental limit on the dark matter lifetime into a constraint on the non-minimal coupling parameter. Figure 5.6 shows this constraint together with the limits derived from the non-observation of exotic signals in the gamma-ray flux at Earth. For most dark matter masses, the CMB constraint is marginally weaker than those derived from present-day gamma-ray data, the only exception being the narrow mass window around $m_\phi \simeq 2\text{--}3$ MeV. Therefore, the CMB data do not preclude an upcoming experiment like e-ASTROGAM [159] observing a spectral feature from dark matter decay in the photon flux at Earth.

6.2 Constraints from dark matter production

As demonstrated in section 3.2, the presence of a non-minimal coupling of dark matter to gravity results, after a transformation into the Einstein frame, in a coupling to the matter energy-momentum tensor. Thus, a large number of effective operators connecting the visible and the dark sector are introduced simultaneously, with correlated Wilson coefficients whose size is determined by the gravity portal coupling ξ . In the early Universe, these can serve to populate the dark sector from the visible sector thermal bath. Whether the present-day dark matter abundance is indeed set by these non-minimal gravitational interactions or not, however, depends on whether there are other types of relevant couplings. For any kind of dark matter produced in the early Universe, its present-day relic abundance is typically set by whatever type of interaction is strongest at early cosmic times. Thus, in order for gravitational interactions to be relevant, other couplings between the dark and visible sector have to be heavily suppressed, *e.g.* due to some symmetry that is only broken by gravity. If this is indeed the case and dark matter interacts only gravitationally with the visible sector, then a WIMP-like freeze-out production in the early Universe is not possible, due to the minute strength of gravitational interactions. If the dark matter particles ever were in thermal equilibrium with the standard model, gravitationally suppressed freeze-out would occur very early and the present-day number density would be unacceptably high [4]. Instead, a relic abundance could have been created via the freeze-in mechanism [31] sketched in section 2.3.

In [160, 161, 162], thermal gravitational dark matter production in the early Universe was studied in detail, in a minimal coupling scenario. Depending on the value of the reheating temperature, the dark matter mass and, to a lesser extent, the spin of the dark matter particle, a relic abundance in accordance with observations can be produced via tree-level graviton exchange, arising from minimal gravitational coupling between the dark and visible sector.

Additionally allowing for a non-minimal coupling of a dark matter field φ to gravity introduces new effective operators, the lowest-dimensional of which have the form (3.4), where the tensor structure of the coupling depends on the specific dark matter scenario. After a transformation into the Einstein frame, these lead to an infinite tower of operators with an increasing number of external dark matter legs, multiplicatively coupled to standard model operators,

$$\sum_{k=1}^{\infty} (\xi \kappa^2 f(\varphi, \{X_{\text{vis}}\}))^k \times \mathcal{O}_{\text{SM}}, \quad (6.5)$$

and suppressed by increasing powers of the Planck mass as well as the non-minimal coupling parameter. (In the expression above, Lorentz indices have been omitted for clarity.) Interestingly, the Planck-mass suppression of the leading effective operators induced this way is \bar{M}_P^{-2} , the same as for the lowest-order graviton mediated processes from minimal coupling. Therefore, the relative strength of interactions induced by the non-minimal operators of (3.4) compared to graviton scattering entirely depends on the value of the gravity portal coupling ξ .

An exception arises only in the scalar singlet scenario. Here, the leading non-minimal operators conserving Lorentz and gauge symmetry are

$$\mathcal{L}_\xi = -\xi^{(1)} M R \phi - \xi^{(2)} R \phi^2. \quad (6.6)$$

The linear $\xi^{(1)}$ -term, allowed only for scalar, uncharged dark matter, results in amplitudes suppressed by a factor M/\bar{M}_P^2 . Therefore, if the scalar mass scale is large enough (*e.g.* $M \simeq \bar{M}_\text{P}$), the Planck mass suppression is partially lifted. In this case, these interactions will dominate over processes induced by minimal gravitational coupling as well as over the quadratic $\xi^{(2)}$ -term in the expression above. Only when the $\xi^{(1)}$ -operator inducing dark matter decay at present times is also responsible for dark matter production in the early Universe can one directly connect the relic abundance with the decay phenomenology. Otherwise, dark matter production and decay will generally be controlled by different model parameters. With these caveats in mind, the present-day dark matter abundance from freeze-in production in the early Universe due to a \mathbb{Z}_2 -breaking non-minimal coupling to gravity can be computed for the scalar singlet scenario introduced in section 4.1. Here, number-changing three-, four-, and five-point interactions can occur, some of which are sketched in figure 6.1. Every external ϕ leg carries with

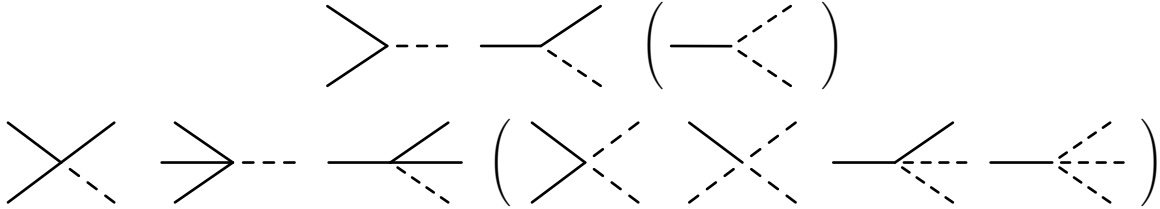


Figure 6.1: *Dark matter production via three- and four-point interactions. Dashed lines indicate dark matter legs, full lines correspond to standard model particles. Subdominant channels in brackets.*

it one power of Planck mass suppression and one power of the non-minimal coupling parameter ($\xi M \kappa$). Therefore, on dimensional grounds, the dominant contribution to the total dark matter production is expected to arise from vertices involving only one dark matter particle, *i.e.* the first and second diagram in the first row, and the first, second and third in the second row. For each of these types of interaction, the resulting present-day dark matter abundance can be computed explicitly.

6.2.1 Relic abundance from coannihilations

Consider first the co-annihilation-type processes described by the first diagram in the second row of figure 6.1. These involve one dark matter leg and three particles from the visible sector thermal bath. Shortly after reheating, the temperature of the thermal bath lies above that of electroweak symmetry breaking. Therefore, the electroweak vacuum is symmetric and all standard model particles are massless, with the possible exception of the four Higgs degrees of freedom themselves, whose mass is determined by the Higgs potential. In the Feynman ($R_{\xi=1}$)

gauge, the Higgs field can be decomposed as

$$\Phi = \left(\frac{1}{\sqrt{2}} \begin{pmatrix} \varphi_H^+ \\ H + i \varphi_H^0 \end{pmatrix} \right), \quad (6.7)$$

where $\varphi_H^\pm, \varphi_H^0$ are the Goldstone degrees of freedom. The Feynman rules and resulting scattering cross sections in this scenario can be derived using standard techniques. (This process can be automated as sketched in appendices B and C). Some general features can already be anticipated at this stage, however. Due to the absence of any explicit mass scales in the theory, the vertices can only depend on the dimensionless standard model couplings and on particle momenta. The dependence on the non-minimal coupling and Planck-mass suppression follow from the form of the non-minimal coupling to gravity. Therefore, on dimensional grounds, the resulting interaction cross sections times relative velocity will have the form

$$\sigma |\mathbf{v}| \propto \frac{(\xi M \kappa)^2}{1 + 6 (\xi M \kappa)^2} \frac{1}{M_{\text{P}}^2} = \frac{\bar{\xi}^2}{M_{\text{P}}^2}, \quad (6.8)$$

modulo phase space factors, times standard model couplings, as summarized in table 6.1. Here,

Vertex	SM coupling
$\phi f' \bar{f} (G, W, Z, \gamma)$	g_s^2, g^2, g^2, e^2
$\phi f' \bar{f} \varphi_H$	$y_f y_{f'}$
$\phi 2\varphi_H (W, Z, \gamma)$	g^2, g^2, e^2
$\phi 2\varphi_H 2(W, Z, \gamma)$	g^4, g^4, e^4
$\phi 4\varphi_H$	λ^2

Table 6.1: Standard model couplings relevant for dark matter production in the early Universe.

φ_H stands for any of the four components of the Higgs doublet, $\varphi_H = H, \varphi_H^0, \varphi_H^\pm$. To determine which of these channels dominate dark matter production, both the running of the coupling constants to energies available in the early Universe and the precise multiplicity of each of the processes have to be taken into account. Compared to the first three, the last two entries are suppressed by additional powers of the coupling constants and can therefore be neglected. Assuming all particles but the dark matter to be massless, the total cross sections for the first three types of processes, for collisions at a center-of-mass energy squared $E_{\text{CM}}^2 = s_{\text{CM}}$, and for a given configuration of spins/polarizations, are

$$\sigma_{\phi V \rightarrow f^{(\prime)} \bar{f}} |\mathbf{v}| = \frac{\bar{\xi}^2}{M_{\text{P}}^2} \frac{s_{\text{CM}}}{2 E_\phi 2 E_V} \frac{3 N_c^{(f)}}{8 \pi} \left(|g_V|^2 + |g_A|^2 \right), \quad (6.9)$$

$$\sigma_{\phi H \rightarrow t \bar{t}} |\mathbf{v}| = \frac{\bar{\xi}^2}{M_{\text{P}}^2} \frac{s_{\text{CM}}}{2 E_\phi 2 E_H} \frac{N_c^{(f)}}{2 \pi} y_t^2, \quad (6.10)$$

$$\sigma_{\phi V \rightarrow \varphi_H \varphi_H} |\mathbf{v}| = \frac{\bar{\xi}^2}{M_{\text{P}}^2} \frac{s_{\text{CM}}}{2 E_\phi 2 E_V} \frac{1}{6 \pi} |g_V S|^2. \quad (6.11)$$

Since the top quark has by far the largest Yukawa coupling y_t among the standard model fermions, scattering with a top-antitop pair is the only relevant channel from the second category in table 6.1. The gauge boson couplings are listed in table 6.2, while table 6.3 shows the vector-scalar couplings for processes involving two Higgs degrees of freedom and a vector boson. With

Gauge boson	g_V	g_A
G	g_s	0
W	$\frac{g}{2\sqrt{2}} V_{\text{CKM}}$	$\frac{g}{2\sqrt{2}} V_{\text{CKM}}$
Z	$\frac{g}{2 \cos \theta_W} (t_3 - 2 Q \sin^2 \theta_W)$	$\frac{g}{2 \cos \theta_W} t_3$
γ	$Q e$	0

Table 6.2: Standard model gauge boson-fermion couplings.

Vertex	$g_V S$
$\phi \gamma \varphi_H^+ \varphi_H^-$	e
$\phi W^\pm \varphi_H^\mp (\varphi_H^0, H)$	$\frac{g}{2}$
$\phi Z \varphi_H^+ \varphi_H^-$	$\frac{g}{2 \cos \theta_W} (\cos^2 \theta_W - \sin^2 \theta_W)$
$\phi Z \varphi_H^0 H$	$\frac{g}{2 \cos \theta_W}$

Table 6.3: Vector-scalar couplings.

these expressions for the scattering cross sections in terms of the center-of-mass energy, the evolution of the dark matter abundance in the early Universe can be computed following [86]. The Boltzmann equation describing the evolution of the number density n_ϕ of a dark matter particle ϕ of mass m_ϕ due to the process $\phi A \leftrightarrow BC$ reads [4]

$$\dot{n}_\phi + 3H n_\phi = - \int d\Pi_\phi d\Pi_A d\Pi_B d\Pi_C (2\pi)^4 \delta^{(4)}(p_\phi + p_A - p_B - p_C) |\mathcal{M}|^2 (f_\phi f_A - f_B f_C), \quad (6.12)$$

where H is the time-dependent Hubble parameter, f_i is the phase space density of particle species i and

$$d\Pi_i = \frac{g_i}{(2\pi)^3} \frac{d^3 p_i}{2E_i}, \quad (6.13)$$

with g_i the number of internal degrees of freedom. Being standard model particles, B and C are in thermal equilibrium, so

$$f_{B,C} = f_{B,C}^{(\text{EQ})} \simeq e^{-E_{B,C}/T}. \quad (6.14)$$

Due to conservation of energy, $f_B^{(\text{EQ})} f_C^{(\text{EQ})} = f_\phi^{(\text{EQ})} f_A^{(\text{EQ})}$, and the right-hand side of the above expression simplifies to

$$\text{RHS} = - \int d\Pi_\phi d\Pi_A d\Pi_B d\Pi_C (2\pi)^4 \delta^{(4)}(\{p_i\}) |\mathcal{M}|^2 (f_\phi f_A - f_\phi^{(\text{EQ})} f_A^{(\text{EQ})}) \quad (6.15)$$

$$= - g_B g_C \int d\Pi_\phi d\Pi_A (f_\phi f_A - f_\phi^{(\text{EQ})} f_A^{(\text{EQ})}) (2E_\phi 2E_A \sigma_{\phi A \rightarrow BC} |\mathbf{v}|). \quad (6.16)$$

In the above expression, the last factor inside the integral is the scattering cross section for the process $\phi A \rightarrow BC$, modulo the normalization prefactors related to the particle flux in collision experiments. In the case of freeze-in production, for as long as interactions are still efficient, the actual dark matter particle abundance lies far below its equilibrium value, $f_\phi \ll f_\phi^{(\text{EQ})}$, while A

remains in equilibrium with the thermal bath throughout, $f_A = f_A^{(\text{EQ})}$. Therefore, the first term in the above sum can be dropped, yielding

$$\dot{n}_\phi + 3H n_\phi \simeq g_B g_C \int d\Pi_\phi d\Pi_A f_\phi^{(\text{EQ})} f_A^{(\text{EQ})} (2E_\phi 2E_A \sigma_{\phi A \rightarrow BC} |\mathbf{v}|) \quad (6.17)$$

$$\equiv g_\phi g_A g_B g_C \langle \sigma v \rangle n_A^{(\text{EQ})} n_\phi^{(\text{EQ})}, \quad (6.18)$$

where $n_i^{(\text{EQ})}$ is the equilibrium number density of particle species i , and $\langle \sigma v \rangle$ is the thermally averaged cross section. To perform this averaging explicitly along the lines of [86], one has to evaluate

$$\dot{n}_\phi + 3H n_\phi = \frac{g_\phi g_A g_B g_C}{4(2\pi)^4} T \int_{m_\phi^2}^{\infty} ds_{\text{CM}} \frac{s_{\text{CM}} - m_\phi^2}{\sqrt{s_{\text{CM}}}} K_1\left(\frac{\sqrt{s_{\text{CM}}}}{T}\right) (2E_\phi 2E_A \sigma_{\phi A \rightarrow BC}(s_{\text{CM}}) |\mathbf{v}|), \quad (6.19)$$

with $K_1(x)$ the modified Bessel function of the second kind of order 1. For cross sections of the form

$$\sigma(s_{\text{CM}}) |\mathbf{v}| = \frac{c_g}{\bar{M}_{\text{P}}^2} \frac{s_{\text{CM}}}{2E_\phi 2E_A}, \quad (6.20)$$

with constant c_g , as in the scenario under discussion, the integral over s_{CM} gives

$$\dot{n}_\phi + 3H n_\phi = \frac{g_\phi g_A g_B g_C}{4(2\pi)^4} \frac{c_g}{\bar{M}_{\text{P}}^2} \left[16 T^6 G_{1,3}^{3,0}\left(\frac{m_\phi^2}{4T^2} \middle| \begin{matrix} 1 \\ 0, 2, 3 \end{matrix} \right) - 2 m_\phi^4 T^2 K_2\left(\frac{m_\phi}{T}\right) \right]. \quad (6.21)$$

Here, $K_2(x)$ is the modified Bessel function of the second kind of order 2, and $G_{p,q}^{m,n}(x)$ is the Meijer G-function. Introducing the dimensionless variables $Y = n_\phi/s$ and $x = m_\phi/T$, where s is the entropy density per comoving volume, one can absorb the change in number density due to the evolution of the scale factor, since

$$\dot{n}_\phi + 3H n_\phi = \dot{Y} s. \quad (6.22)$$

During radiation domination, the entropy density and Hubble parameter at temperature T are given by [4]

$$s(T) = \frac{2\pi^2}{45} g_{*s} T^3, \quad H(T) = 1.67\sqrt{g_*} \frac{T^2}{M_{\text{P}}} = 0.333\sqrt{g_*} \frac{T^2}{\bar{M}_{\text{P}}}, \quad (6.23)$$

with g_*, g_{*s} counting the number of massless degrees of freedom. (Note that the Planck mass $M_{\text{P}} = \sqrt{8\pi} \bar{M}_{\text{P}} \simeq 1.22 \times 10^{19}$ GeV.) Using the fact that $t \propto T^{-2}$ and $H \propto T^2$ during radiation domination, so that $\dot{T} \simeq -HT$ [31, 4], the differential equation for the dark matter yield Y as a function of x reads

$$\frac{dY}{dx} = \frac{x^4}{H(m_\phi) s(m_\phi)} \times \text{RHS} = \lambda' g(x), \quad (6.24)$$

with

$$\lambda' = \frac{g_\phi g_A g_B g_C}{2(2\pi)^4} \frac{c_g}{\bar{M}_{\text{P}}^2} \frac{m_\phi^6}{H(m_\phi) s(m_\phi)}, \quad (6.25)$$

$$g(x) = 8x^{-2} G_{1,3}^{3,0}\left(\frac{x^2}{4} \middle| \begin{matrix} 1 \\ 0, 2, 3 \end{matrix} \right) - x^2 K_2(x). \quad (6.26)$$

The entropy density and Hubble parameter are evaluated at a temperature equal to the dark matter mass $T = m_\phi$. The differential equation for the dark matter abundance can be integrated directly. The amount of dark matter created via interactions since reheating at $x_{\text{rh}} = m_\phi/T_{\text{rh}}$ is

$$Y_{A\phi\leftrightarrow BC}(x) = \lambda' \int_{x_{\text{rh}}}^x dx' g(x'). \quad (6.27)$$

For small x , the integrand can be expanded as $g(x) \simeq 16/x^2 - 2 + \mathcal{O}(x^2)$. This is an excellent approximation: in a freeze-in scenario, interactions are only efficient long before the temperature reaches values close to the particle mass, provided that the reheating temperature is high enough, $x_{\text{rh}} < x_{\text{freeze-in}} < 1$. As $g(x) \propto x^{-2}$, the number density is built up predominantly immediately after reheating and reaches its asymptotic value quickly. To very good approximation, the present-day dark matter abundance is given by

$$Y_{A\phi\leftrightarrow BC}(\infty) = \frac{16 \lambda'}{x_{\text{rh}}}. \quad (6.28)$$

It is sensitive to the value of the reheating temperature, $Y_{A\phi\leftrightarrow BC}(\infty) \propto T_{\text{rh}}/\bar{M}_{\text{P}}$, but independent of the dark matter mass m_ϕ , since $\lambda' \propto m_\phi$. Assuming a flat Friedmann-Robertson-Walker geometry, the corresponding fraction of the total energy density of the Universe today is

$$\Omega_\phi h^2 = h^2 \frac{\rho_\phi}{\rho_{c,0}}, \quad (6.29)$$

with the critical density $\rho_{c,0} = 1.055 \times 10^{-5} h^2 \text{ GeV cm}^{-3}$ [4]. The energy density in dark matter particles is

$$\rho_\phi = m_\phi n_\phi = m_\phi Y(\infty) s_0, \quad (6.30)$$

with the present-day entropy density $s_0 = 2970 \text{ cm}^{-3}$. Putting everything together,

$$0.12 \gtrsim \Omega_{A\phi\leftrightarrow BC} h^2 = 4.062 \times 10^{-3} \times \frac{g_\phi g_A g_B g_C c_g}{\sqrt{g_* g_{*s}}} \left(\frac{m_\phi}{\text{GeV}} \right) \left(\frac{T_{\text{rh}}}{10^9 \text{ GeV}} \right). \quad (6.31)$$

In the scalar singlet scenario in question, $g_\phi = 1$, and if the dark matter abundance freezes in before the temperature drops below the electroweak scale, $g_* = g_{*s} \simeq 106.75$, which leads to

$$0.12 \gtrsim \Omega_{A\phi\leftrightarrow BC} h^2 = 3.683 \times 10^{-6} \times (g_A g_B g_C c_g) \left(\frac{m_\phi}{\text{GeV}} \right) \left(\frac{T_{\text{rh}}}{10^9 \text{ GeV}} \right). \quad (6.32)$$

The last step is to determine the value of $(g_A g_B g_C c_g)$ for each coannihilation channel of (6.9) to (6.11) individually and to sum over all channels to obtain the total abundance created through two-to-two co-scattering.

For dark matter-gluon scattering into a pair of quarks, $\phi G \rightarrow q \bar{q}$, the gluon can be in one of two helicity states, which fixes the spins of the fermions, $g_B = g_C = 1$. An additional color factor $N_c = 4$, so $g_A = 2 \times 4$. Permuting the external legs of the amplitude, one finds the processes $\phi q \rightarrow G q$ and $\phi \bar{q} \rightarrow G \bar{q}$ arising from the same vertex. Here, the spin of the initial (anti-)quark is free, $g_A = 2$, while $g_B = N_c = 3$ and $g_C = 1$. Finally, the vertex $\phi G q \bar{q}$ arises for an overall number of $N_q = 6$ quark flavors, and is proportional to the non-minimal coupling $\bar{\xi}$ and the strong gauge coupling g_s . Thus, for this kind of vertex,

$$\phi G q \bar{q} : \sum_q (g_A g_B g_C c_g) = (2 \times 4 + 2 \times 3 + 2 \times 3) \times 6 \times \frac{3}{8\pi} g_s^2 \bar{\xi}^2 = \frac{45}{\pi} g_s^2 \bar{\xi}^2. \quad (6.33)$$

Adding processes with electroweak gauge bosons and assuming, for simplicity, that all three standard model gauge couplings g_s, g, g' are approximately given by $\alpha_{\text{SM}} = g_{\text{SM}}^2/(4\pi) \simeq 1/43$ at energies around the scale of a hypothesized Grand Unified Theory (GUT) [163], dark matter scattering processes involving fermions and gauge bosons $V = G, W, Z, \gamma$ sum up to

$$\phi V f' \bar{f} : \sum_{f,V} (g_A g_B g_C c_g) \simeq 6.41 \times \bar{\xi}^2, \quad (6.34)$$

with gluon scattering being responsible for roughly two thirds of the abundance generated through the processes of (6.9).

In the second type of interaction (6.10), involving the top Yukawa coupling, the multiplicative factor evaluates to

$$\phi H t \bar{t} : (g_A g_B g_C c_g) \simeq 2.80 \times \bar{\xi}^2. \quad (6.35)$$

Here, it is assumed that y_t does not change significantly running up in energy from the electroweak to the GUT scale, $y_t \simeq 1$ [163].

Dark matter-vector boson scattering with two scalars (6.11), finally, contributes less than a percent to the total abundance,

$$\phi V \varphi_H \varphi_H : \sum_{\varphi_H, V} (g_A g_B g_C c_g) \simeq 0.018 \times \bar{\xi}^2, \quad (6.36)$$

due to the much lower number of degrees of freedom. The other processes listed in table 6.1 are further suppressed by higher powers of the coupling constants. Therefore, to percent-level accuracy, the total abundance of scalar singlet dark matter created via two-to-two scattering processes in the early Universe is given by summing over the contributions from $\phi V f' \bar{f}$ and $\phi H t \bar{t}$, giving

$$0.12 \gtrsim \Omega_{A\phi \leftrightarrow BC} h^2 \simeq 3.392 \times 10^{-5} \times \bar{\xi}^2 \left(\frac{m_\phi}{\text{GeV}} \right) \left(\frac{T_{\text{rh}}}{10^9 \text{ GeV}} \right). \quad (6.37)$$

6.2.2 Relic abundance from (inverse) decays

Another contribution to the dark matter abundance is caused by “inverse decay”-type processes, described by diagrams such as the first in the first row, or the second in the second row of figure 6.1. The corresponding Boltzmann equation for the evolution of the dark matter number density reads [31]

$$\dot{n}_\phi + 3H n_\phi = - \int d\Pi_\phi d\Pi_A d\Pi_B \dots d\Pi_Z (2\pi)^4 \delta^{(4)}(\{p_i\}) |\mathcal{M}|^2 (f_\phi - f_A f_B \dots f_Z), \quad (6.38)$$

for the process $A B \dots Z \leftrightarrow \phi$ with an arbitrary number of initial-state particles. As before, the delta distribution enforces momentum conservation. The right-hand side simplifies significantly. While interactions are still efficient (*i.e.* before the dark matter abundance freezes in), $f_\phi \simeq 0$, while the remaining particles are in contact with the thermal bath, $f_{i \neq \phi} = f_i^{(\text{EQ})} \simeq e^{-E_i/T}$. Furthermore, due to energy conservation, $f_A^{(\text{EQ})} f_B^{(\text{EQ})} \dots f_Z^{(\text{EQ})} = f_\phi^{(\text{EQ})}$ as for the two-to-two annihilations, so

$$\text{RHS} = \int d\Pi_\phi f_\phi^{(\text{EQ})} \int d\Pi_A d\Pi_B \dots d\Pi_Z (2\pi)^4 \delta^{(4)}(\{p_i\}) |\mathcal{M}|^2 \quad (6.39)$$

$$= \int d\Pi_\phi f_\phi^{(\text{EQ})} 2 m_\phi \Gamma_{\phi \rightarrow AB \dots Z}, \quad (6.40)$$

where $\Gamma_{\phi \rightarrow AB\dots Z} \equiv \Gamma_\phi$ is the partial decay rate of ϕ into the final state $A B \dots Z$ in the rest frame of the decaying particle. (For this production channel to exist, the decay must be kinematically allowed.) Since Γ_ϕ is independent of E_ϕ , the remaining phase space integral can be performed straightforwardly, and the Boltzmann equation reads

$$\dot{n}_\phi + 3H n_\phi = g_\phi \frac{m_\phi^2 \Gamma_\phi}{2\pi^2} T K_1(m_\phi/T). \quad (6.41)$$

As before, the dimensionless yield $Y = n_\phi/s$ can be defined, and the Boltzmann equation dY/dx can be solved by direct integration. In contrast to the coannihilation case, as long as the reheating temperature is larger than a few times the dark matter mass (such that dark matter can be produced at all), the present-day dark matter abundance is independent of its precise value T_{rh} ,

$$Y_{\phi \leftrightarrow AB\dots Z}(\infty) \simeq \frac{135 g_\phi}{8\pi^3 (0.333) \sqrt{g_* g_{*s}}} \frac{\bar{M}_\text{P} \Gamma_\phi}{m_\phi^2}. \quad (6.42)$$

Dark matter can also be produced via the conventional decay of bath particles, $A \leftrightarrow \phi B C \dots Z$. In this case, an analogous calculation [31] yields

$$Y_{A \leftrightarrow \phi BC\dots Z}(\infty) \simeq \frac{135 g_A}{8\pi^3 (0.333) \sqrt{g_* g_{*s}}} \frac{\bar{M}_\text{P} \Gamma_A}{m_A^2}. \quad (6.43)$$

For these processes, for kinematical reasons, $m_A > m_\phi + m_B + \dots + m_Z$ is required. For inverse and regular decays, the corresponding present-day dark matter fraction of the total energy density is, respectively [31],

$$\Omega_{\phi \leftrightarrow AB\dots Z} h^2 \simeq \frac{1.12 \times 10^{27}}{\sqrt{g_* g_{*s}}} g_\phi \frac{\Gamma_\phi}{m_\phi}, \quad (6.44)$$

$$\Omega_{A \leftrightarrow \phi BC\dots Z} h^2 \simeq \frac{1.12 \times 10^{27}}{\sqrt{g_* g_{*s}}} g_A \frac{m_\phi \Gamma_A}{m_A^2}. \quad (6.45)$$

As was shown in section 5.1, at energies above the electroweak scale, the dependence of the decay rate of a scalar singlet on its mass is at least as $\Gamma_\phi \simeq \bar{\xi}^2 m_\phi^3 / \bar{M}_\text{P}^2$. Considering for comparison the decay rate of a visible sector particle A with a dark matter particle in the final state, one finds

$$\Gamma_A \simeq \Gamma_{A,\text{SM}} \times \bar{\xi}^2 \times \frac{m_A^2}{32\pi^2 \bar{M}_\text{P}^2}, \quad (6.46)$$

where $\Gamma_{A,\text{SM}}$ is its pure standard-model decay width without a dark matter particle in the final state. As evident from (6.5), the non-minimal coupling to gravity introduces a Planck-mass suppression factor which is compensated by a factor m_A^2 from the phase space integral (the decay process into dark matter has an additional particle in the final state). Unstable standard model particles such as the top quark or the electroweak gauge bosons have decay widths no larger than $\Gamma_{A,\text{SM}} \lesssim \mathcal{O}(\text{GeV})$ [1], so

$$\Omega_{\phi \leftrightarrow AB\dots Z} h^2 \gtrsim 1.02 \times 10^{24} \times \bar{\xi}^2 \frac{m_\phi^2}{\bar{M}_\text{P}^2}, \quad (6.47)$$

$$\Omega_{A \leftrightarrow \phi BC\dots Z} h^2 \lesssim 1.02 \times 10^{24} \times \bar{\xi}^2 \frac{m_\phi^2}{\bar{M}_\text{P}^2} \times \frac{g_A}{32\pi^2} \times \left(\frac{\text{GeV}}{m_\phi} \right). \quad (6.48)$$

The dark matter yield from standard model particle decay will only dominate over inverse decays for dark matter masses below $m_\phi \lesssim g_A/(32\pi^2)$ GeV. Above that mass,

$$\Omega_{A\leftrightarrow\phi BC\dots Z} h^2 \ll \Omega_{\phi\leftrightarrow AB\dots Z} h^2, \quad (6.49)$$

where

$$\Omega_{\phi\leftrightarrow AB\dots Z} h^2 \gtrsim 1.71 \times 10^{-13} \times \xi^2 \left(\frac{m_\phi}{\text{GeV}} \right)^2. \quad (6.50)$$

As the scaling of the total width of the scalar singlet with its mass increases according to table 5.1 as soon as new decay channels open up, the true relic abundance created via inverse decays will be somewhat larger. For figure 6.2, the full dependence $\Gamma_\phi(m_\phi)$ was used, taking into account all partial widths.

6.2.3 Total relic abundance

To obtain the total dark matter abundance, the yields from decays, inverse decays and scattering processes have to be added. Which contribution dominates depends on the dark matter mass and the reheating temperature. In either case, the final abundance of dark matter particles from freeze-in production is proportional to the interaction strength (rather than inversely proportional to it, as in the case of freeze-out). Thus, requiring consistency with the observed dark matter relic density fraction translates into an upper bound on the non-minimal coupling parameter whose precise value may depend on the reheating temperature. Figure 6.2 shows the resulting bounds on the non-minimal coupling ($\xi M \kappa$) as a function of the scalar singlet mass m_ϕ . While in principle it is possible to produce the observed present-day dark matter abundance through scattering via the non-minimal coupling to gravity, the required value of the non-minimal coupling parameter for a given dark matter mass is excluded by the non-observation of decay signals in gamma-ray or cosmic ray observations or by CMB data. Therefore, a scalar singlet dark matter particle would need to have been produced through a different mechanism, *e.g.* a Higgs portal coupling, unrelated to its decay phenomenology.

As argued in the beginning of this section, for any other dark matter candidate, dark matter production through a non-minimal operator (3.4) faces stronger Planck-mass suppression. Unless the non-minimal coupling ξ takes on very large values, the abundance created through the regular, minimal coupling to gravity will be of comparable size. Furthermore, any non-gravitational interaction of the dark matter particle will in turn dominate over gravitational production.

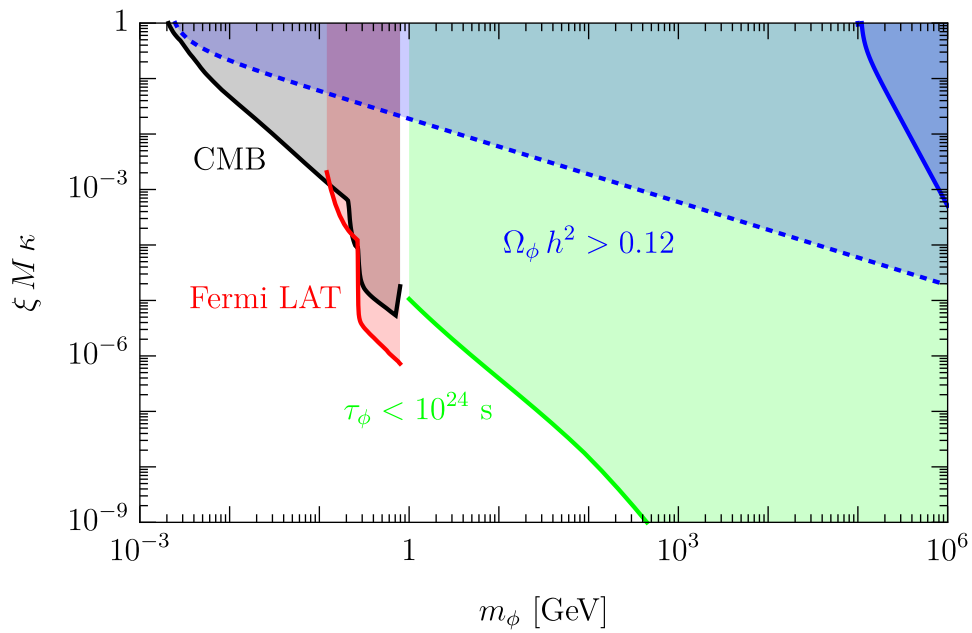


Figure 6.2: Bounds from dark matter production. The dotted (continuous) blue line shows the non-minimal coupling required to produce the observed dark matter relic density via two-to-two scattering (inverse decays). The contribution from regular decays is negligible. Black, red and green lines show the constraints from CMB, gamma-ray and cosmic ray observations, as discussed in sections 6.1, 5.2 and 5.1. Shaded areas are excluded. For the dark matter abundance produced via two-to-two scattering given by (6.37), a high reheating temperature of $T_{\text{rh}} = 10^{16}$ GeV is assumed.

Chapter 7

Inflation in non-minimally coupled scenarios

Theoretical considerations of the early Universe have identified a range of puzzling features about the cosmos in the context of the Λ CDM model. Most notably, the near-perfect flatness of spacetime, the isotropy of the cosmic microwave background across causally disconnected patches of space and the absence of various kinds of relics that arise in certain extensions of the standard model are hard to explain [4]. Inflation offers an attractive way out: by postulating a period of exponential expansion shortly after the big bang, spacetime is flattened, a given causally connected patch is stretched to sizes comparable to the observable universe today, and unwanted relics are diluted sufficiently to be unobservable at present times [164, 165, 166].

7.1 Scalar field dynamics

The basic picture can be illustrated using a simple single-field model that adds a single scalar φ to the standard model, appropriately labelled the inflaton. Typically, it couples very weakly to the standard model degrees of freedom and has a very shallow region in its potential $\mathcal{V}(\varphi)$, enabling a period of “slow-roll” inflation. Starting from the Lagrangian

$$\mathcal{L} = \frac{1}{2} (\partial_\mu \varphi) (\partial^\mu \varphi) - \mathcal{V}(\varphi), \quad (7.1)$$

and under the assumption of a spatially homogenous field, $\partial_i \varphi = 0$, the classical equation of motion reads

$$\ddot{\varphi} + 3H \dot{\varphi} + \frac{d\mathcal{V}}{d\varphi} = 0, \quad (7.2)$$

with H the Hubble rate and dots representing derivatives with respect to cosmic time t . The classical inflaton field behaves as a harmonic oscillator with a frequency determined by its potential and a damping term related to the expansion of spacetime (often referred to as “Hubble friction”). The assumption of spatial homogeneity of the scalar field is a rather mild one, as any pre-existing spatial gradients would be quickly suppressed by the exponential expansion of spacetime [4]. In the slow-roll regime, $\ddot{\varphi} \ll 3H \dot{\varphi}$ and $\ddot{\varphi} \ll d\mathcal{V}/d\varphi$, so the scalar field smoothly drifts down its (shallow) potential, $\dot{\varphi} = -\mathcal{V}'(\varphi)/(3H)$. The energy density attributed to φ is almost constant during this period, leading to the advertised behavior of the scale factor, $a(t) \propto e^{Ht}$ [4].

In order to allow for this slow-roll phase, there are certain requirements on the shape of the scalar potential \mathcal{V} . The precise measurements of the CMB temperature and polarization

fluctuations performed by the Planck collaboration pinpoints the spectral index of curvature perturbations, $n_s = 0.968 \pm 0.006$ (68 % confidence level), and constrains the tensor-to-scalar ratio to values $r < 0.11$ (95 % confidence) [167]. In single-field models of inflation, they can be calculated in terms of the slow-roll parameters,

$$\epsilon = \frac{M_{\text{P}}^2}{2} \frac{(d\mathcal{V}/d\varphi)^2}{\mathcal{V}^2}, \quad (7.3)$$

$$\eta = M_{\text{P}}^2 \frac{d^2\mathcal{V}/d\varphi^2}{\mathcal{V}}, \quad (7.4)$$

and are approximately given by [168]

$$n_s \simeq 1 + 2\eta - 6\epsilon, \quad (7.5)$$

$$r \simeq 16\epsilon. \quad (7.6)$$

Moreover, the number of e-folds during inflation needs to be at least $N \gtrsim 50\text{--}60$ [167], and can be calculated as [168]

$$N = \frac{1}{M_{\text{P}}^2} \int_{\varphi_{\text{f}}}^{\varphi_{\text{i}}} d\varphi \mathcal{V} \left(\frac{d\mathcal{V}}{d\varphi} \right)^{-1}. \quad (7.7)$$

Here, $\varphi_{\text{i,f}}$ refer to the field values at the start and at the end of inflation.

The Planck constraints rule out a number of inflationary models. As an example, one of the simplest inflaton models imaginable, quadratic inflation, has the potential

$$\mathcal{V}(\varphi) = \frac{m_{\varphi}^2}{2} \varphi^2, \quad (7.8)$$

specified by a single parameter, m_{φ}^2 . The field value at the end of inflation can be calculated through the relation $\epsilon(\varphi_{\text{f}}) = 1$. Fixing the number of e-folds N determines the initial field value φ_{i} through (7.7). Finally, to reproduce the observed amplitude of the curvature power spectrum $A_s = (2.14 \pm 0.06) \times 10^{-9}$ [5], the scalar potential needs to satisfy

$$\frac{\mathcal{V}(\varphi_{\text{i}})}{\epsilon(\varphi_{\text{i}})} = (0.027 M_{\text{P}})^4, \quad (7.9)$$

which determines the value of the inflaton mass, $m_{\varphi} = 6(7) \times 10^{-6} M_{\text{P}}$ for $N = 60(50)$ [168]. The resulting values for the spectral index n_s and tensor-to-scalar ratio r are disfavored by Planck data. This should not be too surprising, given the simplicity of this toy model.

7.2 Inflation with non-minimal coupling to gravity

As was shown in [168], extending the basic model (7.1) with a non-minimal coupling to gravity of the form

$$-\frac{1}{2} \xi' \varphi^2 R \quad (7.10)$$

can significantly alter the shape of the potential, depending on the size of the non-minimal coupling. Specifically, for $\xi' = \mathcal{O}(10^{-3})$, the expected values for n_s and r are in agreement with observations [168]. The reason is that the Weyl transformation (3.17) again modifies the kinetic term of the scalar field φ , analogously to (4.6). Performing a field redefinition to bring the

kinetic term into canonical form changes the shape of the potential; specifically, higher-order terms in the scalar field are introduced with coefficients proportional to $m_\varphi^2/M_{\text{P}}^2$ [168]. These serve to flatten the Einstein-frame potential and make the model viable again.

A similar effect can be expected by extending (7.1) not with a quadratic non-minimal operator, but with the linear term

$$\mathcal{L}_\xi = -\xi M \varphi R, \quad (7.11)$$

in the spirit of identifying the inflaton field with the scalar singlet dark matter candidate discussed in sections 4.1 and 5.1. This would constitute an intriguing link between the dynamics of the very early Universe and the various phenomena connected to the dark matter puzzle. In this case, the Einstein frame potential is given by

$$\widehat{\mathcal{V}}(\widehat{\varphi}) = \frac{m_\varphi^2 \varphi^2(\widehat{\varphi})}{2(1 + 2\kappa^2 \xi M \varphi(\widehat{\varphi}))^2}, \quad (7.12)$$

where the relation between the Jordan- and Einstein-frame scalar fields is [52]

$$\widehat{\varphi} = \frac{\sqrt{6}}{\kappa} \left(y - y_0 + \frac{1}{2} \log \frac{(1-y)(1+y_0)}{(1+y)(1-y_0)} \right), \quad (7.13)$$

to all orders in ξ , where

$$y = \sqrt{1 + \frac{1 + 2\kappa^2 \xi M \varphi}{6\xi^2 M^2 \kappa^2}}, \quad y_0 = y|_{\varphi \rightarrow 0}. \quad (7.14)$$

Expression (7.12) explicitly shows the flattening of the potential introduced by the Weyl transformation. While $\widehat{\mathcal{V}}$ is approximately quadratic at small field values, it approaches the constant value

$$\widehat{\mathcal{V}}(\widehat{\varphi}) \rightarrow \frac{m_\varphi^2 \bar{M}_{\text{P}}^4}{8\xi^2 M^2} \quad (7.15)$$

for $\kappa\varphi \gg 1$. Numerically, one finds that it is possible to satisfy the Planck bounds on the spectral index n_s and tensor-to-scalar ratio r within the quadratic inflation model with a linear non-minimal coupling to gravity. For $N = 50$ (60), this requires a non-minimal coupling of either $\xi \simeq 0.61$ (7.4), resulting in a very low tensor-to-scalar ratio $r \simeq 0.011$ (0.0030), or a smaller value of $\xi \simeq 0.15$ (0.0053), with $r \simeq 0.031$ (0.11). In either of these cases, however, the modification of the scalar potential (7.12) is rather minor, and the value for the scalar mass parameter m_φ required to satisfy (7.9) differs only mildly from that of the minimally coupled scenario. A mass of $m_\varphi \simeq 10^{-5} \bar{M}_{\text{P}} \simeq 10^{13}$ GeV, as needed, would correspond to a very heavy dark matter candidate. Indeed, as shown in section 5.1, the non-observation of exotic contributions in gamma-ray and cosmic-ray experiments constrains the non-minimal coupling to be of order $\xi \lesssim 10^{-40}$ in this regime. Therefore, barring an unreasonable amount of running of ξ between the electroweak and Planck scales, it is not possible to describe dark matter and inflation within this setup. Rather, one would need to introduce additional terms in the Lagrangian. A trivial choice would be to include both the linear non-minimal coupling (7.11) and the quadratic one (7.10) discussed in [168], using the latter to bring the scenario in agreement with Planck data and fixing the former to a small enough value to be in line with the constraints from section 5.1. The viability of this scenario was explored in [169].

More generally, non-minimally coupled inflaton fields have found widespread interest, a notable example being the Higgs inflation scenario. Postulating that the standard model Higgs boson plays the role of the inflaton arguably poses the most efficient way of achieving inflation in the early Universe [170]. However, as elegant as this scenario appears at first glance, some of its aspects require further work. In Higgs inflation, the slow-roll regime corresponds to trans-Planckian field values of the canonically normalized scalar field, as it often happens in models of inflation. Lacking a quantum theory of gravity, the question about the applicability of the EFT approach in this regime arises [171, 172]. Moreover, the successful implementation of inflation in this framework crucially relies on the ratio between the flat-space potential \mathcal{V}_H and the square of the non-minimal coupling operator to the Ricci scalar approaching a constant value. This requires a substantial amount of fine-tuning in the coefficients of additional effective operators arising around M_{P}/ξ (*i.e.* below the Planck scale), in the sense that these operators need to be absent to not spoil the asymptotic behavior of the Einstein frame potential [171]. In other words, an asymptotic shift symmetry in this potential is strictly required [173], the origin of which, however, is unknown.

Chapter 8

Conclusions

As outlined in section 2.4, one of the characterising traits of a dark matter particle is its longevity: the absence of exotic contributions in the cosmic-ray, gamma-ray and neutrino fluxes measured at Earth, as well as precise measurements of the cosmic microwave background, allow one to restrict the dark matter lifetime to values $\tau_{\text{DM}} \gtrsim 10^{24}$ s over a large range of masses (*cf.* chapter 5). Unless the dark matter particle is very light, such that its decays are heavily phase space suppressed, this means that there should be an approximate symmetry in place at low energies, *e.g.* a global \mathbb{Z}_2 , that ensures dark matter stability. If this symmetry is broken at high energies, dark matter can still decay, albeit with a very long lifetime. In the EFT framework, this translates to effective operators with a high suppression scale. Indeed, if it turns out that there is no new physics between the electroweak and the Planck scale [174, 70, 69], it is possible that symmetry breaking only occurs gravitationally, at energies around $M_{\text{P}} \simeq 2.4 \times 10^{18}$ GeV.

This thesis provides an account of the main phenomenological implications of a dark matter candidate that has a \mathbb{Z}_2 -breaking, non-minimal coupling to gravity. Section 3.1 described the general form of the relevant effective operators. After identifying the Lorentz structure and the level of suppression of these operators for various dark matter scenarios, section 3.2 and chapter 4 demonstrated how to derive the interaction Lagrangian between the dark matter candidate and the visible sector, and how dark matter decay proceeds through this Lagrangian. The following sections studied, in turn, a scalar singlet, a scalar doublet and a fermionic singlet dark matter candidate in more detail, highlighting similarities and differences between the individual scenarios.

Chapter 5 focused on the derivation of experimental constraints on the size of the non-minimal coupling parameter ξ for the three scenarios under discussion. To this end, a conservative estimate for the total width of the dark matter particle was computed over a large range of dark matter masses and confronted with data from cosmic-ray and gamma-ray experiments. For the singlet scalar candidate, the resulting limits are especially strong. A non-minimal coupling ($\xi M \kappa$) of order unity leads to a dark matter lifetime shorter than the age of the Universe $\tau_{\text{Uni}} \simeq 4 \times 10^{17}$ s down to dark matter masses of $m_\phi \simeq 270$ MeV, the pion pair production threshold. Requiring agreement with data from x-ray and gamma-ray experiments such as COMPTEL, EGRET and Fermi-LAT, as well as measurements of the cosmic microwave background by the Planck satellite allow one to strengthen this constraint to $(\xi M \kappa) \lesssim 5 \times 10^{-5}$ for this value of the dark matter mass, and extending the limits down to $m_\phi \simeq 2$ MeV. A dark matter candidate at the TeV scale would require a heavily suppressed non-minimal coupling of $(\xi M \kappa) \lesssim 1.9 \times 10^{-10}$, hinting at the presence of a mechanism forbidding this type of interaction altogether, such as a dark gauge symmetry.

For a dark matter candidate with non-zero standard model gauge charges or higher spin,

the experimental bounds are significantly weaker, as discussed in sections 5.3 and 5.4. The $SU(2)_L \times U(1)_Y$ charge of the scalar doublet determines the form of the effective operator inducing dark matter decay, leading to a severe suppression of order $(v/\bar{M}_P)^2$ of the partial widths. Consequently, constraining the non-minimal coupling to values below unity requires dark matter masses above $m_{DM} \gtrsim 10^5$ GeV, for both the CP -even and the CP -odd component of the scalar doublet. In the fermion singlet case, the leading effective operator is of even higher mass dimension, leading to additional suppression. In a simple UV extension of the scenario, depending on the mass of the scalar mediator, the experimental bounds are only significant above $m_\chi \gtrsim 10^6$ GeV.

For the scalar singlet, complementary limits can be derived from cosmology. In this scenario, chapter 6 demonstrated the impact of dark matter decays in the early Universe on the cosmic microwave background. Furthermore, the non-minimal gravitational interactions can result in efficient dark matter production via the freeze-in mechanism. Taking into account coannihilation as well as decay processes, it was demonstrated that while in principle, dark matter production can occur in this way, the expected relic abundance from non-minimal gravitational interactions lies well below the measured value of $\Omega_\phi h^2 \simeq 0.12$ [5]. Finally, the possibility of a connection between inflation and dark matter decay was examined. Similarly to the case of Higgs inflation [170], a \mathbb{Z}_2 -breaking non-minimal coupling of the inflaton field to gravity can modify the scalar potential. This leads to a shift in the slow-roll parameters, with consequences for the remaining model parameters. The toy scenario of a scalar singlet inflaton with only a linear non-minimal coupling discussed in section 7.2 is excluded by observations. However, extended models with additional non-minimal couplings and more complex potentials are still viable.

Although the standard model of particle physics and the cosmological Λ CDM framework have met remarkable success in their respective regimes of applicability, many questions about the fundamental workings of nature remain open. Concerning the dark matter puzzle, ongoing advances in detector technologies for direct and indirect detection as well as complementarity with LHC searches give cause for hope: new generations of experiments are setting ever stronger constraints on the dark matter parameter space, allowing us to rule out large numbers of models even in the absence of conclusive signals. On the theory side, dark matter scenarios beyond the traditional WIMP paradigm are seeing more and more attention, further broadening the scope of experiments and opening up new possibilities for detection. Lastly, even if non-gravitational interactions of dark matter fail to manifest themselves experimentally in the near future, it is reassuring to know that even a closer look at its connection to gravity can yield intriguing phenomenological consequences.

Appendix A

Feynman rules for non-minimally coupled dark sectors

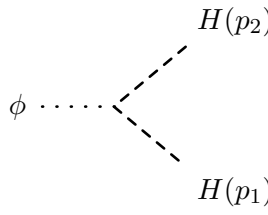
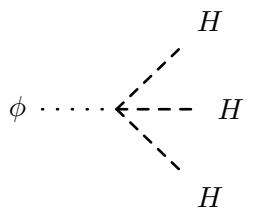
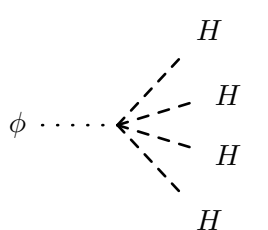
Masses, couplings and other parameters are defined in the main text. All particle momenta (in brackets) are assumed to be outgoing from the vertex and standard model charge flow is indicated by arrows. Time runs from left to right.

A.1 Scalar singlet above 1 GeV

Given the Lagrangian (4.9), the interactions of the non-minimally coupled scalar singlet can be read off straightforwardly. The hat on the scalar singlet is dropped for ease of notation, $\phi \equiv \widehat{\phi}$, and a modified non-minimal coupling is defined as

$$\bar{\xi} \equiv \frac{\xi M \kappa}{\sqrt{1 + 6 (\xi M \kappa)^2}}, \quad (\text{A.1})$$

as before. With these conventions, the Feynman rules read


	$2 i \bar{\xi} \kappa (2 m_H^2 + p_1 \cdot p_2),$
	$12 i \bar{\xi} \kappa \frac{m_H^2}{v},$
	$12 i \bar{\xi} \kappa \frac{m_H^2}{v^2},$



$$i \bar{\xi} \kappa \left(4m_f - \frac{3}{2} \not{p}_1 + \frac{3}{2} \not{p}_2 \right),$$



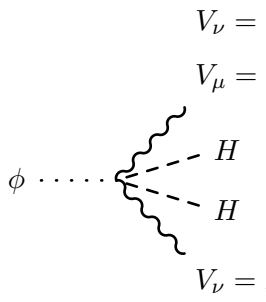
$$4i \bar{\xi} \kappa \frac{m_f}{v},$$



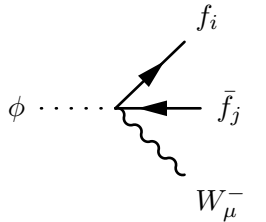
$$-2i \bar{\xi} \kappa m_V^2 \eta^{\mu\nu},$$



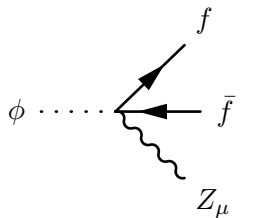
$$-4i \bar{\xi} \kappa \frac{m_V^2}{v} \eta^{\mu\nu},$$



$$-4i \bar{\xi} \kappa \frac{m_V^2}{v^2} \eta^{\mu\nu},$$



$$-3i \bar{\xi} \kappa U_{ij} \frac{g}{\sqrt{2}} \gamma^\mu \frac{1}{2} (1 - \gamma_5),$$



$$-3i \bar{\xi} \kappa \frac{g}{2c_W} \gamma^\mu \left(t_3^{(f)} - 2Q_f s_W^2 - t_3^{(f)} \gamma_5 \right),$$

$$\begin{aligned}
& \text{Diagram 1: } \phi \text{ splits into } f \text{ and } \bar{f} \text{ with } A_\mu \text{ attached.} & -3i\bar{\xi}\kappa Q_f e \gamma^\mu, \\
& \text{Diagram 2: } \phi \text{ splits into } q \text{ and } \bar{q} \text{ with } G_\mu^a \text{ attached.} & -3i\bar{\xi}\kappa g_s \gamma^\mu T_a.
\end{aligned}$$

A.2 Low-mass scalar singlet

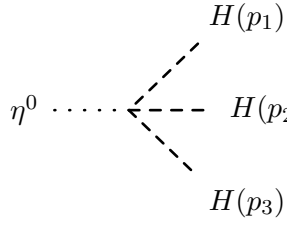
Below the GeV scale, the visible sector is described by the effective Lagrangian (2.36). For a non-minimally coupled scalar singlet, this leads to the interaction Lagrangian (4.16). The Feynman rules for the $\phi f \bar{f}$ - and $\phi f \bar{f} A$ -vertices are identical to the ones at higher energies. Additional vertices with pions and photons take the form

$$\begin{aligned}
& \text{Diagram 1: } \phi \text{ splits into } \pi^0, \pi^- (p_1) \text{ and } \pi^0, \pi^+ (p_2). & 2i\bar{\xi}\kappa \left(2m_{\pi^0, \pi^\pm}^2 + p_1 \cdot p_2 \right), \\
& \text{Diagram 2: } \phi \text{ splits into } A_\nu(k_1) \text{ and } A_\mu(k_2). & i\bar{\xi}\kappa c_{\gamma\gamma} (k_1^\mu k_2^\nu - k_1 \cdot k_2 \eta^{\mu\nu}).
\end{aligned}$$

A.3 Scalar doublet

In the inert doublet model, either of the two neutral components of the second Higgs doublet can be the dark matter candidate, but only the CP -even component η^0 appears in the non-minimal operator. The Feynman rules derived from (4.28) are similar to the scalar singlet case and read

$$\text{Diagram: } \eta^0 \text{ splits into } H(p_1) \text{ and } H(p_2). \quad 2i\xi\kappa^2 v (2m_H^2 + p_1 \cdot p_2),$$



A Feynman diagram showing a dashed line labeled η^0 on the left, which splits into three dashed lines labeled $H(p_1)$, $H(p_2)$, and $H(p_3)$ on the right.

$$2 i \xi \kappa^2 (12 m_H^2 + p_1 \cdot p_2 + p_1 \cdot p_3 + p_2 \cdot p_3),$$



A Feynman diagram showing a dashed line labeled η^0 on the left, which splits into four dashed lines labeled H on the right.

$$60 i \xi \kappa^2 \frac{m_H^2}{v},$$



A Feynman diagram showing a dashed line labeled η^0 on the left, which splits into five dashed lines labeled H on the right.

$$60 i \xi \kappa^2 \frac{m_H^2}{v^2},$$



A Feynman diagram showing a dashed line labeled η^0 on the left, which splits into two solid lines: an arrow labeled $f(p_1)$ pointing up-right and a line with an arrow labeled $\bar{f}(p_2)$ pointing down-right.

$$i \xi \kappa^2 v \left(4 m_f - \frac{3}{2} \not{p}_1 + \frac{3}{2} \not{p}_2 \right),$$



A Feynman diagram showing a dashed line labeled η^0 on the left, which splits into three lines: an arrow labeled $f(p_1)$ pointing up-right, a line with an arrow labeled $\bar{f}(p_2)$ pointing down-right, and a dashed line labeled H pointing down-right.

$$i \xi \kappa^2 \left(8 m_f - \frac{3}{2} \not{p}_1 + \frac{3}{2} \not{p}_2 \right),$$



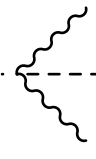


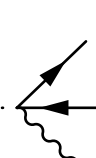

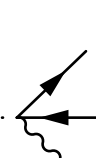

A Feynman diagram showing a dashed line labeled η^0 on the left, which splits into four lines: an arrow labeled f pointing up-right, a line with an arrow labeled \bar{f} pointing down-right, and two dashed lines labeled H pointing down-right.

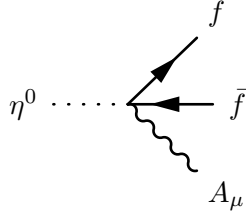
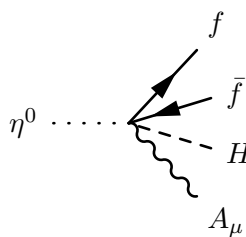
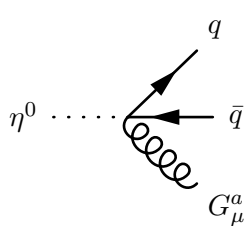
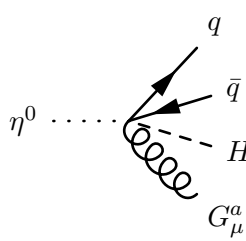
$$8 i \xi \kappa^2 \frac{m_f}{v},$$



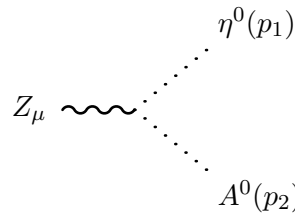
A Feynman diagram showing a dashed line labeled η^0 on the left, which splits into two wavy lines. The top wavy line is labeled $V_\mu = Z_\mu, W_\mu^+$ and the bottom wavy line is labeled $V_\nu = Z_\nu, W_\nu^-$.

$$-2 i \xi \kappa^2 v m_V^2 \eta^{\mu\nu},$$

$\eta^0 \cdots \cdots$ 	$-6 i \xi \kappa^2 m_V^2 \eta^{\mu\nu},$
$\eta^0 \cdots \cdots$ 	$-12 i \xi \kappa^2 \frac{m_V^2}{v} \eta^{\mu\nu},$
$\eta^0 \cdots \cdots$ 	$-12 i \xi \kappa^2 \frac{m_V^2}{v^2} \eta^{\mu\nu},$
$\eta^0 \cdots \cdots$ 	$-3 i \xi \kappa^2 v U_{ij} \frac{g}{\sqrt{2}} \gamma^\mu \frac{1}{2} (1 - \gamma_5),$
$\eta^0 \cdots \cdots$ 	$-3 i \xi \kappa^2 U_{ij} \frac{g}{\sqrt{2}} \gamma^\mu \frac{1}{2} (1 - \gamma_5),$
$\eta^0 \cdots \cdots$ 	$-3 i \xi \kappa^2 v \frac{g}{2 c_W} \gamma^\mu \left(t_3^{(f)} - 2 Q_f s_W^2 - t_3^{(f)} \gamma_5 \right),$
$\eta^0 \cdots \cdots$ 	$-3 i \xi \kappa^2 \frac{g}{2 c_W} \gamma^\mu \left(t_3^{(f)} - 2 Q_f s_W^2 - t_3^{(f)} \gamma_5 \right),$

	$-3 i \xi \kappa^2 v Q_f e \gamma^\mu,$
	$-3 i \xi \kappa^2 Q_f e \gamma^\mu,$
	$-3 i \xi \kappa^2 v g_s \gamma^\mu T_a,$
	$-3 i \xi \kappa^2 g_s \gamma^\mu T_a.$

If the CP -odd component A^0 is lighter than η^0 , decays proceed through the three-point vertex

	$\frac{g}{2 c_W} (p_2^\mu - p_1^\mu),$
---	--

where the virtual η^0 subsequently decays through the non-minimal operator. The tree-level amplitudes for the decay $A^0 \rightarrow ZX$ are identical to the ones for $\eta^0 \rightarrow X$, multiplied by the factor

$$\epsilon_\mu(p_Z) \frac{g}{2 c_W} (2 p_{A^0}^\mu - p_Z^\mu) \frac{i}{(p_{A^0} - p_Z)^2 - m_{\eta^0}^2},$$

where the momenta of A^0 and Z are assumed to be incoming and outgoing, respectively.

A.4 Fermion singlet

In the fermion singlet scenario, the lowest-dimensional non-minimal operator results in the interaction term (4.33). As justified in the main text, the tree-level χ decay amplitudes in this EFT formulation are fully analogous to the ones for the CP -even component of the scalar doublet η^0 , multiplied by a fermionic current,

$$i\mathcal{M}_\chi = \frac{1}{2\sqrt{2}M^2} \bar{u}(p_\nu) (1 - \gamma_5) u(p_\chi) \times i\mathcal{M}_{\eta^0}, \quad (\text{A.2})$$

where ξ is to be reinterpreted as the non-minimal coupling of the fermion. These effective operators can be understood to arise from a UV completion of the theory. In section 4.3, the example of a scalar mediator was discussed. In that case, the decay amplitudes are modified according to (4.37),

$$i\mathcal{M}_\chi = \frac{y_j}{2\sqrt{2}} \frac{1}{(p_\chi - p_\nu)^2 - m_{\eta^0}^2} \bar{u}(p_\nu) (1 - \gamma_5) u(p_\chi) \times i\mathcal{M}_{\eta^0}. \quad (\text{A.3})$$

Appendix B

Generating Feynman rules with the *FeynRules* package for *Mathematica*

When studying phenomenological implications of concrete extensions of the standard model, it is often necessary to determine their impact on scattering cross sections or decay rates. As a first step towards that goal, one typically needs to extract the Feynman rules of the theory from its Lagrangian. As this extraction follows a universal procedure, it can be greatly accelerated through automation. The *FeynRules* package [120] for *Mathematica* is one such implementation. In this appendix, the procedure of obtaining the Feynman rules for a non-minimally coupled dark matter candidate will be sketched.

As an input to *FeynRules*, the user needs to specify the model under discussion. For extensions of the standard model, it is advisable to start with its pre-installed implementation and add to it the new physics one is interested in. Concretely, one needs to define all new fields, all couplings and other parameters (such as particle masses), as well as new gauge groups, if applicable. Adding a Dirac fermion singlet to the standard model, for example, is accomplished by including

```
F[5] == {
  ClassName      -> ChiDM,
  SelfConjugate  -> False,
  ParticleName   -> "chidm",
  Mass           -> {mchi, Internal},
  Width         -> {wchi, Internal},
  FullName      -> "ChiDM"
}
```

after the list of standard model fermions. In the first line, the new field is identified as a fermion and uniquely numbered. The mass and width given in lines five and six need to be specified as external parameters later in the model file, via

```
mchi == {
  ParameterType -> External,
  Description   -> "DM mass"
},
wchi == {
  ParameterType -> External,
  Description   -> "DM width"
}
```

Additional new parameters include the non-minimal coupling constant ξ , the mass scale M as well as the inverse reduced Planck mass κ . These are implemented analogously, by adding

```
xiDM == {
  ParameterType -> External,
  Value         -> 1,
  TeX           -> \[Xi],
  InteractionOrder -> {nmDM,1},
  Description    -> "Non-minimal coupling parameter"
},
MDM == {
  ParameterType -> External,
  Value         -> 1,
  TeX           -> M,
  Description    -> "DM coupling mass scale"
},
kappaDM == {
  ParameterType -> External,
  Value         -> 1,
  TeX           -> \[Kappa],
  Description    -> "Inverse reduced Planck mass"
}
```

to the model file. The numerical values given above are defaults and can be modified later. Lastly, the interactions of the fermion singlet have to be specified through its Lagrangian. The free dark matter Lagrangian is

```
LDM := Block[{mu4},
  I*( anti[ChiDM].Ga[mu4].del[ChiDM,mu4]
    - del[anti[ChiDM],mu4].Ga[mu4].ChiDM )/2]
- mchi anti[ChiDM].ChiDM;
```

while the interaction Lagrangian (4.33) in the fermion singlet scenario is entered as

```
Lint := ME[i1,i2] kappaDM^2 /Sqrt[2] xiDM /MDM^2 *
  (vev + H) (anti[ChiDM].ve + anti[ve].ChiDM) * TSM[i1,i2];
```

where built-in functions can be used for hermitian conjugation or metric tensors. The standard model energy-momentum tensor needs to be specified appropriately. The modified model file can then be imported to an interactive *Mathematica* session. After starting *FeynRules* and importing the model, a list of Feynman rules can be generated through the

```
FeynmanRules[LSM + LDM + Lint]
```

command. To use the model in Monte Carlo event generators like *MadGraph*, a Universal FeynRules Output folder [121] can be created automatically by entering

```
WriteUFO[LSM + LDM + Lint]
```

into the notebook session.

Appendix C

Computing decay rates and scattering cross sections with *MadGraph*

The Universal FeynRules Output format provides an interface between the analytical tools contained in the *FeynRules* package [120] and numerical Monte Carlo generators like *MadGraph* [122]. For a given set of model parameters, these can be used to explicitly determine scattering cross sections or partial widths. In the case of the fermion singlet discussed in section 4.3, for example, one can straightforwardly determine all tree-level partial widths for a fixed dark matter mass in this way. The folder generated by *FeynRules* can be directly imported into *MadGraph*. Next, one needs to enter the process of interest, fix the values of free parameters, and can then generate events. This is accomplished with the commands

```
import model smfs_xi
generate chidm > w+ w- h h h ve nmDM=1
output ~/Desktop/chiWW3Hnu
launch ~/Desktop/chiWW3Hnu
0
set param_card default
set mchi 1.e6
set kappadm 1.0
set xidm 1.0
set mdm 1.0
set nevents 10000
0
```

After rescaling the result with the proper prefactor $\xi^2 M^{-4} \bar{M}_p^{-4}$, this allows one to determine the partial width of the process $\chi \rightarrow WW H H H \nu$ at a dark matter mass of $m_\chi = 10^6$ GeV. To obtain multiple benchmark points at different masses, *MadGraph* can be operated in scripted mode. Among its output files is an `.html` document listing the results of different runs for a given process, which allows for convenient exporting to plotting or analysis software.

Appendix D

High-multiplicity phase-space integrals

Although the *FeynRules-MadGraph* pipeline allows for convenient and efficient computation of decay rates or scattering cross sections, it can be instructive (and useful for debugging purposes) to perform these calculations manually. The general formula for the decay of a particle φ into n final-state particles is [175]

$$d\Gamma_{\varphi \rightarrow n} = \frac{\mathcal{N}}{2m_0} |\mathcal{M}|^2 d\Phi_n, \quad (\text{D.1})$$

with m_0 the mass of the initial particle, $|\mathcal{M}|^2$ the unpolarized matrix element squared, \mathcal{N} a symmetry factor connected with final-state particle multiplicity, and $d\Phi_n$ the differential n -body phase space volume

$$d\Phi_n = (2\pi)^2 \delta^{(4)}\left(p_\varphi - \sum_{j=1}^n p_j\right) \prod_{i=1}^n \frac{d^3 p_i}{(2\pi)^3 2E_i}. \quad (\text{D.2})$$

While the general two-body phase space integral can be calculated analytically, the presence of three or more massive particles in the final state makes the calculation significantly more complex. Nevertheless, these phase-space integrals can be evaluated numerically, following a systematic approach. For the multi-body decay processes under discussion in this thesis, it is advantageous to split the evaluation into a chain of sequential two-body decays of virtual intermediate states. The phase-space element $d\Phi_n$ is a Lorentz invariant quantity. As a matter of fact, this also holds for all of the intermediate two-body phase-space integrals $d\Phi_2$ individually. Therefore, each of these two-body decays can be computed in its respective center-of-mass frame and afterwards boosted into the dark matter rest frame. This simplifies the calculation significantly. In an n -body decay, one introduces $(n - 2)$ intermediate virtual states. This way, the $(3n - 4)$ integrals that need to be performed in $d\Phi_n$ (three integrals per final-state particle, minus four due to net momentum conservation) are transformed into $(2n - 2)$ angular integrals over polar and azimuthal angles $\{\theta\}, \{\phi\}$, defined in their respective center-of-mass frames, and $(n - 2)$ integrals over the squared intermediate virtual state energies $\{s\}$.

For illustration, consider the decay of φ with initial momentum p_0 into a three-body final state with final-state momenta p_1, p_2 and p_3 . One can now split this process into $p_0 \rightarrow p_{12} p_3$, $p_{12} \rightarrow p_1 p_2$, with p_{12} the momentum of a virtual intermediate particle. The full three-body phase space can then be written as

$$d\Phi_3 = \frac{ds_{12}}{2\pi} d\Phi_2(m_0^2, \sqrt{s_{12}}, m_3) d\Phi_2(s_{12}, m_1, m_2), \quad (\text{D.3})$$

where the integration limits of the Mandelstam variable $s_{12} = p_{12}^2 = (p_1 + p_2)^2$ are

$$(m_1 + m_2)^2 \leq s_{12} \leq (m_0 - m_3)^2. \quad (\text{D.4})$$

The two-body phase space at center-of-mass energy \sqrt{s} for final-state masses m_1 and m_2 is

$$d\Phi_2(s, m_1, m_2) = \frac{1}{32\pi^2} \lambda(s, m_1, m_2) d\Omega_{12}. \quad (\text{D.5})$$

where

$$\lambda(s, m_1, m_2) = \sqrt{1 - 2 \frac{m_1^2 + m_2^2}{s} + \frac{(m_1^2 - m_2^2)^2}{s^2}} \quad (\text{D.6})$$

and $d\Omega_{12} = d\phi_{12} d(\cos\theta_{12})$, with the polar and azimuthal angles measured in the center-of-mass frame of particles 1 and 2. Scalar products between four-vectors, $p_i \cdot p_j$, can introduce angular dependence to the matrix element \mathcal{M} . To express these inner products in terms of the angles defined in the decomposition (D.3), one can proceed iteratively. In the center-of-mass system of particles 1 and 2, their four-momenta are

$$p_{1,(12)}^\mu = \begin{pmatrix} \sqrt{|\mathbf{p}_1|^2 + m_1^2} \\ |\mathbf{p}_1| \sin\theta_{12} \cos\phi_{12} \\ |\mathbf{p}_1| \sin\theta_{12} \sin\phi_{12} \\ |\mathbf{p}_1| \cos\theta_{12} \end{pmatrix}, \quad p_{2,(12)}^\mu = \begin{pmatrix} \sqrt{|\mathbf{p}_1|^2 + m_2^2} \\ -|\mathbf{p}_1| \sin\theta_{12} \cos\phi_{12} \\ -|\mathbf{p}_1| \sin\theta_{12} \sin\phi_{12} \\ -|\mathbf{p}_1| \cos\theta_{12} \end{pmatrix}, \quad (\text{D.7})$$

where the magnitude of the three-momentum is

$$|\mathbf{p}_1| = \frac{\sqrt{s_{12}}}{2} \lambda(s_{12}, m_1, m_2) \quad (\text{D.8})$$

(and $\mathbf{p}_2 = -\mathbf{p}_1$ due to momentum conservation). They can be transformed into the center-of-mass frame of the decaying particle φ through an appropriate Lorentz transformation,

$$p_{i,(CM)}^\mu = \Lambda_\nu^\mu(m_0^2, \sqrt{s_{12}}, m_3, \theta_{123}, \phi_{123}) p_{i,(12)}^\nu, \quad (\text{D.9})$$

where m_0^2 specifies the center-of-mass energy squared in the target frame, $\sqrt{s_{12}} = \sqrt{p_{12}^2}$ is the mass of the virtual intermediate state and m_3 that of the remaining particle. The Lorentz transformation is composed of a boost from the rest frame of the virtual intermediate state into that of φ and a rotation by the angles θ_{123}, ϕ_{123} , defined in the center-of-mass frame of φ . For arbitrary center-of-mass energies s , particle masses m_1 and m_2 and angles θ, ϕ , it reads

$$\Lambda_\nu^\mu(s, m_1, m_2, \theta, \phi) = \begin{pmatrix} \gamma & -\gamma\bar{\beta}_1 & -\gamma\bar{\beta}_2 & -\gamma\bar{\beta}_3 \\ -\gamma\bar{\beta}_1 & \frac{(\gamma-1)\bar{\beta}_1^2}{\beta^2} + 1 & \frac{(\gamma-1)\bar{\beta}_1\bar{\beta}_2}{\beta^2} & \frac{(\gamma-1)\bar{\beta}_1\bar{\beta}_3}{\beta^2} \\ -\gamma\bar{\beta}_2 & \frac{(\gamma-1)\bar{\beta}_2\bar{\beta}_1}{\beta^2} & \frac{(\gamma-1)\bar{\beta}_2^2}{\beta^2} + 1 & \frac{(\gamma-1)\bar{\beta}_2\bar{\beta}_3}{\beta^2} \\ -\gamma\bar{\beta}_3 & \frac{(\gamma-1)\bar{\beta}_3\bar{\beta}_1}{\beta^2} & \frac{(\gamma-1)\bar{\beta}_3\bar{\beta}_2}{\beta^2} & \frac{(\gamma-1)\bar{\beta}_3^2}{\beta^2} + 1 \end{pmatrix}, \quad (\text{D.10})$$

where

$$\bar{\beta}^{-2} = 1 + \frac{4m_1^2}{s} \lambda(s, m_1, m_2)^{-2}, \quad \gamma = \frac{1}{\sqrt{1 - \bar{\beta}^2}} = \frac{\sqrt{s}}{2m_1} \sqrt{\lambda(s, m_1, m_2)^2 + \frac{4m_1^2}{s}}, \quad (\text{D.11})$$

and

$$\vec{\beta} = \begin{pmatrix} \bar{\beta}_1 \\ \bar{\beta}_2 \\ \bar{\beta}_3 \end{pmatrix} = \begin{pmatrix} \cos \theta \cos \phi & -\sin \phi & \sin \theta \cos \phi \\ \cos \theta \sin \phi & \cos \phi & \sin \theta \sin \phi \\ -\sin \theta & 0 & \cos \theta \end{pmatrix} \begin{pmatrix} 0 \\ 0 \\ -\bar{\beta} \end{pmatrix} = \begin{pmatrix} -\sin \theta \cos \phi \bar{\beta} \\ -\sin \theta \sin \phi \bar{\beta} \\ -\cos \theta \bar{\beta} \end{pmatrix}. \quad (\text{D.12})$$

In the case at hand (D.9), the angles θ_{123} and ϕ_{123} determine the direction of the p_{12} - p_3 decay axis, measured in the φ rest frame, while θ_{12} and ϕ_{12} specify the direction of p_1 and p_2 , in the center-of-mass frame of the intermediate state. Once the matrix element squared and the phase space volume are expressed purely in terms of s_{12} , the angles θ_{12} , θ_{123} , ϕ_{12} and ϕ_{123} , as well as the particle masses m_0, m_1, m_2, m_3 , the total decay rate can be obtained by numerical integration.

This procedure can be generalized straightforwardly to the case of general n -body decays. With the definition $\Sigma_{ij\dots k} = m_i + m_j + \dots + m_k$, one can split up the four-, five- and six-body phase-space integrals appearing in chapter 5 as

$$d\Phi_4 = \frac{ds_{12}}{2\pi} \frac{ds_{34}}{2\pi} d\Phi_2(m_0^2, \sqrt{s_{12}}, \sqrt{s_{34}}) d\Phi_2(s_{12}, m_1, m_2) d\Phi_2(s_{34}, m_3, m_4), \quad (\text{D.13})$$

where

$$\Sigma_{12}^2 \leq s_{12} \leq (m_0 - \Sigma_{34})^2, \quad (\text{D.14})$$

$$\Sigma_{34}^2 \leq s_{34} \leq (m_0 - \sqrt{s_{12}})^2, \quad (\text{D.15})$$

$$d\Phi_5 = \frac{ds_{12}}{2\pi} \frac{ds_{345}}{2\pi} \frac{ds_{45}}{2\pi} d\Phi_2(m_0^2, \sqrt{s_{12}}, \sqrt{s_{345}}) d\Phi_2(s_{12}, m_1, m_2) d\Phi_2(s_{345}, m_3, \sqrt{s_{45}}) d\Phi_2(s_{45}, m_4, m_5), \quad (\text{D.16})$$

with

$$\Sigma_{12}^2 \leq s_{12} \leq (m_0 - \Sigma_{345})^2, \quad (\text{D.17})$$

$$\Sigma_{345}^2 \leq s_{345} \leq (m_0 - \sqrt{s_{12}})^2, \quad (\text{D.18})$$

$$\Sigma_{45}^2 \leq s_{45} \leq (\sqrt{s_{345}} - m_3)^2, \quad (\text{D.19})$$

and

$$d\Phi_6 = \frac{ds_{12}}{2\pi} \frac{ds_{3456}}{2\pi} \frac{ds_{456}}{2\pi} \frac{ds_{56}}{2\pi} d\Phi_2(m_0^2, \sqrt{s_{12}}, \sqrt{s_{3456}}) d\Phi_2(s_{12}, m_1, m_2) d\Phi_2(s_{3456}, m_3, \sqrt{s_{456}}) d\Phi_2(s_{456}, m_4, \sqrt{s_{56}}) d\Phi_2(s_{56}, m_5, m_6), \quad (\text{D.20})$$

with the integration region given by

$$\Sigma_{12}^2 \leq s_{12} \leq (m_0 - \Sigma_{3456})^2, \quad (\text{D.21})$$

$$\Sigma_{3456}^2 \leq s_{3456} \leq (m_0 - \sqrt{s_{12}})^2, \quad (\text{D.22})$$

$$\Sigma_{456}^2 \leq s_{456} \leq (\sqrt{s_{3456}} - m_3)^2, \quad (\text{D.23})$$

$$\Sigma_{56}^2 \leq s_{56} \leq (\sqrt{s_{456}} - m_4)^2. \quad (\text{D.24})$$

The transformation of the four-momenta in these decays is a straightforward generalization of (D.9). The four-momentum $p_{4,(\text{CM})}$ in a five-body decay, for example, is

$$p_{4,(\text{CM})}^\mu = \Lambda_\nu^\mu(m_0^2, \sqrt{s_{12}}, \sqrt{s_{345}}, \theta_{12345}, \phi_{12345}) \Lambda_\rho^\nu(s_{345}, m_3, \sqrt{s_{45}}, \theta_{345}, \phi_{345}) p_{4,(45)}^\rho, \quad (\text{D.25})$$

where $p_{4,(45)}^\rho$ is the four-momentum in the center-of-mass frame of particles 4 and 5, in analogy to (D.7). The expressions for the other four-momenta can be obtained in the same way through successive Lorentz transformations.

In principle, the splitting configurations listed above are chosen arbitrarily. However, depending on the form of the matrix element, choosing the right splitting (or, alternatively, choosing the right momentum assignment for the final-state particles) can be highly advantageous computationally. The above splitting is particularly well-suited for decays like $\varphi \rightarrow WW + nH$ or $\varphi \rightarrow f\bar{f} + nH$, as the only momentum product appearing in their matrix elements is $p_1 \cdot p_2 = (s_{12} - m_1^2 - m_2^2) / 2$, without any angular dependence.

Appendix E

Energy spectra of cascade decays

If a particle undergoes a decay cascade, *i.e.* if the final-state particles of the primary decay are unstable themselves, one might be interested in the energy spectrum of the stable daughter particles at the end of the cascade process. One example was given in section 6.1, where the impact of injecting electron-positron pairs and photons into the cosmological fluid on the cosmic microwave background was studied. Here, above a certain minimum mass, a dark matter particle ϕ decays into muons and pions with significant branching ratios (*cf.* figure 5.4). The muons subsequently decay almost exclusively into electrons and neutrino-antineutrino pairs [1], while charged pions mostly decay into muons (with a branching fraction of 99.99 % [1]). Neutral pions, in turn, decay into a pair of photons 98.82 % of the time [1]. Electron spectra for the decay chain $\pi \rightarrow \mu \rightarrow e$ have been known for a long time [176]. For arbitrary multi-step decays (also including multi-body final states), a simple Monte Carlo-based approach can be used to determine the final energy spectra, as will be sketched in the following.

Consider the decay chain $P_0 \rightarrow P_1 \rightarrow P_2$. The energy spectrum $(dN_2/dE_2)_1$ of particle P_2 produced in a decay is typically given in the rest frame of particle P_1 . The energy E_2 is not a Lorentz invariant quantity, however, so if measured in the rest frame of P_0 , the energy spectrum $(dN_2/dE_2)_0$ will be different. More specifically, E_2 is the 0-component of the four-momentum of particle P_2 , so it transforms as

$$p_{2,(0)}^0 = \Lambda_{\mu}^0(\gamma_1, \theta_1, \phi_1) p_{2,(1)}^{\mu} \quad (\text{E.1})$$

where $\Lambda_{\mu}^{\nu}(\gamma_1, \theta_1, \phi_1)$ is composed of two rotations and a boost, similar to (D.10), and relates the P_1 rest frame to that of P_0 . Explicitly,

$$E_{2,(0)} = \gamma_1 E_{2,(1)} + \cos \theta_1 \sqrt{\gamma_1^2 - 1} \sqrt{E_{2,(1)}^2 - m_2^2}, \quad (\text{E.2})$$

where $\gamma_1 = E_{1,(0)}/m_1$ is the boost factor of particle P_1 in the rest frame of P_0 . Given the energy spectrum $(dN_1/dE_1)_0$ of P_1 in the rest frame of P_0 and the spectrum $(dN_2/dE_2)_1$ of P_2 in the rest frame of P_1 , the final spectrum $(dN_2/dE_2)_0$ can be obtained by

- Randomly drawing a large number of energies $E_{1,(0)}$, distributed according to the spectrum $(dN_1/dE_1)_0$, and normalizing them by m_1 to obtain a sample of boost factors γ_1 ,
- Randomly drawing an equal number of energies $E_{2,(1)}$ distributed according to $(dN_2/dE_2)_1$,
- Randomly drawing sets of polar and azimuthal angles, with flat distributions for $\cos \theta_1$ and ϕ_1 ,
- Transforming each energy $E_{2,(1)}$ in the sample according to (E.2),

- And binning, normalizing and interpolating the transformed energy spectra.

The accuracy of this approach can easily be adjusted through the number of “events” generated (a practical choice is $\mathcal{O}(10^6)$). Moreover, the procedure can be trivially extended to cascade decays with additional intermediate steps by successively performing additional Lorentz transformations in (E.1). This is necessary for the decay chain $\phi \rightarrow \pi^+\pi^-$, $\pi \rightarrow \mu \rightarrow e$, for example. Particle spectra generated in this way were cross-checked against existing literature, *e.g.* the electron spectra from [176], and excellent agreement was found. For the determination of the CMB limits discussed in section 6.1, the dark matter decay channels $\gamma\gamma$, e^+e^- , $e^+e^-\gamma$, $\mu^+\mu^-$, $\mu^+\mu^-\gamma$, $\pi^0\pi^0$ and $\pi^+\pi^-$ were considered, together with $\mu^+ \rightarrow e^+\bar{\nu}_\mu\nu_e$, $\pi^0 \rightarrow \gamma\gamma$ and $\pi^+ \rightarrow \mu^+\nu_\mu$ (and the processes with their antiparticles, were applicable). The resulting spectra $(dN_e/dE)_f$ and $(dN_\gamma/dE)_f$ for each final state f are the ones entering (6.1).

Acknowledgements

I am immensely thankful to my supervisor Alejandro Ibarra, for giving me the chance to pursue my doctoral studies at T30d. His comprehensive expertise, profound intuition, and unflagging enthusiasm for physics made for a truly inspiring time in his group. I want to thank him, as well as my collaborator Oscar Catà, for many stimulating and fruitful discussions. Whenever I hit a technical or conceptual roadblock, I could count on both to guide me back on track, and learn something new along the way.

Secondly, I wish to thank all members of T30d — both scientific and administrative! — of the past 4.5 years for providing such a warm and lively scientific environment, based on deep mutual respect and a common thirst for knowledge. You were a wonderful set of colleagues, and I feel privileged to have been working with you. Likewise, I am very grateful for the time I could spend at the MPP during my studies. With my office in Garching, I wish I could have had a closer connection to the theory groups at Föhringer Ring. Through the MPP's generous travel opportunities, I was able to join the wider HEP/astroparticle physics community on many occasions around the world.

I want to thank my parents, as well as my siblings, for their unconditional love and support, and for providing a safe base camp for this adventure. Even when the going gets tough, you are always there.

Last, but certainly not least, I want to shout out to the folks of office 1122, past and present, official and unofficial — you know who you are. Could I have done it without you? Maybe! But I would have missed out on an awful lot of BBQ sessions, Friday-afternoon rants, discussions on physics (or politics), and general gossip and banter. Enjoying time with one's colleagues is one thing, but true privilege is to share an office with friends. Cheers!

Bibliography

- [1] C. Patrignani et al. Review of Particle Physics. *Chin. Phys.*, C40(10):100001, 2016. doi:10.1088/1674-1137/40/10/100001.
- [2] Georges Aad et al. Observation of a new particle in the search for the Standard Model Higgs boson with the ATLAS detector at the LHC. *Phys. Lett.*, B716:1–29, 2012. arXiv:1207.7214, doi:10.1016/j.physletb.2012.08.020.
- [3] Serguei Chatrchyan et al. Observation of a new boson at a mass of 125 GeV with the CMS experiment at the LHC. *Phys. Lett.*, B716:30–61, 2012. arXiv:1207.7235, doi:10.1016/j.physletb.2012.08.021.
- [4] Edward W. Kolb and Michael S. Turner. The Early Universe. *Front. Phys.*, 69:1–547, 1990.
- [5] P. A. R. Ade et al. Planck 2015 results. XIII. Cosmological parameters. *Astron. Astrophys.*, 594:A13, 2016. arXiv:1502.01589, doi:10.1051/0004-6361/201525830.
- [6] Gianfranco Bertone, Dan Hooper, and Joseph Silk. Particle dark matter: Evidence, candidates and constraints. *Phys. Rept.*, 405:279–390, 2005. arXiv:hep-ph/0404175, doi:10.1016/j.physrep.2004.08.031.
- [7] V. C. Rubin, N. Thonnard, and W. K. Ford, Jr. Rotational properties of 21 SC galaxies with a large range of luminosities and radii, from NGC 4605 /R = 4kpc/ to UGC 2885 /R = 122 kpc/. *Astrophys. J.*, 238:471, 1980. doi:10.1086/158003.
- [8] Massimo Persic, Paolo Salucci, and Fulvio Stel. The Universal rotation curve of spiral galaxies: 1. The Dark matter connection. *Mon. Not. Roy. Astron. Soc.*, 281:27, 1996. arXiv:astro-ph/9506004, doi:10.1093/mnras/281.1.27, 10.1093/mnras/278.1.27.
- [9] Julio F. Navarro, Carlos S. Frenk, and Simon D. M. White. The Structure of cold dark matter halos. *Astrophys. J.*, 462:563–575, 1996. arXiv:astro-ph/9508025, doi:10.1086/177173.
- [10] M. Milgrom. A Modification of the Newtonian dynamics as a possible alternative to the hidden mass hypothesis. *Astrophys. J.*, 270:365–370, 1983. doi:10.1086/161130.
- [11] Douglas Clowe, Marusa Bradac, Anthony H. Gonzalez, Maxim Markevitch, Scott W. Randall, Christine Jones, and Dennis Zaritsky. A direct empirical proof of the existence of dark matter. *Astrophys. J.*, 648:L109–L113, 2006. arXiv:astro-ph/0608407, doi:10.1086/508162.

- [12] Marusa Bradac, Steven W. Allen, Tommaso Treu, Harald Ebeling, Richard Massey, R. Glenn Morris, Anja von der Linden, and Douglas Applegate. Revealing the properties of dark matter in the merging cluster MACSJ0025.4-1222. *Astrophys. J.*, 687:959, 2008. [arXiv:0806.2320](#), [doi:10.1086/591246](#).
- [13] George F. Smoot et al. Structure in the COBE differential microwave radiometer first year maps. *Astrophys. J.*, 396:L1–L5, 1992. [doi:10.1086/186504](#).
- [14] G. Hinshaw et al. Nine-Year Wilkinson Microwave Anisotropy Probe (WMAP) Observations: Cosmological Parameter Results. *Astrophys. J. Suppl.*, 208:19, 2013. [arXiv:1212.5226](#), [doi:10.1088/0067-0049/208/2/19](#).
- [15] Michael S. Turner. Coherent Scalar Field Oscillations in an Expanding Universe. *Phys. Rev.*, D28:1243, 1983. [doi:10.1103/PhysRevD.28.1243](#).
- [16] Wayne Hu, Rennan Barkana, and Andrei Gruzinov. Cold and fuzzy dark matter. *Phys. Rev. Lett.*, 85:1158–1161, 2000. [arXiv:astro-ph/0003365](#), [doi:10.1103/PhysRevLett.85.1158](#).
- [17] Gerard Jungman, Marc Kamionkowski, and Kim Griest. Supersymmetric dark matter. *Phys. Rept.*, 267:195–373, 1996. [arXiv:hep-ph/9506380](#), [doi:10.1016/0370-1573\(95\)00058-5](#).
- [18] G. F. Chapline. Cosmological effects of primordial black holes. *Nature*, 253:251, January 1975. [doi:10.1038/253251a0](#).
- [19] Bernard Carr, Florian Kuhnel, and Marit Sandstad. Primordial Black Holes as Dark Matter. *Phys. Rev.*, D94(8):083504, 2016. [arXiv:1607.06077](#), [doi:10.1103/PhysRevD.94.083504](#).
- [20] Patrick J. Fox, Roni Harnik, Joachim Kopp, and Yuhsin Tsai. Missing Energy Signatures of Dark Matter at the LHC. *Phys. Rev.*, D85:056011, 2012. [arXiv:1109.4398](#), [doi:10.1103/PhysRevD.85.056011](#).
- [21] Daniel Abercrombie et al. Dark Matter Benchmark Models for Early LHC Run-2 Searches: Report of the ATLAS/CMS Dark Matter Forum. 2015. [arXiv:1507.00966](#).
- [22] R. Agnese et al. New Results from the Search for Low-Mass Weakly Interacting Massive Particles with the CDMS Low Ionization Threshold Experiment. *Phys. Rev. Lett.*, 116(7):071301, 2016. [arXiv:1509.02448](#), [doi:10.1103/PhysRevLett.116.071301](#).
- [23] Andi Tan et al. Dark Matter Results from First 98.7 Days of Data from the PandaX-II Experiment. *Phys. Rev. Lett.*, 117(12):121303, 2016. [arXiv:1607.07400](#), [doi:10.1103/PhysRevLett.117.121303](#).
- [24] D. S. Akerib et al. Results from a search for dark matter in the complete LUX exposure. *Phys. Rev. Lett.*, 118(2):021303, 2017. [arXiv:1608.07648](#), [doi:10.1103/PhysRevLett.118.021303](#).
- [25] E. Aprile et al. Dark Matter Search Results from a One Ton-Year Exposure of XENON1T. *Phys. Rev. Lett.*, 121(11):111302, 2018. [arXiv:1805.12562](#), [doi:10.1103/PhysRevLett.121.111302](#).

-
- [26] F. Petricca et al. First results on low-mass dark matter from the CRESST-III experiment. In *15th International Conference on Topics in Astroparticle and Underground Physics (TAUP 2017) Sudbury, Ontario, Canada, July 24-28, 2017*, 2017. URL: <http://inspirehep.net/record/1637341/files/arXiv:1711.07692.pdf>, arXiv:1711.07692.
- [27] M. Ackermann et al. Searching for Dark Matter Annihilation from Milky Way Dwarf Spheroidal Galaxies with Six Years of Fermi Large Area Telescope Data. *Phys. Rev. Lett.*, 115(23):231301, 2015. arXiv:1503.02641, doi:10.1103/PhysRevLett.115.231301.
- [28] Gaëlle Giesen, Mathieu Boudaud, Yoann Génolini, Vivian Poulin, Marco Cirelli, Pierre Salati, and Pasquale D. Serpico. AMS-02 antiprotons, at last! Secondary astrophysical component and immediate implications for Dark Matter. *JCAP*, 1509(09):023, 2015. arXiv:1504.04276, doi:10.1088/1475-7516/2015/09/023, 10.1088/1475-7516/2015/9/023.
- [29] M. G. Aartsen et al. Search for dark matter annihilations in the Sun with the 79-string IceCube detector. *Phys. Rev. Lett.*, 110(13):131302, 2013. arXiv:1212.4097, doi:10.1103/PhysRevLett.110.131302.
- [30] Kim Griest and David Seckel. Three exceptions in the calculation of relic abundances. *Phys. Rev.*, D43:3191–3203, 1991. doi:10.1103/PhysRevD.43.3191.
- [31] Lawrence J. Hall, Karsten Jedamzik, John March-Russell, and Stephen M. West. Freeze-In Production of FIMP Dark Matter. *JHEP*, 03:080, 2010. arXiv:0911.1120, doi:10.1007/JHEP03(2010)080.
- [32] Yonit Hochberg, Eric Kuflik, Tomer Volansky, and Jay G. Wacker. Mechanism for Thermal Relic Dark Matter of Strongly Interacting Massive Particles. *Phys. Rev. Lett.*, 113:171301, 2014. arXiv:1402.5143, doi:10.1103/PhysRevLett.113.171301.
- [33] R. Foot and S. Vagnozzi. Dissipative hidden sector dark matter. *Phys. Rev.*, D91:023512, 2015. arXiv:1409.7174, doi:10.1103/PhysRevD.91.023512.
- [34] Thomas Hambye. On the stability of particle dark matter. *PoS*, IDM2010:098, 2011. arXiv:1012.4587, doi:10.22323/1.110.0098.
- [35] Scott Willenbrock. Symmetries of the standard model. In *Physics in D $\hat{=}$ 4. Proceedings, Theoretical Advanced Study Institute in elementary particle physics, TASI 2004, Boulder, USA, June 6-July 2, 2004*, pages 3–38, 2004. arXiv:hep-ph/0410370.
- [36] Edward Witten. Symmetry and Emergence. *Nature Phys.*, 14:116–119, 2018. arXiv:1710.01791, doi:10.1038/nphys4348.
- [37] Steven Weinberg. A New Light Boson? *Phys. Rev. Lett.*, 40:223–226, 1978. doi:10.1103/PhysRevLett.40.223.
- [38] John Preskill, Mark B. Wise, and Frank Wilczek. Cosmology of the Invisible Axion. *Phys. Lett.*, B120:127–132, 1983. [URL(1982)]. doi:10.1016/0370-2693(83)90637-8.
- [39] Marco Cirelli, Nicolao Fornengo, and Alessandro Strumia. Minimal dark matter. *Nucl. Phys.*, B753:178–194, 2006. arXiv:hep-ph/0512090, doi:10.1016/j.nuclphysb.2006.07.012.
-

- [40] Oscar Cata and Alejandro Ibarra. Dark Matter Stability without New Symmetries. *Phys. Rev.*, D90(6):063509, 2014. [arXiv:1404.0432](#), [doi:10.1103/PhysRevD.90.063509](#).
- [41] Lotty Ackerman, Matthew R. Buckley, Sean M. Carroll, and Marc Kamionkowski. Dark Matter and Dark Radiation. *Phys. Rev.*, D79:023519, 2009. [277(2008)]. [arXiv:0810.5126](#), [doi:10.1103/PhysRevD.79.023519](#), [10.1142/9789814293792_0021](#).
- [42] Jonathan L. Feng, Manoj Kaplinghat, Huitzu Tu, and Hai-Bo Yu. Hidden Charged Dark Matter. *JCAP*, 0907:004, 2009. [arXiv:0905.3039](#), [doi:10.1088/1475-7516/2009/07/004](#).
- [43] Renata Kallosh, Andrei D. Linde, Dmitri A. Linde, and Leonard Susskind. Gravity and global symmetries. *Phys. Rev.*, D52:912–935, 1995. [arXiv:hep-th/9502069](#), [doi:10.1103/PhysRevD.52.912](#).
- [44] Tom Banks and Nathan Seiberg. Symmetries and Strings in Field Theory and Gravity. *Phys. Rev.*, D83:084019, 2011. [arXiv:1011.5120](#), [doi:10.1103/PhysRevD.83.084019](#).
- [45] V. Berezhinsky, Anjan S. Joshipura, and J. W. F. Valle. Gravitational violation of R-parity and its cosmological signatures. *Phys. Rev.*, D57:147–151, 1998. [arXiv:hep-ph/9608307](#), [doi:10.1103/PhysRevD.57.147](#).
- [46] Eduard Masso, Francesc Rota, and Gabriel Zsembinszki. Planck-scale effects on global symmetries: Cosmology of pseudo-Goldstone bosons. *Phys. Rev.*, D70:115009, 2004. [arXiv:hep-ph/0404289](#), [doi:10.1103/PhysRevD.70.115009](#).
- [47] M. S. Boucenna, R. A. Lineros, and J. W. F. Valle. Planck-scale effects on WIMP dark matter. *Front.in Phys.*, 1:34, 2013. [arXiv:1204.2576](#), [doi:10.3389/fphy.2013.00034](#).
- [48] Yann Mambrini, Stefano Profumo, and Farinaldo S. Queiroz. Dark Matter and Global Symmetries. *Phys. Lett.*, B760:807–815, 2016. [arXiv:1508.06635](#), [doi:10.1016/j.physletb.2016.07.076](#).
- [49] Sebastian Inghütt. Dark matter decays from non-minimal coupling to gravity. Master’s thesis, Technical University of Munich, 11 2015.
- [50] Oscar Catà, Alejandro Ibarra, and Sebastian Inghütt. Dark matter decays from non-minimal coupling to gravity. *Phys. Rev. Lett.*, 117(2):021302, 2016. [arXiv:1603.03696](#), [doi:10.1103/PhysRevLett.117.021302](#).
- [51] Oscar Catà, Alejandro Ibarra, and Sebastian Inghütt. Dark matter decay through gravity portals. *Phys. Rev.*, D95(3):035011, 2017. [arXiv:1611.00725](#), [doi:10.1103/PhysRevD.95.035011](#).
- [52] Oscar Catà, Alejandro Ibarra, and Sebastian Inghütt. Sharp spectral features from light dark matter decay via gravity portals. *JCAP*, 1711(11):044, 2017. [arXiv:1707.08480](#), [doi:10.1088/1475-7516/2017/11/044](#).
- [53] J. C. Kapteyn. First Attempt at a Theory of the Arrangement and Motion of the Sidereal System. *Astrophys. J.*, 55:302–328, 1922. [doi:10.1086/142670](#).
- [54] J H Oort. The force exerted by the stellar system in the direction perpendicular to the galactic plane and some related problems. *Bull. Astron. Inst. Netherlands*, 6:249–287, 1932. URL: <http://cds.cern.ch/record/436532>.

-
- [55] F. Zwicky. Die Rotverschiebung von extragalaktischen Nebeln. *Helv. Phys. Acta*, 6:110–127, 1933. [Gen. Rel. Grav.41,207(2009)]. doi:10.1007/s10714-008-0707-4.
- [56] F Zwicky. On the masses of nebulae and clusters of nebulae. *Astrophys. J.*, 86:217–246, 1937. URL: <http://cds.cern.ch/record/437296>.
- [57] M. S. Roberts and R. N. Whitehurst. The rotation curve and geometry of M31 at large galactocentric distances. *Astrophysical Journal*, 201:327–346, October 1975. doi:10.1086/153889.
- [58] A. N. Taylor, S. Dye, Thomas J. Broadhurst, N. Benitez, and E. van Kampen. Gravitational lens magnification and the mass of abell 1689. *Astrophys. J.*, 501:539, 1998. arXiv:astro-ph/9801158, doi:10.1086/305827.
- [59] Pieter van Dokkum et al. A galaxy lacking dark matter. *Nature*, 555(7698):629–632, 2018. arXiv:1803.10237, doi:10.1038/nature25767.
- [60] Nicolas F. Martin, Michelle L. M. Collins, Nicolas Longeard, and Erik Tollerud. Current Velocity Data on Dwarf Galaxy NGC 1052-DF2 do not Constrain it to Lack Dark Matter. *The Astrophysical Journal Letters*, 859:L5, May 2018. arXiv:1804.04136, doi:10.3847/2041-8213/aac216.
- [61] Chervin F. P. Laporte, Adriano Agnello, and Julio F. Navarro. Reconciling mass estimates of ultradiffuse galaxies. *Monthly Notices of the Royal Astronomical Society*, 484:245–251, Mar 2019. arXiv:1804.04139, doi:10.1093/mnras/sty2891.
- [62] Ignacio Trujillo, Michael A. Beasley, Alejandro Borlaff, Eleazar R. Carrasco, Arianna Di Cintio, Mercedes Filho, Matteo Monelli, Mireia Montes, Javier Roman, Tomas Ruiz-Lara, Jorge Sanchez Almeida, David Valls-Gabaud, and Alexandre Vazdekis. A distance of 13 Mpc resolves the claimed anomalies of the galaxy lacking dark matter. *arXiv e-prints*, page arXiv:1806.10141, Jun 2018. arXiv:1806.10141.
- [63] J. Aalbers et al. DARWIN: towards the ultimate dark matter detector. *JCAP*, 1611:017, 2016. arXiv:1606.07001, doi:10.1088/1475-7516/2016/11/017.
- [64] B. J. Mount et al. LUX-ZEPLIN (LZ) Technical Design Report. 2017. arXiv:1703.09144.
- [65] Kentaro Miuchi et al. First underground results with NEWAGE-0.3a direction-sensitive dark matter detector. *Phys. Lett.*, B686:11–17, 2010. arXiv:1002.1794, doi:10.1016/j.physletb.2010.02.028.
- [66] E. Daw et al. The DRIFT Directional Dark Matter Experiments. *EAS Publ. Ser.*, 53:11–18, 2012. arXiv:1110.0222, doi:10.1051/eas/1253002.
- [67] Q. Riffard et al. Dark Matter directional detection with MIMAC. In *Proceedings, 48th Rencontres de Moriond on Very High Energy Phenomena in the Universe: La Thuile, Italy, March 9-16, 2013*, pages 227–230, 2013. arXiv:1306.4173.
- [68] Michael Leyton. Directional dark matter detection with the DMTPC m³ experiment. *J. Phys. Conf. Ser.*, 718(4):042035, 2016. doi:10.1088/1742-6596/718/4/042035.
- [69] Morad Aaboud et al. Search for dark matter and other new phenomena in events with an energetic jet and large missing transverse momentum using the ATLAS detector. *JHEP*, 01:126, 2018. arXiv:1711.03301, doi:10.1007/JHEP01(2018)126.
-

- [70] Albert M Sirunyan et al. Search for dark matter produced with an energetic jet or a hadronically decaying W or Z boson at $\sqrt{s} = 13$ TeV. *JHEP*, 07:014, 2017. arXiv:1703.01651, doi:10.1007/JHEP07(2017)014.
- [71] David E. Kaplan, Markus A. Luty, and Kathryn M. Zurek. Asymmetric Dark Matter. *Phys. Rev.*, D79:115016, 2009. arXiv:0901.4117, doi:10.1103/PhysRevD.79.115016.
- [72] Serguei Chatrchyan et al. Search for invisible decays of Higgs bosons in the vector boson fusion and associated ZH production modes. *Eur. Phys. J.*, C74:2980, 2014. arXiv:1404.1344, doi:10.1140/epjc/s10052-014-2980-6.
- [73] Georges Aad et al. Search for massive, long-lived particles using multitrack displaced vertices or displaced lepton pairs in pp collisions at $\sqrt{s} = 8$ TeV with the ATLAS detector. *Phys. Rev.*, D92(7):072004, 2015. arXiv:1504.05162, doi:10.1103/PhysRevD.92.072004.
- [74] M. Ackermann et al. The spectrum of isotropic diffuse gamma-ray emission between 100 MeV and 820 GeV. *Astrophys. J.*, 799:86, 2015. arXiv:1410.3696, doi:10.1088/0004-637X/799/1/86.
- [75] R. Abbasi et al. Constraints on the Extremely-high Energy Cosmic Neutrino Flux with the IceCube 2008-2009 Data. *Phys. Rev.*, D83:092003, 2011. [Erratum: Phys. Rev.D84,079902(2011)]. arXiv:1103.4250, doi:10.1103/PhysRevD.84.079902, 10.1103/PhysRevD.83.092003.
- [76] L. Accardo et al. High Statistics Measurement of the Positron Fraction in Primary Cosmic Rays of 0.5–500 GeV with the Alpha Magnetic Spectrometer on the International Space Station. *Phys. Rev. Lett.*, 113:121101, 2014. doi:10.1103/PhysRevLett.113.121101.
- [77] M. Aguilar et al. Antiproton Flux, Antiproton-to-Proton Flux Ratio, and Properties of Elementary Particle Fluxes in Primary Cosmic Rays Measured with the Alpha Magnetic Spectrometer on the International Space Station. *Phys. Rev. Lett.*, 117(9):091103, 2016. doi:10.1103/PhysRevLett.117.091103.
- [78] Marco Cirelli, Gennaro Corcella, Andi Hektor, Gert Hutsi, Mario Kadastik, Paolo Panci, Martti Raidal, Filippo Sala, and Alessandro Strumia. PPC 4 DM ID: A Poor Particle Physicist Cookbook for Dark Matter Indirect Detection. *JCAP*, 1103:051, 2011. [Erratum: JCAP1210,E01(2012)]. arXiv:1012.4515, doi:10.1088/1475-7516/2012/10/E01, 10.1088/1475-7516/2011/03/051.
- [79] Dan Hooper and Lisa Goodenough. Dark Matter Annihilation in The Galactic Center As Seen by the Fermi Gamma Ray Space Telescope. *Phys. Lett.*, B697:412–428, 2011. arXiv:1010.2752, doi:10.1016/j.physletb.2011.02.029.
- [80] Alejandro Ibarra, David Tran, and Christoph Weniger. Indirect Searches for Decaying Dark Matter. *Int. J. Mod. Phys.*, A28:1330040, 2013. arXiv:1307.6434, doi:10.1142/S0217751X13300408.
- [81] Vanda Silveira and A. Zee. SCALAR PHANTOMS. *Phys. Lett.*, 161B:136–140, 1985. doi:10.1016/0370-2693(85)90624-0.
- [82] John McDonald. Gauge singlet scalars as cold dark matter. *Phys. Rev.*, D50:3637–3649, 1994. arXiv:hep-ph/0702143, doi:10.1103/PhysRevD.50.3637.

-
- [83] Paolo Gondolo and Graciela Gelmini. Cosmic abundances of stable particles: Improved analysis. *Nucl. Phys.*, B360:145–179, 1991. doi:10.1016/0550-3213(91)90438-4.
- [84] James M. Cline, Kimmo Kainulainen, Pat Scott, and Christoph Weniger. Update on scalar singlet dark matter. *Phys. Rev.*, D88:055025, 2013. [Erratum: *Phys. Rev.* D92,no.3,039906(2015)]. arXiv:1306.4710, doi:10.1103/PhysRevD.92.039906, 10.1103/PhysRevD.88.055025.
- [85] Peter Athron et al. Status of the scalar singlet dark matter model. *Eur. Phys. J.*, C77(8):568, 2017. arXiv:1705.07931, doi:10.1140/epjc/s10052-017-5113-1.
- [86] Joakim Edsjo and Paolo Gondolo. Neutralino relic density including coannihilations. *Phys. Rev.*, D56:1879–1894, 1997. arXiv:hep-ph/9704361, doi:10.1103/PhysRevD.56.1879.
- [87] Carlos E. Yaguna. The Singlet Scalar as FIMP Dark Matter. *JHEP*, 08:060, 2011. arXiv:1105.1654, doi:10.1007/JHEP08(2011)060.
- [88] R. D. Peccei and Helen R. Quinn. Constraints Imposed by CP Conservation in the Presence of Instantons. *Phys. Rev.*, D16:1791–1797, 1977. doi:10.1103/PhysRevD.16.1791.
- [89] Frank Wilczek. Problem of Strong p and t Invariance in the Presence of Instantons. *Phys. Rev. Lett.*, 40:279–282, 1978. doi:10.1103/PhysRevLett.40.279.
- [90] Camilo Garcia-Cely, Alejandro Ibarra, Anna S. Lamperstorfer, and Michel H. G. Tytgat. Gamma-rays from Heavy Minimal Dark Matter. *JCAP*, 1510(10):058, 2015. arXiv:1507.05536, doi:10.1088/1475-7516/2015/10/058.
- [91] Marco Cirelli, Thomas Hambye, Paolo Panci, Filippo Sala, and Marco Taoso. Gamma ray tests of Minimal Dark Matter. *JCAP*, 1510(10):026, 2015. arXiv:1507.05519, doi:10.1088/1475-7516/2015/10/026.
- [92] Alejandro Ibarra, David Tran, and Christoph Weniger. Decaying Dark Matter in Light of the PAMELA and Fermi LAT Data. *JCAP*, 1001:009, 2010. arXiv:0906.1571, doi:10.1088/1475-7516/2010/01/009.
- [93] Marco Cirelli, Emmanuel Moulin, Paolo Panci, Pasquale D. Serpico, and Aion Viana. Gamma ray constraints on Decaying Dark Matter. *Phys. Rev.*, D86:083506, 2012. arXiv:1205.5283, doi:10.1103/PhysRevD.86.083506, 10.1103/PhysRevD.86.109901.
- [94] Arman Esmaili and Pasquale Dario Serpico. Are IceCube neutrinos unveiling PeV-scale decaying dark matter? *JCAP*, 1311:054, 2013. arXiv:1308.1105, doi:10.1088/1475-7516/2013/11/054.
- [95] Albert Einstein. The Foundation of the General Theory of Relativity. *Annalen Phys.*, 49(7):769–822, 1916. [65(1916)]. doi:10.1002/andp.200590044, 10.1002/andp.19163540702.
- [96] Sean M. Carroll. *Spacetime and geometry: An introduction to general relativity*. Addison-Wesley, 2004. URL: <http://www.slac.stanford.edu/spires/find/books/www?cl=QC6:C37:2004>.
- [97] Clifford M. Will. The Confrontation between general relativity and experiment. *Living Rev. Rel.*, 9:3, 2006. arXiv:gr-qc/0510072, doi:10.12942/lrr-2006-3.
-

- [98] Robert H. Sanders and Stacy S. McGaugh. Modified Newtonian dynamics as an alternative to dark matter. *Ann. Rev. Astron. Astrophys.*, 40:263–317, 2002. [arXiv:astro-ph/0204521](#), [doi:10.1146/annurev.astro.40.060401.093923](#).
- [99] Thomas P. Sotiriou and Valerio Faraoni. $f(R)$ Theories Of Gravity. *Rev. Mod. Phys.*, 82:451–497, 2010. [arXiv:0805.1726](#), [doi:10.1103/RevModPhys.82.451](#).
- [100] Jorge C. Romao and Joao P. Silva. A resource for signs and Feynman diagrams of the Standard Model. *Int. J. Mod. Phys.*, A27:1230025, 2012. [arXiv:1209.6213](#), [doi:10.1142/S0217751X12300256](#).
- [101] F. Englert and R. Brout. Broken Symmetry and the Mass of Gauge Vector Mesons. *Phys. Rev. Lett.*, 13:321–323, 1964. [157(1964)]. [doi:10.1103/PhysRevLett.13.321](#).
- [102] Peter W. Higgs. Broken Symmetries and the Masses of Gauge Bosons. *Phys. Rev. Lett.*, 13:508–509, 1964. [160(1964)]. [doi:10.1103/PhysRevLett.13.508](#).
- [103] G. S. Guralnik, C. R. Hagen, and T. W. B. Kibble. Global Conservation Laws and Massless Particles. *Phys. Rev. Lett.*, 13:585–587, 1964. [162(1964)]. [doi:10.1103/PhysRevLett.13.585](#).
- [104] J. Gasser and H. Leutwyler. Chiral Perturbation Theory to One Loop. *Annals Phys.*, 158:142, 1984. [doi:10.1016/0003-4916\(84\)90242-2](#).
- [105] Jalal Abdallah et al. Simplified Models for Dark Matter Searches at the LHC. *Phys. Dark Univ.*, 9-10:8–23, 2015. [arXiv:1506.03116](#), [doi:10.1016/j.dark.2015.08.001](#).
- [106] Daniele Alves. Simplified Models for LHC New Physics Searches. *J. Phys.*, G39:105005, 2012. [arXiv:1105.2838](#), [doi:10.1088/0954-3899/39/10/105005](#).
- [107] Georges Aad et al. Search for direct production of charginos, neutralinos and sleptons in final states with two leptons and missing transverse momentum in pp collisions at $\sqrt{s} = 8$ TeV with the ATLAS detector. *JHEP*, 05:071, 2014. [arXiv:1403.5294](#), [doi:10.1007/JHEP05\(2014\)071](#).
- [108] Jessica Goodman, Masahiro Ibe, Arvind Rajaraman, William Shepherd, Tim M. P. Tait, and Hai-Bo Yu. Constraints on Dark Matter from Colliders. *Phys. Rev.*, D82:116010, 2010. [arXiv:1008.1783](#), [doi:10.1103/PhysRevD.82.116010](#).
- [109] Giorgio Busoni, Andrea De Simone, Johanna Gramling, Enrico Morgante, and Antonio Riotto. On the Validity of the Effective Field Theory for Dark Matter Searches at the LHC, Part II: Complete Analysis for the s -channel. *JCAP*, 1406:060, 2014. [arXiv:1402.1275](#), [doi:10.1088/1475-7516/2014/06/060](#).
- [110] Kathryn M. Zurek. Multi-Component Dark Matter. *Phys. Rev.*, D79:115002, 2009. [arXiv:0811.4429](#), [doi:10.1103/PhysRevD.79.115002](#).
- [111] Keith R. Dienes and Brooks Thomas. Dynamical Dark Matter: I. Theoretical Overview. *Phys. Rev.*, D85:083523, 2012. [arXiv:1106.4546](#), [doi:10.1103/PhysRevD.85.083523](#).
- [112] John F. Donoghue. General relativity as an effective field theory: The leading quantum corrections. *Phys. Rev.*, D50:3874–3888, 1994. [arXiv:gr-qc/9405057](#), [doi:10.1103/PhysRevD.50.3874](#).

-
- [113] Jose A. R. Cembranos. Dark Matter from R2-gravity. *Phys. Rev. Lett.*, 102:141301, 2009. arXiv:0809.1653, doi:10.1103/PhysRevLett.102.141301.
- [114] Fuminobu Takahashi and Eiichiro Komatsu. Gravitational Dark Matter Decay and the ATIC/PPB-BETS Excess. 2009. arXiv:0901.1915.
- [115] Taishi Katsuragawa and Shinya Matsuzaki. Dark matter in modified gravity? *Phys. Rev.*, D95(4):044040, 2017. arXiv:1610.01016, doi:10.1103/PhysRevD.95.044040.
- [116] Yong Tang and Yue-Liang Wu. Pure Gravitational Dark Matter, Its Mass and Signatures. *Phys. Lett.*, B758:402–406, 2016. arXiv:1604.04701, doi:10.1016/j.physletb.2016.05.045.
- [117] Laura Lopez Honorez, Emmanuel Nezri, Josep F. Oliver, and Michel H. G. Tytgat. The Inert Doublet Model: An Archetype for Dark Matter. *JCAP*, 0702:028, 2007. arXiv:hep-ph/0612275, doi:10.1088/1475-7516/2007/02/028.
- [118] Riccardo Barbieri, Lawrence J. Hall, and Vyacheslav S. Rychkov. Improved naturalness with a heavy Higgs: An Alternative road to LHC physics. *Phys. Rev.*, D74:015007, 2006. arXiv:hep-ph/0603188, doi:10.1103/PhysRevD.74.015007.
- [119] Elena Jeron. Decay of vectorial dark matter through a gravity channel. Master’s thesis, Ludwig-Maximilians-Universität München, 8 2017.
- [120] Adam Alloul, Neil D. Christensen, Céline Degrande, Claude Duhr, and Benjamin Fuks. FeynRules 2.0 - A complete toolbox for tree-level phenomenology. *Comput. Phys. Commun.*, 185:2250–2300, 2014. arXiv:1310.1921, doi:10.1016/j.cpc.2014.04.012.
- [121] Celine Degrande, Claude Duhr, Benjamin Fuks, David Grellscheid, Olivier Mattelaer, and Thomas Reiter. UFO - The Universal FeynRules Output. *Comput. Phys. Commun.*, 183:1201–1214, 2012. arXiv:1108.2040, doi:10.1016/j.cpc.2012.01.022.
- [122] J. Alwall, R. Frederix, S. Frixione, V. Hirschi, F. Maltoni, O. Mattelaer, H. S. Shao, T. Stelzer, P. Torrielli, and M. Zaro. The automated computation of tree-level and next-to-leading order differential cross sections, and their matching to parton shower simulations. *JHEP*, 07:079, 2014. arXiv:1405.0301, doi:10.1007/JHEP07(2014)079.
- [123] Mikhail A. Shifman, A. I. Vainshtein, M. B. Voloshin, and Valentin I. Zakharov. Low-Energy Theorems for Higgs Boson Couplings to Photons. *Sov. J. Nucl. Phys.*, 30:711–716, 1979. [Yad. Fiz.30,1368(1979)].
- [124] Nilendra G. Deshpande and Ernest Ma. Pattern of Symmetry Breaking with Two Higgs Doublets. *Phys. Rev.*, D18:2574, 1978. doi:10.1103/PhysRevD.18.2574.
- [125] Camilo Garcia-Cely, Michael Gustafsson, and Alejandro Ibarra. Probing the Inert Doublet Dark Matter Model with Cherenkov Telescopes. *JCAP*, 1602(02):043, 2016. arXiv:1512.02801, doi:10.1088/1475-7516/2016/02/043.
- [126] Yeong Gyun Kim and Kang Young Lee. The Minimal model of fermionic dark matter. *Phys. Rev.*, D75:115012, 2007. arXiv:hep-ph/0611069, doi:10.1103/PhysRevD.75.115012.

- [127] Mathias Garny, Alejandro Ibarra, and Stefan Vogl. Signatures of Majorana dark matter with t-channel mediators. *Int. J. Mod. Phys.*, D24(07):1530019, 2015. [arXiv:1503.01500](#), [doi:10.1142/S0218271815300190](#).
- [128] S. Desai et al. Search for dark matter WIMPs using upward through-going muons in Super-Kamiokande. *Phys. Rev.*, D70:083523, 2004. [Erratum: *Phys. Rev.*D70,109901(2004)]. [arXiv:hep-ex/0404025](#), [doi:10.1103/PhysRevD.70.083523](#), [10.1103/PhysRevD.70.109901](#).
- [129] R. Abbasi et al. Search for dark matter from the Galactic halo with the IceCube Neutrino Telescope. *Phys. Rev.*, D84:022004, 2011. [arXiv:1101.3349](#), [doi:10.1103/PhysRevD.84.022004](#).
- [130] R. Abbasi et al. A Search for UHE Tau Neutrinos with IceCube. *Phys. Rev.*, D86:022005, 2012. [arXiv:1202.4564](#), [doi:10.1103/PhysRevD.86.022005](#).
- [131] A. Achterberg et al. Multi-year search for a diffuse flux of muon neutrinos with AMANDA-II. *Phys. Rev.*, D76:042008, 2007. [Erratum: *Phys. Rev.*D77,089904(2008)]. [arXiv:0705.1315](#), [doi:10.1103/PhysRevD.76.042008](#), [10.1103/PhysRevD.77.089904](#).
- [132] P. Abreu et al. A Search for Ultra-High Energy Neutrinos in Highly Inclined Events at the Pierre Auger Observatory. *Phys. Rev.*, D84:122005, 2011. [Erratum: *Phys. Rev.*D84,029902(2011)]. [arXiv:1202.1493](#), [doi:10.1103/PhysRevD.85.029902](#), [10.1103/PhysRevD.84.122005](#).
- [133] P. W. Gorham et al. Observational Constraints on the Ultra-high Energy Cosmic Neutrino Flux from the Second Flight of the ANITA Experiment. *Phys. Rev.*, D82:022004, 2010. [Erratum: *Phys. Rev.*D85,049901(2012)]. [arXiv:1003.2961](#), [doi:10.1103/PhysRevD.82.022004](#), [10.1103/PhysRevD.85.049901](#).
- [134] Arman Esmaili, Alejandro Ibarra, and Orlando L. G. Peres. Probing the stability of superheavy dark matter particles with high-energy neutrinos. *JCAP*, 1211:034, 2012. [arXiv:1205.5281](#), [doi:10.1088/1475-7516/2012/11/034](#).
- [135] Laura Covi, Michael Grefe, Alejandro Ibarra, and David Tran. Neutrino Signals from Dark Matter Decay. *JCAP*, 1004:017, 2010. [arXiv:0912.3521](#), [doi:10.1088/1475-7516/2010/04/017](#).
- [136] Alejandro Ibarra, Anna S. Lamperstorfer, and Joseph Silk. Dark matter annihilations and decays after the AMS-02 positron measurements. *Phys. Rev.*, D89(6):063539, 2014. [arXiv:1309.2570](#), [doi:10.1103/PhysRevD.89.063539](#).
- [137] E. Churazov et al. INTEGRAL observations of the cosmic X-ray background in the 5-100 keV range via occultation by the Earth. *Astron. Astrophys.*, 2006. [*Astron. Astrophys.*467,529(2007)]. [arXiv:astro-ph/0608250](#), [doi:10.1051/0004-6361:20066230](#).
- [138] G. Weidenspointner, M. Varendorff, S. C. Kappadath, K. Bennett, H. Bloemen, R. Diehl, W. Hermsen, G. G. Lichti, J. Ryan, and V. Schönfelder. The cosmic diffuse gamma-ray background measured with comptel. *AIP Conference Proceedings*, 510(1):467–470, 2000. URL: <https://aip.scitation.org/doi/abs/10.1063/1.1307028>, [arXiv:https://aip.scitation.org/doi/pdf/10.1063/1.1307028](#), [doi:10.1063/1.1307028](#).

-
- [139] A. W. Strong, I. V. Moskalenko, and O. Reimer. A new determination of the extragalactic diffuse gamma-ray background from egret data. *Astrophys. J.*, 613:956–961, 2004. [arXiv:astro-ph/0405441](#), [doi:10.1086/423196](#).
- [140] Marcello Ciafaloni, Paolo Ciafaloni, and Denis Comelli. Bloch-Nordsieck violating electroweak corrections to inclusive TeV scale hard processes. *Phys. Rev. Lett.*, 84:4810–4813, 2000. [arXiv:hep-ph/0001142](#), [doi:10.1103/PhysRevLett.84.4810](#).
- [141] Marcello Ciafaloni, Paolo Ciafaloni, and Denis Comelli. Electroweak Bloch-Nordsieck violation at the TeV scale: ‘Strong’ weak interactions? *Nucl. Phys.*, B589:359–380, 2000. [arXiv:hep-ph/0004071](#), [doi:10.1016/S0550-3213\(00\)00508-3](#).
- [142] Paolo Ciafaloni and Denis Comelli. Electroweak evolution equations. *JHEP*, 11:022, 2005. [arXiv:hep-ph/0505047](#), [doi:10.1088/1126-6708/2005/11/022](#).
- [143] G. Bell, J. H. Kuhn, and J. Rittinger. Electroweak Sudakov Logarithms and Real Gauge-Boson Radiation in the TeV Region. *Eur. Phys. J.*, C70:659–671, 2010. [arXiv:1004.4117](#), [doi:10.1140/epjc/s10052-010-1489-x](#).
- [144] Alejandro Ibarra, Sergio Lopez Gehler, and Miguel Pato. Dark matter constraints from box-shaped gamma-ray features. *JCAP*, 1207:043, 2012. [arXiv:1205.0007](#), [doi:10.1088/1475-7516/2012/07/043](#).
- [145] V. Schoenfelder, H. Aarts, K. Bennett, H. de Boer, J. Clear, W. Collmar, A. Connors, A. Deerenberg, R. Diehl, A. von Dordrecht, J. W. den Herder, W. Hermsen, M. Kippen, L. Kuiper, G. Lichti, J. Lockwood, J. Macri, M. McConnell, D. Morris, R. Much, J. Ryan, G. Simpson, M. Snelling, G. Stacy, H. Steinle, A. Strong, B. N. Swanenburg, B. Taylor, C. de Vries, and C. Winkler. Instrument description and performance of the Imaging Gamma-Ray Telescope COMPTEL aboard the Compton Gamma-Ray Observatory. *Astrophysical Journal Supplement Series*, 86:657–692, June 1993. [doi:10.1086/191794](#).
- [146] D. J. Thompson et al. Calibration of the Energetic Gamma-Ray Experiment Telescope (EGRET) for the Compton Gamma-Ray Observatory. *Astrophys. J. Suppl.*, 86:629–656, 1993. [doi:10.1086/191793](#).
- [147] R. Rando and for the Fermi LAT Collaboration. Post-launch performance of the Fermi Large Area Telescope. *ArXiv e-prints*, July 2009. [arXiv:0907.0626](#).
- [148] Paolo Ciafaloni, Denis Comelli, Antonio Riotto, Filippo Sala, Alessandro Strumia, and Alfredo Urbano. Weak Corrections are Relevant for Dark Matter Indirect Detection. *JCAP*, 1103:019, 2011. [arXiv:1009.0224](#), [doi:10.1088/1475-7516/2011/03/019](#).
- [149] Jennifer A. Adams, Subir Sarkar, and D. W. Sciama. CMB anisotropy in the decaying neutrino cosmology. *Mon. Not. Roy. Astron. Soc.*, 301:210–214, 1998. [arXiv:astro-ph/9805108](#), [doi:10.1046/j.1365-8711.1998.02017.x](#).
- [150] Xue-Lei Chen and Marc Kamionkowski. Particle decays during the cosmic dark ages. *Phys. Rev.*, D70:043502, 2004. [arXiv:astro-ph/0310473](#), [doi:10.1103/PhysRevD.70.043502](#).
- [151] Nikhil Padmanabhan and Douglas P. Finkbeiner. Detecting dark matter annihilation with CMB polarization: Signatures and experimental prospects. *Phys. Rev.*, D72:023508, 2005. [arXiv:astro-ph/0503486](#), [doi:10.1103/PhysRevD.72.023508](#).
-

- [152] J. Chluba and R. A. Sunyaev. The evolution of CMB spectral distortions in the early Universe. *Mon. Not. Roy. Astron. Soc.*, 419:1294–1314, 2012. [arXiv:1109.6552](#), doi:10.1111/j.1365-2966.2011.19786.x.
- [153] Tracy R. Slatyer, Nikhil Padmanabhan, and Douglas P. Finkbeiner. CMB Constraints on WIMP Annihilation: Energy Absorption During the Recombination Epoch. *Phys. Rev.*, D80:043526, 2009. [arXiv:0906.1197](#), doi:10.1103/PhysRevD.80.043526.
- [154] Silvia Galli, Tracy R. Slatyer, Marcos Valdes, and Fabio Iocco. Systematic Uncertainties In Constraining Dark Matter Annihilation From The Cosmic Microwave Background. *Phys. Rev.*, D88:063502, 2013. [arXiv:1306.0563](#), doi:10.1103/PhysRevD.88.063502.
- [155] Christoph Weniger, Pasquale D. Serpico, Fabio Iocco, and Gianfranco Bertone. CMB bounds on dark matter annihilation: Nucleon energy-losses after recombination. *Phys. Rev.*, D87(12):123008, 2013. [arXiv:1303.0942](#), doi:10.1103/PhysRevD.87.123008.
- [156] Tracy R. Slatyer. Indirect Dark Matter Signatures in the Cosmic Dark Ages II. Ionization, Heating and Photon Production from Arbitrary Energy Injections. *Phys. Rev.*, D93(2):023521, 2016. [arXiv:1506.03812](#), doi:10.1103/PhysRevD.93.023521.
- [157] Tracy R. Slatyer and Chih-Liang Wu. General Constraints on Dark Matter Decay from the Cosmic Microwave Background. *Phys. Rev.*, D95(2):023010, 2017. [arXiv:1610.06933](#), doi:10.1103/PhysRevD.95.023010.
- [158] Tracy R. Slatyer. Indirect dark matter signatures in the cosmic dark ages. I. Generalizing the bound on s-wave dark matter annihilation from Planck results. *Phys. Rev.*, D93(2):023527, 2016. [arXiv:1506.03811](#), doi:10.1103/PhysRevD.93.023527.
- [159] A. De Angelis et al. The e-ASTROGAM mission. *Exper. Astron.*, 44(1):25–82, 2017. [arXiv:1611.02232](#), doi:10.1007/s10686-017-9533-6.
- [160] Mathias Garny, McCullen Sandora, and Martin S. Sloth. Planckian Interacting Massive Particles as Dark Matter. *Phys. Rev. Lett.*, 116(10):101302, 2016. [arXiv:1511.03278](#), doi:10.1103/PhysRevLett.116.101302.
- [161] Mathias Garny, Andrea Palessandro, McCullen Sandora, and Martin S. Sloth. Theory and Phenomenology of Planckian Interacting Massive Particles as Dark Matter. *JCAP*, 1802(02):027, 2018. [arXiv:1709.09688](#), doi:10.1088/1475-7516/2018/02/027.
- [162] Yong Tang and Yue-Liang Wu. On Thermal Gravitational Contribution to Particle Production and Dark Matter. *Phys. Lett.*, B774:676–681, 2017. [arXiv:1708.05138](#), doi:10.1016/j.physletb.2017.10.034.
- [163] H. Arason, D. J. Castano, B. Keszthelyi, S. Mikaelian, E. J. Piard, Pierre Ramond, and B. D. Wright. Renormalization group study of the standard model and its extensions. 1. The Standard model. *Phys. Rev.*, D46:3945–3965, 1992. doi:10.1103/PhysRevD.46.3945.
- [164] Alan H. Guth. The Inflationary Universe: A Possible Solution to the Horizon and Flatness Problems. *Phys. Rev.*, D23:347–356, 1981. [Adv. Ser. Astrophys. Cosmol.3,139(1987)]. doi:10.1103/PhysRevD.23.347.

-
- [165] Andrei D. Linde. A New Inflationary Universe Scenario: A Possible Solution of the Horizon, Flatness, Homogeneity, Isotropy and Primordial Monopole Problems. *Phys. Lett.*, 108B:389–393, 1982. [Adv. Ser. Astrophys. Cosmol.3,149(1987)]. doi:10.1016/0370-2693(82)91219-9.
- [166] Andreas Albrecht and Paul J. Steinhardt. Cosmology for Grand Unified Theories with Radiatively Induced Symmetry Breaking. *Phys. Rev. Lett.*, 48:1220–1223, 1982. [Adv. Ser. Astrophys. Cosmol.3,158(1987)]. doi:10.1103/PhysRevLett.48.1220.
- [167] P. A. R. Ade et al. Planck 2015 results. XX. Constraints on inflation. *Astron. Astrophys.*, 594:A20, 2016. arXiv:1502.02114, doi:10.1051/0004-6361/201525898.
- [168] Tommi Tenkanen. Resurrecting Quadratic Inflation with a non-minimal coupling to gravity. *JCAP*, 1712(12):001, 2017. arXiv:1710.02758, doi:10.1088/1475-7516/2017/12/001.
- [169] Soo-Min Choi, Yoo-Jin Kang, Hyun Min Lee, and Kimiko Yamashita. Unitary inflaton as decaying dark matter. 2019. arXiv:1902.03781.
- [170] Fedor L. Bezrukov and Mikhail Shaposhnikov. The Standard Model Higgs boson as the inflaton. *Phys. Lett.*, B659:703–706, 2008. arXiv:0710.3755, doi:10.1016/j.physletb.2007.11.072.
- [171] J. L. F. Barbon and J. R. Espinosa. On the Naturalness of Higgs Inflation. *Phys. Rev.*, D79:081302, 2009. arXiv:0903.0355, doi:10.1103/PhysRevD.79.081302.
- [172] C. P. Burgess, Hyun Min Lee, and Michael Trott. Comment on Higgs Inflation and Naturalness. *JHEP*, 07:007, 2010. arXiv:1002.2730, doi:10.1007/JHEP07(2010)007.
- [173] F. Bezrukov, A. Magnin, M. Shaposhnikov, and S. Sibiryakov. Higgs inflation: consistency and generalisations. *JHEP*, 01:016, 2011. arXiv:1008.5157, doi:10.1007/JHEP01(2011)016.
- [174] A. M. Sirunyan et al. Search for new physics in final states with an energetic jet or a hadronically decaying W or Z boson and transverse momentum imbalance at $\sqrt{s} = 13$ TeV. *Phys. Rev.*, D97(9):092005, 2018. arXiv:1712.02345, doi:10.1103/PhysRevD.97.092005.
- [175] Michael E. Peskin and Daniel V. Schroeder. *An Introduction to quantum field theory*. Addison-Wesley, Reading, USA, 1995. URL: <http://www.slac.stanford.edu/~mpeskin/QFT.html>.
- [176] J. H. Scanlon and S. N. Milford. Energy Spectra of Electrons from π - μ -e Decays in Interstellar Space. *Astrophysical Journal*, 141:718, February 1965. doi:10.1086/148156.